8-2009

Coupled Flow Discrete Element Method Application in Granular Porous Media using Open Source Codes

Feng Chen
University of Tennessee - Knoxville

To the Graduate Council:

I am submitting herewith a dissertation written by Feng Chen entitled "Coupled Flow Discrete Element Method Application in Granular Porous Media using Open Source Codes." I have examined the final electronic copy of this dissertation for form and content and recommend that it be accepted in partial fulfillment of the requirements for the degree of Doctor of Philosophy, with a major in Civil Engineering.

<div align="right">Eric C. Drumm, Major Professor</div>

We have read this dissertation and recommend its acceptance:

Georges A. Guiochon, Dayakar Penumadu, Baoshan Huang, Richard Bennett

<div align="right">Accepted for the Council:
Dixie L. Thompson</div>

<div align="right">Vice Provost and Dean of the Graduate School</div>

(Original signatures are on file with official student records.)

To the Graduate Council:

I am submitting herewith a dissertation written by Feng Chen entitled "Coupled Flow Discrete Element Method Application in Granular Porous Media using Open Source Codes." I have examined the final electronic copy of this dissertation for form and content and recommend that it be accepted in partial fulfillment of the requirements for the degree of Doctor of Philosophy, with a major in Civil Engineering.

_____
Eric C. Drumm, Major Professor

We have read this dissertation
and recommend its acceptance:

_____
Georges A. Guiochon

_____
Dayakar Penumadu

_____
Baoshan Huang

_____
Richard Bennett

Accepted for the Council:

_____
Carolyn R. Hodges
Vice Provost and Dean of the Graduate School

Coupled Flow Discrete Element Method Application in Granular Porous Media using Open Source Codes

A Dissertation Presented for
the Doctor of Philosophy
Degree
The University of Tennessee, Knoxville

Feng Chen
August 2009

Acknowledgements

I would like to gratefully acknowledge the enthusiastic supervision of Prof. Eric C Drumm and Prof. Georges Guiochon for their continuous interest, support and guidance during this PhD research. I thank Prof. Baoshan Huang of his help during the 5 year studying and living in University of Tennessee, Knoxville. The text of this Thesis has benefited from valuable comments from Dr. Penumadu and Dr. Bennett.

I am grateful to all my friends Xiang Shu, Qiao Dong, Hao Wu and Jingsong Chen for their help. Finally, I am forever indebted to my wife Yiping Qu's support, my parents and my sister in Shanghai for their understanding, endless patience and encouragement.

致谢

余自丁丑年入同济求学，甲申年入美利坚国田纳西大学攻读博士，至公元二零零九年春末夏初本文定稿，不觉十二载矣，回顾往事，历历在目，依稀昨日。枫生性驽钝，惟勤奋自勉，徐图渐进，然漫漫长路坎坷荆棘，所幸得助甚多，借此片纸，聊表谢忱。

本文之撰写，自选题至方法，自整体至细节，皆得艾瑞克.壮姆导师悉心指点；亦幸遇乔治.古笙教授，满腹经纶，高瞻远瞩；更受黄公宝山教授垂教之恩，博我之寡陋，并助我之急难，惜恩长笔短，不可尽述。

子曰，立身行道，以显父母，若非父母自幼之言传身教，潜移默化，万不敢妄想今日之拙论。枫不肖，为闻道而远行，令父母挂念在他乡。今双亲不远万里与余在异国重逢，枫跪而叩谢，不知何以为报。

妻瞿氏奕萍，贤良端淑，与余比翼他乡，不计居所之简陋，不厌生活之艰辛，风雨同舟，已一又余载，此文之成，妻之功伟矣，枫不胜感激涕零。

Abstract

The flow of fluid through an assembly of particles is of interest to a range of fields such as civil engineering, powder technology, and liquid chromatography. The Discrete Element Method (DEM) is a numerical approximation used to model the interaction of particles and fluid. This study starts with the verification of the open source 3D DEM code (YADE) by investigating simple, one and two-particle contact problems, and DEM results are shown to compare very well with the classical 1D vibration solutions.

2D and 3D simulations of particles flowing through a hopper were then investigated. The stability of the sinkhole repair for a range of rock particle diameters (relative to the sinkhole throat diameter) was investigated by presenting a statistical description to describe the gradual transition from unstable to stable behavior.

This was followed by an investigation of a fluid-solid two phase flow system. The fluid phase is modeled by solving the averaged Navier-Stokes equation using the Finite Volume Method (FVM) and the solid phase was modeled using the DEM. A framework was developed to couple two open source codes: YADE-OpenDEM for the DEM and OpenFOAM for the computational fluid dynamics. The particle-fluid interaction is quantified using a semi-empirical relationship proposed by Ergun (1952). 1D solutions for the classic upward seepage flow and consolidation were obtained and compared well with the analytical solutions. These verification problems were also used to explore the appropriate time step size for both the fluid and mechanical solution processes, and the choice of the viscous damping coefficient.

Finally, the coupled DEM-CFD code is used in the solution of a classical 2D seepage problem of flow beneath a sheet pile and the slurry packing of a chromatography column. For the sheet pile problem, both the quantity of seepage and the pressure gradient leading to the quick condition are investigated. The effect of the fluid volume size relative to particle size was also investigated. For the packing of a chromatography column, the method was able to reproduce the "wall effects" during the axial upward compression procedure, providing a displacement field similar to that observed in experiments.

Table of Contents

List of Figures

x

List of Tables

1 Introduction

1.1 Background

Materials such as soils and rocks, as well as assemblies of particles such as those used to pack chromatography columns, are often treated as porous media. "A porous medium or a porous material is a solid (often called frame or matrix) permeated by an interconnected network of pores (voids) filled with a fluid (liquid or gas)" (Wikipedia 2007). In the field of geotechnical engineering, the interaction between soil particles and pore water is encountered in many problems. Specifically, the seepage flow problem with the hydraulic gradient and the seepage flow velocity tending towards the critical value which leads to a quick condition or liquefaction.

In high performance liquid chromatography, columns of porous silica are packed by subjecting slurry to a large fluid pressure differential to form a dense assembly of particles. The efficiency of the column is governed by radial and axial uniformity of the porosity. Improvement in the analytical capability of the coupled flow through assemblies of particles can positively impact both geotechnical engineering and HPLC, not to mention the field of powder technology. Currently three main categories of simulation schemes exist to solve the coupled flow problems, including

• Continuum mechanics approach

• Lattice Boltzmann method

• Semi-discrete-continuum method

The **continuum approach** averages the physics across many particles and thereby treats the material as a continuum on a macro scale level. In the case of solid-like granular behavior as in soil mechanics, the continuum approach usually treats the material as elastic or elasto-plastic, in the case of liquid-like or gas-like granular flow, the continuum approach may treat the material as a fluid and then models it with the finite element method or other methods available from continuum mechanics. Such approaches, however, overlook macroscopic system properties observed in experimental inquiries, while the microscale particle-fluid interactions have limited resolution.

The **lattice Boltzmann method** (LBM) is a discrete simulation method for complex fluid systems based on the Boltzmann equation on a micro geometrical level (Succi 2001). Traditional computational fluid dynamics (CFD) solves the conservation equations of macroscopic properties (i.e., mass, momentum, and energy) numerically while LBM tracks a typical volume element of fluid which is composed of a limited number of particles that are represented by a particle velocity distribution function which displays the particle stream and collision behavior for each fluid component at each grid point.

The **semi-discrete-continuum** method, which is the topic in this study, is adopted for coupled particle-fluid modeling. The fluid phase is modeled at the macroscopic scale by solving the momentum and continuity equations using traditional computational fluid dynamics. The solid phase, on the other hand, is modeled in microscopic scale using the **discrete element method** (DEM). The semi-implicit finite volume method (FVM) discretization for fluid flow is coupled with the explicit discrete element method for particles.

1.2 Previous and related studies

There are analyses of dry soils using DEM (Bathurst and Rothenburg 1988; Dobry and Ng 1992; Peron et al. 2009; Thornton and Liu 2000) and also investigations in which pore fluid pressure of a soil element is evaluated based on the mean confining stresses required to ensure constant volume deformations (Evgin 2000). However, a more realistic approach capable of considering coupled formulations including the skeleton deformation, pore fluid flow, and resultant interactions is possible with the semi-discrete-continuum approach originally proposed by Tsuji et al. (1993). Tanaka et al. (1993), Kawaguchi et al. (1998), and Yuu et al. (2000) continued with this approach with fluidized beds in powder technology using the DEM for the particles and the FVM for the fluid. However, there has been only limited application of this analysis geotechnical engineering: (El Shamy and Zeghal 2005; Suzuki et al. 2007), there is also coupled flow analysis using the DEM-FVM coupled approach with the fluid phase simplified into a Darcy flow field (Shafipour and Soroush 2008).

For the solution of problems of practical interest, with a reasonable number of particles, a fast and robust software platform is required. Unlike the finite element method (FEM) for which many codes exist, there are very few DEM codes available. Most are developed according the developers' specific requirements, which leads to an investigation of current existing DEM codes. Meanwhile, robust CFD codes are also required to complete the coupled flow approach.

1.2.1 DEM codes

The Discrete (or Distinct) Element Method (DEM) is a set of numerical methods for computing the motion of an assembly of particles. The method was originally applied by Cundall and Strack in 1979 (Cundall and Strack 1979) to problems in rock mechanics. In general, the discrete element can be of various shapes, e.g. tetrahedral, polyhedral, elliptic etc. However, this study only involves spherical particles.

Discrete element methods are processor intensive and this limits either the length of a simulation or the number of particles. A proper software platform is necessary for DEM simulation. Commercially available DEM software packages for spherical particles include:

• PFC2D and PFC3D (Itasca Inc. 2004a) Particle Flow Code in 2/3 Dimensions.

• Chute Maven (Hustrulid and Mustoe 1996) Spherical Discrete Element Modeling in 3 Dimensions.

• EDEM (DEM Solutions 2009) General-purpose DEM simulation with CAD import of particle and machine geometry. EDEM is able to couple the commercial fluid code Fluent (Fluent Inc. 2006) with its own port.

As in the well known PFC2D/3D code, the use of DEM software is typically "code" based which means the input of a specific application is a set of codes from the software end-user. PFC2D/3D created its own FISH programming language and a group of commands to describe the user input (particle and wall description). The disadvantage is that the kernel of the commercial code remained a black box for the end-user and the documentation of the software relies entirely on the software company. Limited and incomplete documentation restrict the ability of end-users to extend their applications to other fields unless the expected code module has already been provided by the software vendor. Such software design seriously limits the application and development of the DEM, and limits the ability to fully understand the computation process.

Open source is a development method for software that harnesses the power of distributed peer review and transparency of process. The promise of open source code is better quality, higher reliability, more flexibility, lower cost, and an end to predatory vendor lock-in (Open Source Initiative 2007). The source code documentation is written text that accompanies computer software. It both explains how it operates or how to use it, and may mean different things to people in different roles. Compared to code based DEM software, the documentation of open source code is even more important for end-users. The open source codes thus provide a transparent process to the end-users such that even a beginner-level programmer can contribute to the document which in turn might be very constructive for the DEM development. Currently open source and non-commercial
DEM codes include:

• BALL and TRUBAL (Cundall 1978): distinct element method (in FORTRAN), originally written by P. Cundall and currently maintained by C. Thornton. (Non-commercial)

• SDEC (Donzé and Magnier 1997): Spherical Discrete Element Code. (Non-commercial)

• YADE (Kozicki and Donzé 2008): Yet Another Dynamic Engine, some functions are re-implemented from SDEC, GPL license. (Open source)

• Pasimodo (Popp and Schiehlen 2008): Multi-purpose particle-based simulation methods. (Non-commercial) software.
In this study, YADE is employed for the discrete element modeling for the solid particles.

1.2.2 CFD codes

Computational fluid dynamics (CFD) (J. Anderson 1995) is one of the branches of fluid mechanics that uses numerical methods and algorithms to solve and analyze problems that involve fluid flows. CFD is also computationally intensive to perform the millions of calculations required to simulate the interaction of fluids and gases with the complex structures encountered in engineering.

Currently most CFD software, either commercial or open source, uses the finite volume discretization to solve the velocity and pressure field from the Navier-Stokes equations, following a pressure correction approach originally proposed by Partankar (1980). The fundamental steps are to iteratively solve the momentum equations first for velocity, and then enforce the velocity to obey continuity equations by correction of the pressure within each time step (transient problem) or iteration (for steady state problem).

Well known commercial CFD codes include:
  • Fluent (Fluent Inc. 2006): Famous ANSYS suite of CAE simulation solutions.
  • StarCD (CD-adapco Group 2001): Powerful engineering simulation (CAE) solutions for fluid flow, heat transfer and stress.

Open source CFD codes include:
  • OpenFOAM (OpenCFD Ltd 2008): A general purpose open-source CFD code. OpenFOAM is written in C++ and uses an object oriented approach for finite volume discretization and uses un-structured grids.
  • Overture (Brown et al. 1999): A large object-oriented C++ framework for solving PDE's with overlapping structured grids.

- FEniCS (Logg 2009): Organized as a collection of sub projects/components, including finite element fluid solver parts.

In this study, an averaged Navier-Stokes equation (Anderson and Jackson 1967) is used for the description of the pore fluid phase, and the fluid field is solved using the finite volume method with the PISO algorithm (Issa 1986) using the open source code OpenFOAM. The transient PISO solver for incompressible laminar Newtonian fluids provided by OpenFOAM has been customized and incorporated into YADE as a dynamically linked library, which constitutes the major coding contribution of this dissertation.

1.3 Present contributions

This study currently makes the following contributions to the application of discrete element method in geotechnical engineering and the field of chromatography:

Chapter 1 "Prediction/Verification of Particle Motion in One Dimension with the Discrete-Element Method" is a paper published as:

Feng Chen, Eric. C. Drumm and Georges Guiochon, Prediction/Verification of particle motion in one dimension with the Discrete Element Method, International Journal of Geomechanics, Vol. 7, No. 5, 2007

In this paper:
(1)   Instead of using an existing commercial DEM code, open source codes are primarily used in this study. This takes advantages of code reuse, the ability to make improvements and learn how the computations are actually being performed, and receive community feedback.
(2)   Analytical solutions of two different yet simple particle contact problems with various types of damping are obtained. The numerical results from the open source code YADE are compared with the analytical solutions and commercial code PFC2D solutions. It is shown that the three results agree well with each other, provided the initial conditions in the two codes are manipulated to be the same, which provides good verification for YADE. The availability of simple verification problems is important to develop confidence in the DEM solutions and facilitate growth of the method.
(3)   A customized user-written YADE routine is implemented for viscous damping, which has been made available to the YADE user community.
(4)   The routine **ConvergenceEstimator** using the ratio of maximum unbalanced force over maximum contact force is implemented in YADE as the convergence criterion to judge whether the whole particle system has reached (or is close to) the equilibrium state. YADE did not have a convergence routine previously, and this routine will be made available to the YADE user community.

Chapter 2 "Simulation of Graded Rock Fill for Sinkhole Repair in Particle Flow Model" and **Chapter 3** "3D DEM analysis of Graded Rock Fill Sinkhole Repair: Particle Size Effects on the Probability of Stability" were similar papers published as:

Feng Chen , Ozgur Alturk , Eric C. Drumm, Simulation of Graded Rock Fill for Sinkhole Repair in Particle Flow Model, Geoshanghai 2006 International conference, June 6-8, 2006

and

Feng Chen, Eric. C. Drumm, Georges Guiochon, 3D DEM Analysis Of Graded Rock Fill Sinkhole Repair: Particle Size Effects On The Probability Of Stability, 2009 Transportation Research Board Conference (Presentation).

In these papers:
(1)   A series of discrete element simulations of the idealized placement of graded rock fill for sinkhole repair were conducted both in 2D and 3D. This is essentially the classic "sand in the funnel" problem.
(2)   Simulations were performed and stability was investigated for a range of mean particle diameters relative to the sinkhole throat diameter. For a given throat diameter, there is a particle size below which a stable arch will not develop over the throat, and there is a larger diameter above which a stable arch will consistently develop. Due to random nature of the particle simulation, there was an intermediate range of particle diameters for which a stable arch may or may not develop, suggesting that stability was not described by a simple stable/not stable mechanism. A statistical approach using logistic regression was used to develop a relation for the unstable to stable transition. It was determined that the mean particle size for a 95% probability of stability was independent of funnel angle, and was about 0.47 times the sinkhole throat diameter. This compares favorably with the empirical value of 0.5 recommended in the literature for stabilizing sinkholes with graded rock fills.
(3)   It is shown the transition in mean particle size from a stable to an unstable assembly of particles is a continuous smooth function rather than a step function from both 2D and 3D analysis.

Chapter 4 "Discrete element simulation of particle-fluid interaction using a software coupling approach":
(1)   The basic finite volume discretization for solving the averaged Navier-Stokes equations with variable porosity terms included is derived using the PISO (Pressure-Implicit with Splitting of Operators) algorithm (reference), following this approach:
  • The transient solver for incompressible laminar Newtonian fluid in the open source code OpenFOAM was extended to a customized solver considering the porosity and the fluid-particle interaction term.
  • A framework of code coupling with YADE and OpenFOAM is then provided.
(2)   A customized YADE routine FluidDragForceEngine is written to wrap the customized fluid solver and incorporate it into the YADE main mechanical loop. Particle information from the discrete element code and fluid-particle interaction terms from the fluid solver communicate using dynamically linked library technique under the Linux platform. Such a coupling method also provides a hint for incorporating other types of open source code and extends the field of DEM application.
Chapter 5 "Coupled Discrete Element and Finite Volume Solution of Two Classical Soil Mechanics Problems" is a paper under review in Computers and Geotechnics as:

Feng Chen, Eric. C. Drumm, Georges Guiochon, Coupled Discrete Element and Finite Volume Solution of Two Classical Soil Mechanics Problems, 2008, Submitted for Computers and Geotechnics

(1)   The coupled open source codes have been used and the solution process verified through the solution of two simple classical soil mechanics problems: one dimensional idealizations of the classic upward seepage flow/quick condition problem and the time rate of consolidation settlement problem. It is shown that the coupled DEM solution can produce results very similar to the well known analytical solutions for both problems. The results for both problems were obtained without the assumption of Darcy's law, but are based on the basic Navier-Stokes equation for the fluid phase and on the particle motion equation for the solid phase.
(2)   In the case of the upward seepage flow problem, the numerical solution also yields results for the transient pore water pressure distribution at early stages of the solution, and produces the displacement of the uppermost particle in the column under quick conditions. The results were shown to agree well with those from the analytical solution and two other DEM solutions.
(3)   For the consolidation problem, the solutions for pressure and particle displacement were provided with a range of consolidation times that are typically of interest in practice.
(4)   Although of little practical interest, the DEM was also shown to be able to simulate the development of the excess pore water pressure distribution at very early solution times, where the classical solution would assume a uniform pore pressure throughout the domain equal to the applied stress P0.
(5)   In addition to the solution of the two classical verification problems, two key issues in the numerical solution of coupled fluid/solid systems were discussed: the dependence on time step size for both the fluid and mechanical solution processes and the choice of viscous damping coefficients. The effects of these parameters on the solution was investigated, and while these effects are expected to be problem dependent, the paper provides some insight into how sensitive the results may be to the choice of these parameters.
Chapter 6 "Coupled Discrete Element and Finite Volume Solution for 2D Fluid Flow in Soil Mechanics" is a future paper manuscript:
Feng Chen, Eric. C. Drumm, Georges Guiochon, (2009) "Coupled Discrete Element and Finite Volume Solution for 2D Fluid Flow in Soil Mechanics" to be submitted for "International Journal of Geomechanics", ASCE
(1)   A coupled DEM-CFD model is created for the fluid flow under sheet pile similar to Lambe and Whitman's classical problem.
(2)   An equal pressure gradient scaling law is used to limit the number of particles in the simulation yet reproducing the desired problem behavior. The use of large scale particles is important if practical scale problems are to be solved in the absence of parallel computation environmental.
(3)   The calculated pressure contours and quantity of flow from the model agree well with the classical solution from flow net. The finite volume method is able to present the transient pressure development during the early stages of the simulation. The particle movements and contact forces when the exit gradient approaches the critical condition is also discussed. By taking the advantage of DEM, the model is also able to simulate the particle migration and the loss of contact forces between particles as the critical gradient is reached, which is not easy to

obtain through traditional continuum approach and can be a starting point for future coupled flow modeling.

Chapter 7 "Coupled Discrete Element and Finite Volume Solution for Packing of a Chromatography Column" is a future paper manuscript:

Feng Chen, Eric. C. Drumm, Georges Guiochon, (2009), "Coupled Discrete Element and Finite Volume Solution for Packing of a Chromatography Column" to be submitted for "Journal of Chromatography A".

(1)   The coupled DEM-CFD method is used to simulate the slurry packing of a chromatography column. The geometry was significantly simplified to conserve computational effort. The particle diameter was assumed to be approximately 100 times that typically used for silica packing material, and the cylindrical shape was approximated by planar flow. The coupled method is able to produce the "wall effects" due to shearing in the packing under the axial upward compression procedure, providing a displacement field similar to that observed in experiments. These wall effects lead to a heterogeneous column packing and lower column efficiency.

(2)   Although the experimentally observed parabolic shaped velocity distribution was not repeated, the packing of a very heterogeneous column was simulated in spite of what is likely an insufficient number of the particles in the column. This relationship is expected to be different if a larger number of particles within the fluid cell were used (at least 1000 particles per fluid cell) which would likely need to be performed under a parallel computational environment.

2 Prediction/Verification of particle motion in one dimension with the discrete element method

The discrete (or distinct) element method (DEM) is a family of numerical methods for predicting the motion of a large number of particles like molecules or particles of soil (Jensen et al. 2001; Williams et al. 1985; Yao and Anandarajah 2003). Various DEM codes are available, although it has been suggested (Richards et al. 2004) that the basic underpinnings of these codes are similar and follow the early work of Cundall and Strack (1979). While the codes may be fundamentally the same, different implementations may provide slightly different results due to subtle difference in the manner in which the method is implemented. Regardless of the code chosen, good practice would suggest that before investigating practical problems involving thousands of particles, the DEM analyst should verify the solution process through the investigation of simple problems for which an analytical solution is known. However, most of the example problems available in the literature or provided by code developers lack closed form solutions.

This section investigates some simple 1-D vibration problems which can serve as verification problems, and compares the solution from the DEM with that from the analytical solution. It is demonstrated that identical results can be obtained from the open source 3-D code YADE (Galizzi and Kozicki 2005) and the well known commercial 2-D code PFC2D (Itasca Inc. 2004a). However, due to subtle differences in the two implementations, in order to get the desired results to the closed form verification problems, an understanding is required of the difference in how solution timesteps are used, material contact stiffness is specified and damping is controlled. These issues are discussed in the paper, and an appendix provides details on some differences in the PFC2D and YADE implementations.

The DEM method was originally applied by Cundall and Strack (1979) to problems in rock mechanics. For the solution of vibration systems, the theoretical basis of the method can be viewed as an extension of finite difference method (Thomson 1993). The DEM method assumes that the particles are rigid, but inter-particle deformation is approximated by overlapping between particles using a simple force displacement law. Single rigid particle motion is predicted by Newton's second law of motion.

The discrete element can be of various shapes, such as disk, tetrahedron or polyhedron, etc. However this paper will only focus on spherical particle motion which is restricted to one dimension and translational motion only. The translational motion of the particle is described in terms of its position y, velocity $\dot{y}$, and acceleration $\ddot{y}$ of the sphere center. The concept of one dimensional motion described in this paper can be easily extended to two or three dimension problems in multiple degrees of freedom with generalized position, velocity and acceleration including rotational motion.
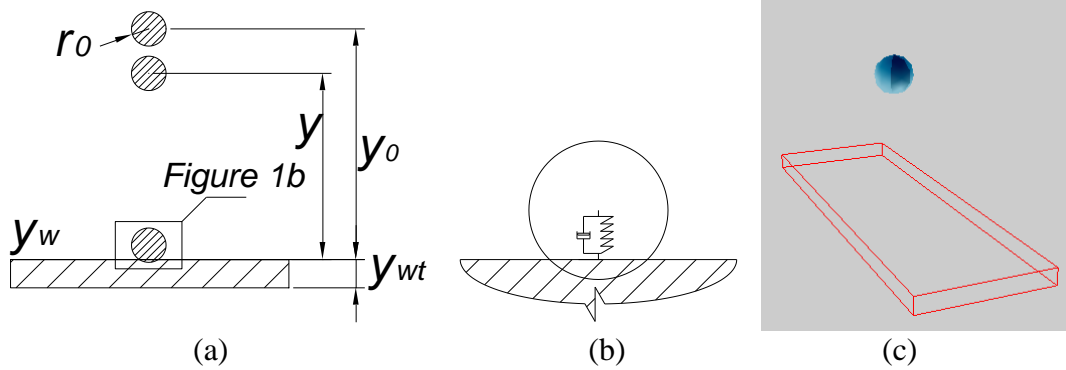
Figure 2.1 First verification problem: Free fall of a single particle. (a) schematic of single particle in free fall; (b) particle boundary contact model; and (c) the single particle free fall model in YADE.

Computational requirements in DEM simulations of practical problems with large numbers of particles are inevitably demanding. The method requires efficient algorithms to track the positions, velocities and directions of large numbers of particles, to detect the particle pair that will create the next collision and to calculate the collision behavior. The algorithms employed in DEM codes may differ less than one might expect, since many codes have developed from a limited number of original sources. For example, most codes likely follow the original concept and the code developed by Cundall that now underpins the PFC2D/3D code (Itasca Inc. 2004a). Although there are similar solutions in literature in which various code developers implement the method, difference in the codes make the solution and comparison of results for basic linear elastic verification problems difficult. This is not the case in the finite element method (FEM), for example, for a simple linear elastic problem; every FEM program should yield the same result. However, for the discrete element method, even the simplest problem can yield slightly different results due to different calculation procedures. This paper will focus on the basic parameter input and solution by DEM using an open source code YADE, (Galizzi and Kozicki 2005) and the commercial code PFC2D (Itasca Inc. 2004a).

2.1 A description of particle system parameters

In this section we will clarify the geometry and physical parameters of the spherical particle systems used in this paper.

2.1.1 Geometry Parameters

As shown in Figure 2.1, the geometry parameters of a single spherical particle in 1D space can be defined using the particle radius r_0 and the particle center position y. The static wall or system boundary can be defined using its position y_w and thickness y_{wt}.

2.1.2 Physical Parameters

The macroscopic elastic properties, including density, Young's modulus E_{ab}, and Poisson's ratio v, are considered to be the input parameters for the discrete-element model. Young's modulus and Poisson's ratio can be converted to the normal and shear stiffness constants K_n and K_s,

respectively, used in the calculation process via the "macro–micro" relationship provided by Hentz et al. (2004):

$$K_n = \frac{E_{ab}\tilde{A}_{\text{int}}}{D_{eq}^{ab}}\left[\frac{1+\alpha_k}{\beta_k\ (1+\nu)\ +\gamma_k\ (1-\alpha_k)}\right] \qquad (2.1)$$

$$K_s = K_n\left(\frac{1-\alpha_k\nu}{1+\nu}\right) \qquad (2.2)$$

where:

$$\tilde{A}_{\text{int}} = \pi\ \min\ (r_a, r_b)^2$$

$$D_{eq}^{ab} = r_a + r_b$$

$$E_{ab} = \frac{E_a E_b}{E_a + E_b}$$

where E_a and E_b=Young's moduli of the two contacting objects of radius r_a and r_b, and α_k, β_k, and γ_k=fitting parameters (Hentz et al. 2004). YADE uses default values of α_k=2.65, β_k =0.65, and γ_k=1.0 which were used for the particle systems here. Note that when a contact forms, it is assumed that the two contacting objects will act in series, and therefore the normal contact stiffness will be calculated using:

$$K_n = \frac{K_{n,a}K_{n,b}}{K_{n,a} + K_{n,b}} \qquad (2.3)$$

where the subscripts a and b refer to the two contact objects (either particle or boundary). The previous geometry and physical parameters are considered to be the basic parameters for the problem; other parameters including particle mass ($m=\rho g$) can be derived from the basic parameters. For the 1D problems investigated here, there is no shear stiffness term K_s, and the system stiffness, $k=K_n$.

2.2 First Verification Problem: Free Fall and Contact of a Single Particle

This single degree-of-freedom system will be investigated without damping, and with the two types of damping most common in the DEM: Viscous damping and local or nonviscous damping (Cundall 1987).

2.2.1 Undamped Free Fall of a Single Particle

The problem will start with the single particle free fall under gravity from its initial position y_0 as shown in Figure 2.1 which will contact a static (fixed) wall and then rebound after the contact. When the particle boundary reaches the static wall, the contact procedure is considered purely elastic and no energy loss occurs during the contact. The calculation will begin at time $t=0$ and end when the particle returns to its initial position for the first time.

2.2.1.1 Free-Fall Stage

The particle motion for the free-fall stage is easily obtained via

$$\ddot{y} = g$$

$$\dot{y} = \int \ddot{y}dt = gt$$

(2.4)

$$y = \int \dot{y}dt = \frac{1}{2}gt^2$$

2.2.1.2 Contact Stage

The end of the free fall stage will be at the time the particle boundary reaches the static wall boundary at which time the contact stage begins. The contact with the static wall can be regarded as a vibration problem of a single mass-spring system with initial velocity, $v_0 = \sqrt{2gh_0} = \sqrt{2g\ y_0 - r_0}$ and the spring stiffness is obtained via Eq. (2.3). Therefore, from the theory of vibration, the following differential equation can be obtained:

$$\ddot{y} + \left[g - \frac{k_c}{m}\ r_0 - y\ \right] = 0$$

(2.5)

With the initial boundary condition:

$$\dot{y}\big|_{t=0} = v_0, \ y\big|_{t=0} = r_0$$

(2.6)

The solution is a portion of the classical harmonic motion in one period provided in Appendix 2.A.

2.2.1.3 Rebound Stage

The rebound stage, in the absence of damping, is the opposite of the free fall stage where the motion equations can be expressed as

$$\ddot{y} = g$$

(2.7)

$$\dot{y} = v_0 + \int \ddot{y}dt = v_0 + gt$$

(2.8)

$$y = r_0 + \int \dot{y}dt = r_0 + v_0 t + \frac{1}{2}gt^2$$

(2.9)

2.2.2 Free Fall of a Single Particle under Viscous Damping

General viscous damping (Bishop and D. C. Johnson 1960) can be applied to the single-particle system presented earlier, where the magnitude of the damping force is linearly proportional to the velocity with the direction opposite to the particle velocity, and can be expressed as

$$F_{d\_viscous} = -c\dot{y}$$

(2.10)

11

where the coefficient c=viscous damping constant. In many discrete-element formulations (Itasca 2004) for the contact model, c is indirectly defined through the viscous damping coefficient β (Ginsberg and Genin 1984):

$$c = \beta c_{critical} \tag{2.11}$$

The critical damping constant c is given by:

$$c_{critical} = 2\sqrt{\bar{m}k} \tag{2.12}$$

where k=contact stiffness and $\bar{m}$ =equivalent mass of the contacting objects. In the case of particle-boundary contact, $\bar{m}$ is taken as the particle mass, whereas in the case of particle–particle contact, $\bar{m}$ is taken as the equivalent mass of the two particles which can be taken as (Itasca Inc. 2004a).

$$\bar{m} = \frac{m_1 m_2}{m_1 + m_2} \tag{2.13}$$

Viscous damping is characterized by the critical damping ratio β. When β=1, the system is said to be critically damped, meaning that the response decays to zero at the most rapid rate. Also, β=1 represents the transition from an oscillatory response, when β<1, to an exponentially decaying response when β>1. When β<1, the system is said to be under-damped, or lightly damped, and when β>1, the system is said to be over-damped, or heavily damped.

Note that viscous damping exists only during the particle contact and therefore during the free drop and rebound stage, the damping effect does not exist (Itasca Inc. 2004a). The dashpot acts in parallel with the contact stiffness as shown in Figure 2.1(b).

In this subsection we will describe the analytical solution for one calculation cycle with viscous damping during the contact stage.

2.2.2.1 Free-Drop Stage

The free-drop stage is exactly the same as the undamped case from Eq. (2.4).

2.2.2.2 Contact Stage

The contact stage can be described by the differential equation in the following form:

$$\ddot{y} - \left[k \left(r_0 - y \right) + mg - c\dot{y} \right] = 0 \tag{2.14}$$

where c=damping proportion constant. The initial boundary condition for the contact stage is defined as

$$\dot{y}\big|_{t=0} = v_0, \ y\big|_{t=0} = r_0 \tag{2.15}$$

The solution for the above-mentioned differential equation in the contact stage is provided in Appendix 2.A.

2.2.2.3 Rebound Stage

The rebound stage is the opposite procedure of the free fall with initial velocity at the end of the contact stage:
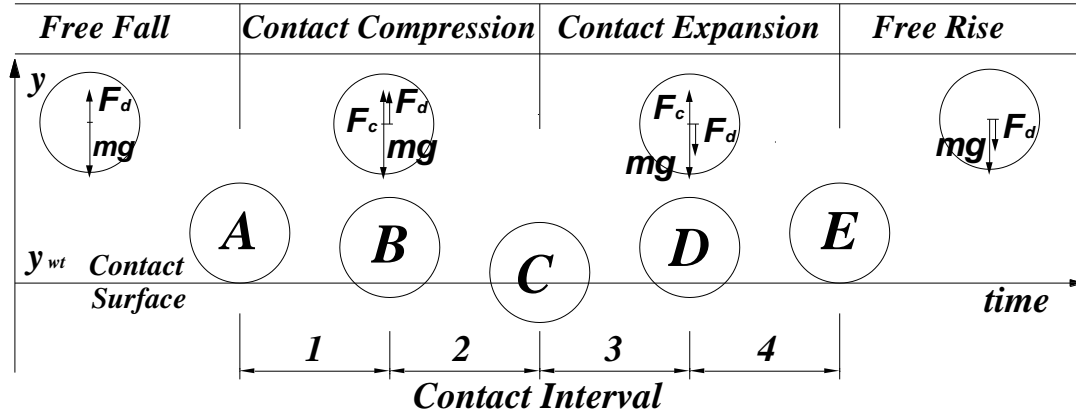
Figure 2.2 Vertical position of particle center versus time for during various contact intervals: local (non-viscous) damping model

$$v_0 = \dot{y}_c \tag{2.16}$$

2.2.3 Free Fall of a Single Particle under Local Damping

Local damping or nonviscous damping (Cundall 1987) is frequency independent damping similar to the hysteretic damping model and can be expressed as:

$$F_{d\_local} = -\alpha \left| F_{unbal} \right| \mathrm{sgn}\ \dot{y} \tag{2.17}$$

Where α is the local damping constant; F_{unbal} is the composite force, which is defined as the vector sum of all applied forces on a single object (either particle or boundary) excluding the damping force; the term sgn $\dot{y}$ is defined as +1, 0, or -1, according to the value of $\dot{y}$ as positive, zero, or negative, respectively. In a one-dimensional problem, the vector sum (composite force) can be considered as the scalar sum of all applied forces.

Note that only accelerating motion is damped and the damping constant α is non-dimensional. The local damping force is scaled to the resultant composite force (unbalanced force) and always opposes the motion.

Local damping is used to simulate energy loss due to particle interaction (Itasca Inc. 2004a), and may not be appropriate for a typical single particle contact problem. However, it is applied to the single particle problem here as verification. With local damping, the free fall motion is also damped as if the particle was falling through a viscous liquid.

2.2.3.1 The free fall stage with local damping

The damped single particle free fall using the local damping mechanism can be expressed as:

$$\ddot{y} = g\ 1-\alpha \tag{2.18}$$

$$\dot{y} = \int \ddot{y} dt = g\ 1-\alpha\ t \tag{2.19}$$

$$y = \int \dot{y} dt = \frac{1}{2} g \left(1 - \alpha \right) t^2 \tag{2.20}$$

2.2.3.2 Contact Stage

The contact stage using local damping uses the absolute value for the resultant unbalanced force. Therefore, the sign of the damping force will change according to the particle position which can be described in terms of four time intervals as depicted in Figure 2.2. The differential equation for the contact stage is best described in terms of four intervals during the contact:

Contact Interval 1: From the Initial Contact A, to the Equilibrium Position B (Figure 2.2): In this interval the gravitational force is larger than the contact force (spring force) in which $F_{contact} < mg$, and the damping force is opposite to the velocity with the magnitude:

$$\left| F_d \right| = mg - F_{contact} = mg - k \left(r_0 - y \right) \tag{2.21}$$

The differential equation can be expressed as:

$$\ddot{y} - \left[k \left(r_0 - y \right) + mg \right] \frac{1-\alpha}{m} = 0 \tag{2.22}$$

With the initial boundary condition:

$$\dot{y} \big|_{t=0} = \sqrt{2g \left(y_0 - r_0 \right) \left(1 - \alpha \right)}, \quad y \big|_{t=0} = r_0 \tag{2.23}$$

The solution is provided in Appendix 2.A under "Closed-Form Solution for the Single Ball Problem during Contact with Local Damping."

The elapsed time corresponding to the equilibrium position y_B can be obtained by solving the previous equation with:

$$\ddot{y} = 0 \tag{2.24}$$

The position at the equilibrium position y_B, which is an inflection point on the trajectory in the (y, t) space, where the contact force equals the gravitational force is

$$y_B = r_0 - \frac{mg}{k} \tag{2.25}$$

Contact Interval 2: From the Equilibrium Position B, to the Maximum Deformation Position C (Figure 2.2): In this stage $F_{contact} < mg$ and the magnitude of the damping force:

$$\left| F_d \right| = F_{contact} - mg = k \left(r_0 - y \right) - mg \tag{2.26}$$

The damping force acts in the direction opposite to the velocity, and the differential equation can be expressed as:

$$\ddot{y} - \left[k \left(r_0 - y \right) + mg \right] \frac{1+\alpha}{m} = 0 \tag{2.27}$$

With the boundary condition:

14

$$\dot{y}=v_B, y\big|_{t=0}=y_B \tag{2.28}$$

The time corresponding to the maximum deformation position can be obtained by solving:
$$\dot{y}=0 \tag{2.29}$$

Contact Interval 3: From the Maximum Deformation Position C, to the Equilibrium Position D (Figure 2.2): In this interval the gravitational force is smaller than the contact force with $F_{contact}>mg$, the magnitude of the damping force is the same as in Stage 2, whereas the direction of the damping force is opposite to the contact force and therefore the differential equation can be obtained as

$$\ddot{y}-\left[k\left(r_0-y\right)+mg\right]\frac{1-\alpha}{m}=0 \tag{2.30}$$

with the initial boundary condition:
$$\dot{y}=0, y\big|_{t=0}=y_C \tag{2.31}$$

Similarly, the elapsed time from the maximum deformation position to the equilibrium point D, which is the second inflection point on the trajectory in the (*y, t*) space, can be obtained by solving:
$$y=y_D \tag{2.32}$$

Contact Interval 4: From the Equilibrium Position D, to the End of the Contact E (Figure 2.2): The final stage of the contact is described by the similar differential equation as in Stage 1, but the damping force will change sign. The magnitude of the damping force is:
$$\left|F_d\right|=mg-F_{contact}=mg-k\left(r_0-y\right) \tag{2.33}$$

The differential equation for Interval 4 can be expressed as:
$$\ddot{y}-\left[k\left(r_0-y\right)+mg\right]\frac{1+\alpha}{m}=0 \tag{2.34}$$

with the initial boundary condition:
$$\dot{y}=\dot{y}_D, y\big|_{t=0}=y_B \tag{2.35}$$

2.2.3.3 Rebound Stage
The rebound stage with the local damping effect is slightly different from the free fall stage as the damping force will change sign, and therefore the equation of motion can be expressed as:
$$\ddot{y}=\left(1+\alpha\right)g \tag{2.36}$$

$$\dot{y}=\dot{y}_E+\left(1+\alpha\right)gt \tag{2.37}$$

$$y = r_0 + \int \dot{y}dt = r_0 + \dot{y}_E t + \frac{1}{2}g \left(1+\alpha\right)t^2 \tag{2.38}$$

The previous analytical solution can also be defined as one calculation cycle for a single falling particle and the next calculation cycle will repeat from Stage 1 to Stage 4 (Figure 2.2), but with a change in the initial boundary condition to reflect the conditions at the end of Stage 4 in the previous calculation cycle.

2.3 Calculation Procedure in the Discrete-Element Method

This section describes the preliminary procedure for the discrete element method in one dimension. As noted in the introduction, the DEM uses the law of motion and the law of force–displacement in its finite difference calculation. The basic steps of the DEM can be summarized as follows.

1. Calculate the basic geometry and physical properties of the particles;
2. Determine the time step for the current iteration;
3. For each time step:
   - Calculate the contact force between the particles using the geometry parameters of the particles, add the force vector to the unbalanced force vector, based on the force–displacement law;
   - Calculate the body force of each particles, for the case described in this paper, the gravitational force is then added to the unbalanced force vector;
   - Apply the damping effect (force) to the resultant unbalanced force;
   - Use the resultant unbalanced force in the previous step to calculate the acceleration for each particle, which by Newton's second law of motion:

$$\ddot{y}_{i,t} = \frac{F_{unbal,i,t}}{m_{i,t}} \tag{2.39}$$

   - Perform the time integration to obtain the velocity and position for each time step. The open source code YADE uses the leap-frog scheme (Hockney 1970) for time integration from acceleration to velocity and position.

4. Return to Step 2 if variable time steps are employed or Step 3 for fixed time steps.

As in most numerical approximation schemes, the selection of time step size is very important in the discrete-element calculation, as an excessively large time step will lead to numerical instability, whereas too small a time step will make the finite difference calculation computationally intensive. Cook et al. (Cook et al. 2001) suggested that the critical (maximum allowed) timestep $t_{critical}$ for a single mass–spring system with no rotational stiffness is:

$$t_{critical} = 2\sqrt{\frac{m}{k_{trans}}} \tag{2.40}$$

where k_{trans}=contact stiffness for translational motion in single degree-of-freedom system and m=mass of the single particle. Additional discussion of the time step considering the infinite series of point masses and springs in the DEM is provided by Itasca (2004a):

$$t_{critical} = \sqrt{\frac{m}{k_{trans}}}$$

$\qquad\qquad\qquad\qquad\qquad\qquad\qquad\qquad$ **(2.41)**

In any case, the time step must be made short enough to provide adequate precision for the response history. Accuracy of any finite difference method is improved by reducing the length of the time step which will in turn minimize the amplification of errors from one step to subsequent time steps. However, as computational effort is a concern in the DEM solution of practical problems, variable time step algorithms are used. From Eq. (2.3) or (2.40), as the stiffness decreases (as is the case of the particle–particle or particle–boundary contact) the allowable time step size increases. For this reason, solution schemes with variable time steps are often used.

2.4 Comparison between the Analytical Solution and the DEM for Single Degree-of-Freedom System

A comparison of the analytical solution using the theory of vibration and the numerical solution using the discrete-element method is presented in this section.

(a)

17
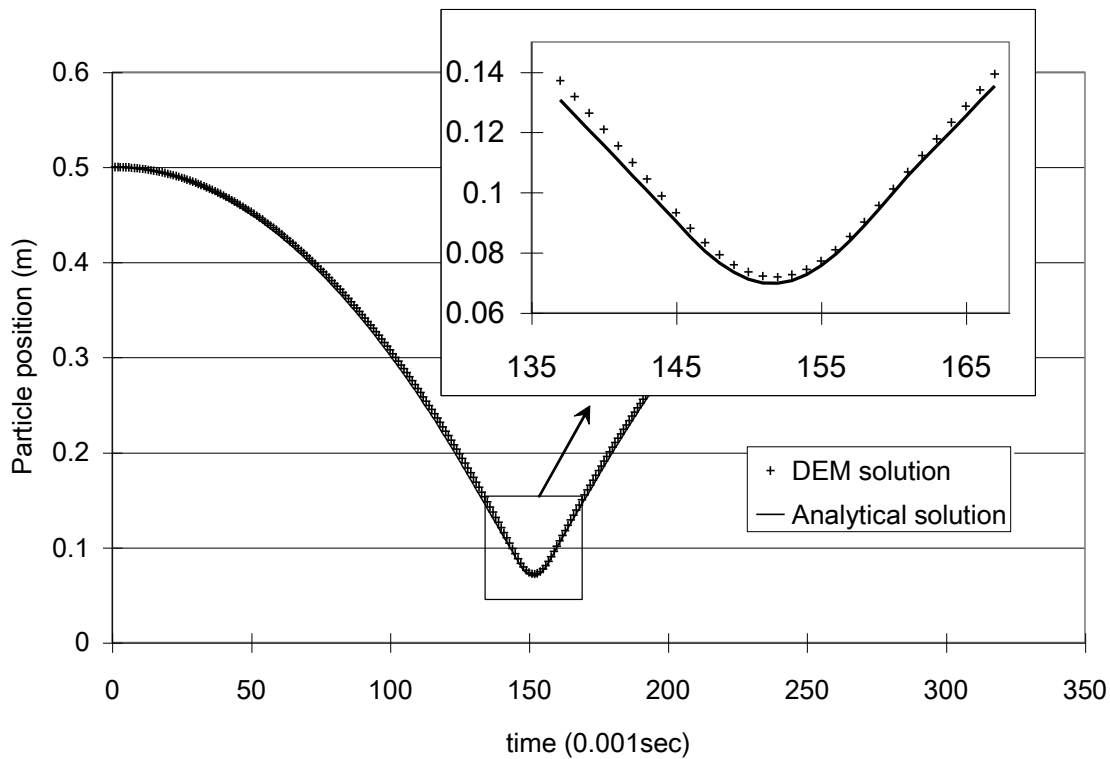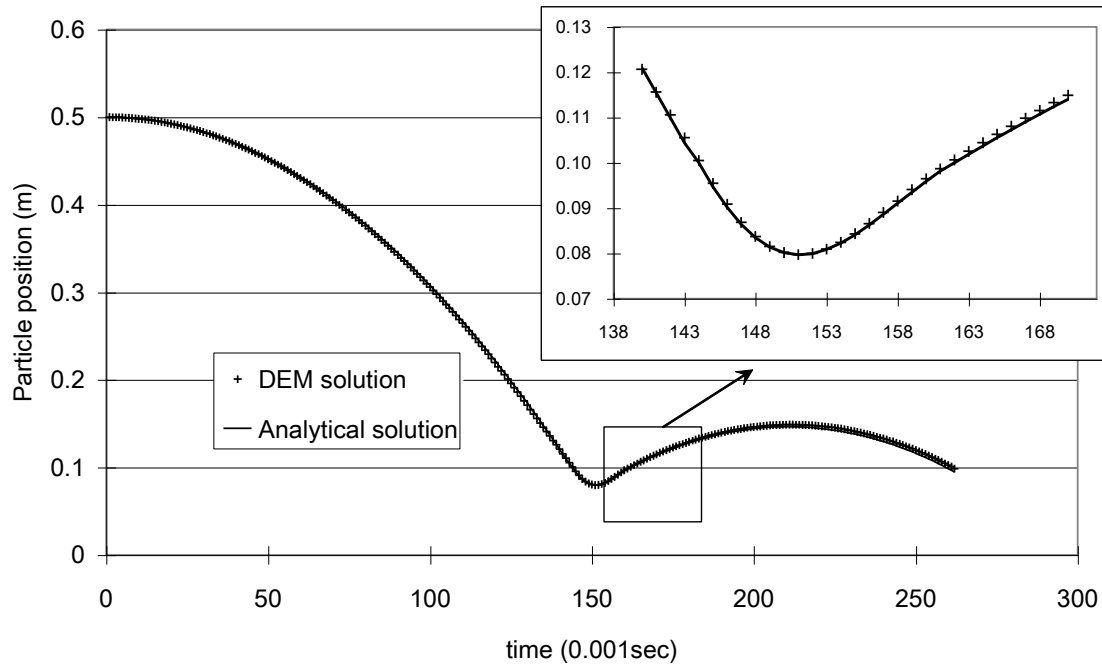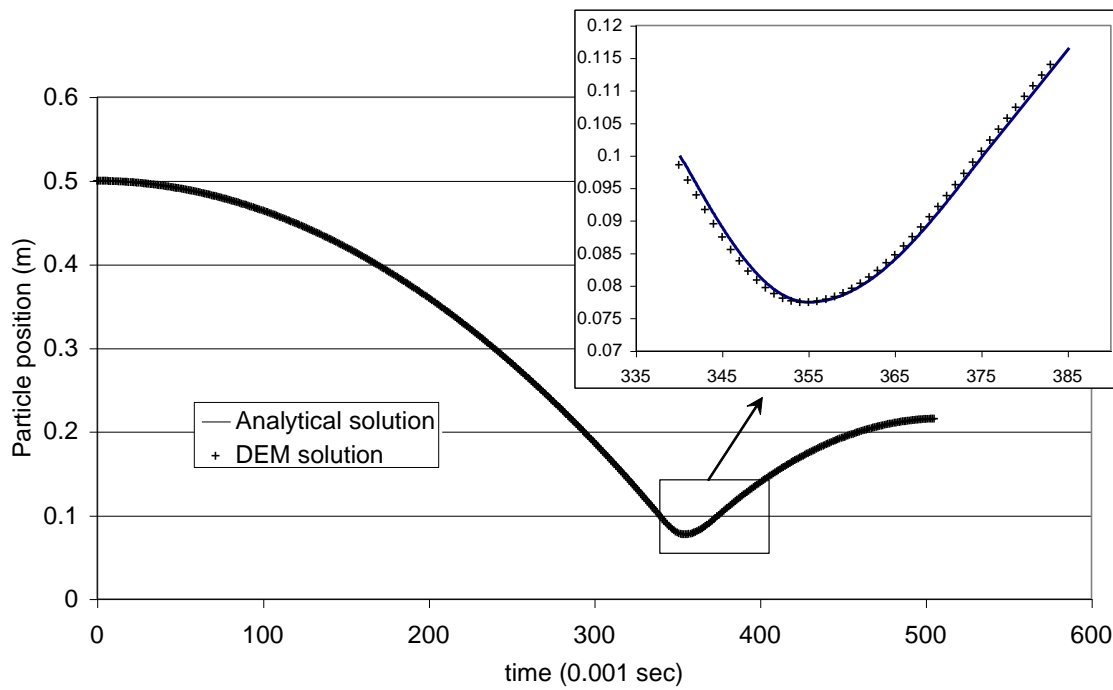
Figure 2.3 Comparison between analytical and discrete-element solution of one particle free fall with (a) no damping effect; (b) viscous damping effect β=0.3; and (c) local damping effect α=0.3

18

Table 2.1 Basic Particle Parameters for First and Second Verification Problems

Parameter	Value	Unit
Particle radius	0.1	m
Particle density (Particle 1)	2,600	kg/m^3
Particle density (Particle 2)	5,200	kg/m^3
Particle Young's modulus	1.6916	MPa
Particle Poisson's ratio	0	
Boundary Young's modulus	5.0748	MPa
Boundary Poisson's ratio	0	
Gravity field	-9.81	m/s^2

The input parameters for Verification Problem 1 are listed in Table 2.1. Note that the values of Young's modulus and Poisson's ratio in this example were chosen such that the particle–particle contact stiffness and the particle-boundary stiffness were equal.

Three comparisons are made for the particle free fall:

1. Without damping Figure 2.3(a);
2. With viscous damping, with the viscous damping coefficient β=0.3 Figure 2.3(b);
3. With local damping, with the local damping coefficient α=0.3 Figure 2.3(c).

The time step chosen for the discrete-element solution is $t=1.0\times10^{-3}$s, which is less than 1/3 of the time step determined from Eq. (2.41) where $t_{critical}=3.33\times10^{-3}$s. A comparison of the particle position versus time for the analytical and DEM solutions is shown in Figure 2.3 for the three damping cases. Note that with viscous damping Figure 2.3(b), the free fall motion is the same as in the solution without damping Figure 2.3(a), but that local damping Figure 2.3(c) reduces the time to rebound. The very small difference between the DEM results and analytical results are shown in the insets of Figure 2.3(a)–(c). As the time step is reduced the two solutions will converge. The results attributed to the DEM shown in Figure 2.3 were obtained with both the commercial code PFC2D and the open source code YADE. The results from the two codes are not distinguished because the results from the two codes agree to 11 significant digits. However, due to differences in the manner in which the DEM is implemented in the two codes, this degree of agreement exists only because the YADE solution in the first time step was manipulated to produce the results obtained from PFC2D. Appendix 2.C provides details about the differences in the two implementations, and how YADE was manipulated. It is suggested that this appendix provides insight into the PFC2D time step implementation, supplements the PFC2D user guide, and may be of interest to the users of that code.
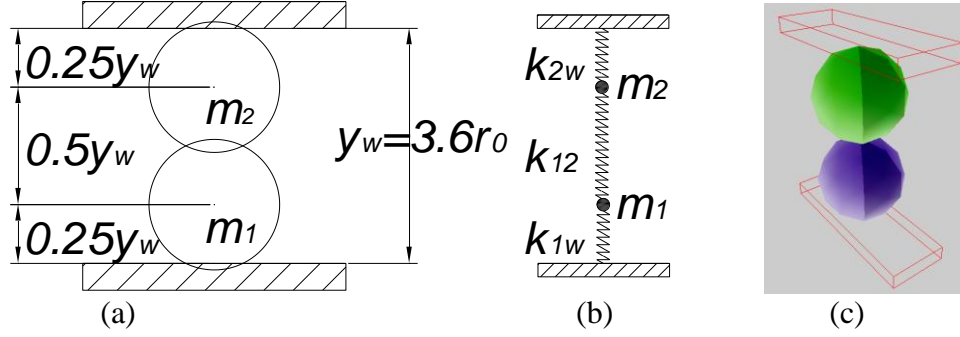
Figure 2.4 Second verification problem: compressed two-particle system. (a) Schematic of stacked two particles; (b) simplified spring contact model; and (c) the stacked two-particle model in YADE.

2.5 Second Verification Problem: Stacked Two-Particle System Compressed between Two Boundaries

The two degree-of-freedom system, as shown in Figure 2.4, can also be solved through analytical solution using a similar procedure as for the single degree-of-freedom systems. However, the expressions of such solutions can be very complicated unless the boundaries are positioned such that the two particles remain in contact at all times (do not separate), which is the case investigated here. The idealized 1D model can then be depicted as a pair of mass–spring systems. In this section we will give the displacement history of the two degree-of-freedom system for the undamped case, the viscous damping case, and the local damping case. The analytical solution for the two ball contact problem is provided in Appendix 2.B.

A system of two stacked particles, both with r_0=0.1m but of different density, is placed between two static walls or boundaries as shown in Figure 2.4. The lower and upper layer boundaries are placed at y_{w1}=0 and y_{w2}=3.6r_0, and the initial position of the two particles $y_1|_{t=0}$=0.25y_{w2}, $y_2|_{t=0}$=0.75y_{w2} such that the balls are initially compressed. The initial geometry of the two particles is such that during particle movement, the particles and the walls remain in contact at all times, i.e., the contact spring will always be in compression, making the problem comparable to a two degree-of-freedom vibration problem in one dimension. The physical parameters of the particles and the static walls are the same as in the single-particle system investigated previously, except that the lower particle has twice the density as the upper particle. This results in the more general problem with two balls of differing mass. This produces an equivalent mass (Eq. (2.13)):

$$m_{12} = \frac{m_1 m_2}{m_1 + m_2} = \frac{2m \cdot m}{2m + m} = \frac{2}{3} m$$

Similar to the response of the previous 1D problems, once released the two particles will start to vibrate, and if no damping is applied the vibration will continue, whereas if damping is applied, the response will decay to the equilibrium position.

20

(a)

(b)

21
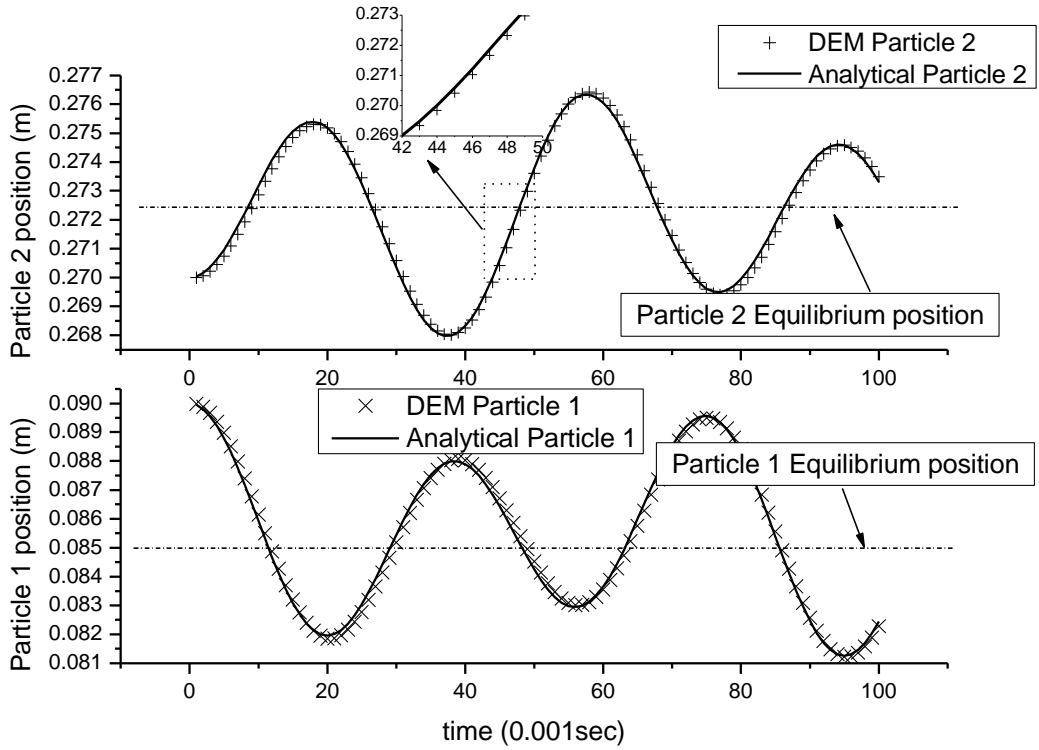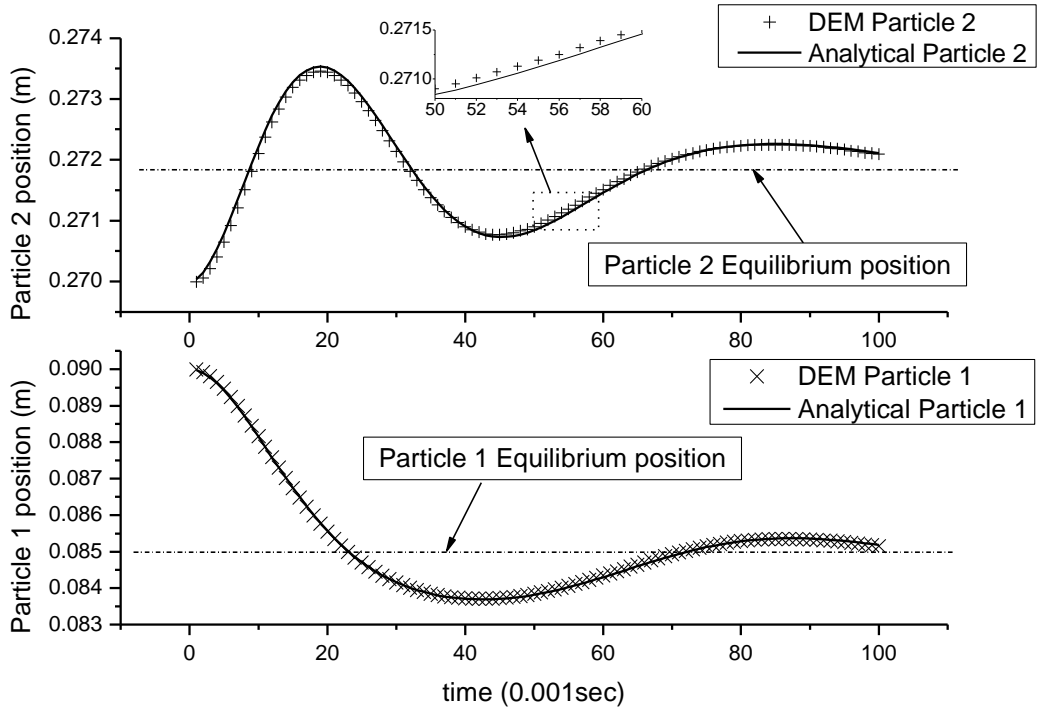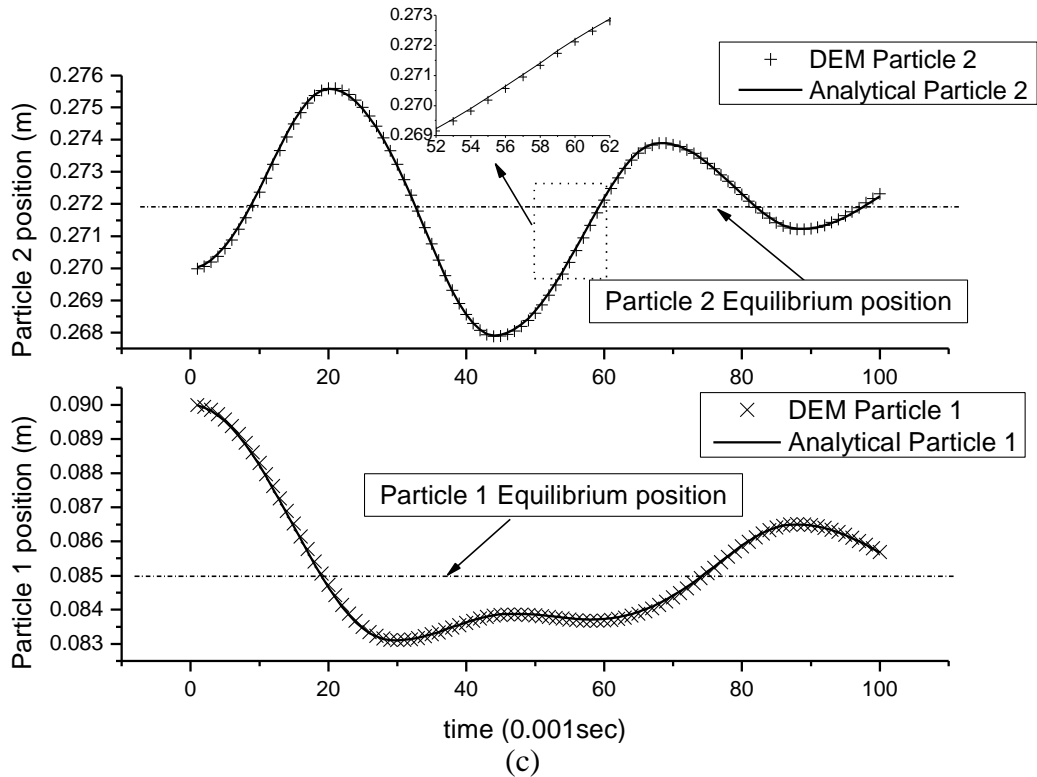
Figure 2.5 Position history for stacked two particles with (a) no damping effect; (b) viscous damping effect β=0.3; and (c) local damping effect α=0.3

The three cases of damping investigated previously are compared. The early position history for the two particles versus time is as shown in Figure 2.5(a) without damping, in Figure 2.5(b) with viscous damping β=0.3, and in Figure 2.5(c) with local damping α =0.3. From Figure 2.5(b) and (c), it is evident that the two particles are approaching their equilibrium positions. The DEM solution is shown to agree well with the classical solution.

2.6 Closure

The discrete-element method is a powerful tool for investigating the response of assemblies of particles. To gain an understanding of the solution process, and assure that the results are interpreted properly, it is often useful to solve simple verification problems. This is particularly true in view of the nature of code documentation which cannot anticipate all users' questions. Simple one and two-particle contact vibration problems were investigated with the DEM, including cases of no damping, viscous damping, and internal damping, the latter being the form of damping commonly found in DEM codes. As anticipated, it was found that the results from a well known commercial 2D code (PFC2D) and the open source 3D code (YADE) yield excellent solutions to these problems. Slight differences between the two DEM solutions were observed, and although these differences were minor and not likely to be important in most problems, the basis of these differences was explored. It was found that a high level of agreement between the results of the two codes was obtained when the YADE solution was manipulated in the first time step to change the calculated velocity and omit the effects of damping. It is suggested that the

solution of simple problems is good practice when using numerical codes developed by others, and a means to answer questions that are not addressed in typical code documentation.

Appendix

Appendix 2.A Analytical Solutions for the Single-Particle System in the First Verification Problem

2.A.1 *Closed-Form Solution for the Single Ball Problem during Contact without Damping*

The closed-form solution for Eq. (2.5) with the initial boundary condition in Eq. (2.6) is listed as:

$$y\ t\ = -\sqrt{2g\ y_0 - r_0}\ \sqrt{\frac{m}{k}}\sin\left(\sqrt{\frac{k}{m}}t\right) + \frac{mg}{k}\cos\left(\sqrt{\frac{k}{m}}t\right) + \left(r_0 - \frac{mg}{k}\right) \qquad (2.42)$$

The contact time can be obtained by solving the following equation:

$$y\ t\ = r_0 \qquad (2.43)$$

And therefore the contact time is:

$$t_{contact} = \sqrt{\frac{m}{k}}\arctan\left(\frac{\sqrt{2kmg\ y_0 - r_0}}{2k\ y_0 - r_0\ - mg}, -\frac{2k\ y_0 - r_0\ + mg}{2k\ y_0 - r_0\ - mg}\right) \qquad (2.44)$$

2.A.2 *Closed-Form Solution for the Single Ball Problem during Contact with Viscous Damping*

Closed-form solution for Eq. (2.15) is provided as follows:

$$y = -\frac{1}{2}\frac{\exp\left(-\frac{c - \sqrt{c^2 - 4km}\ t}{2m}\right) m\ \sqrt{c^2 - 4km}\ -gc - 2k\sqrt{2gh_0}\ - gc^2 + 4mgk}{k\ 4km - c^2}$$

$$-\frac{1}{2}\frac{\exp\left(-\frac{c + \sqrt{c^2 - 4km}\ t}{2m}\right) m\ \sqrt{c^2 - 4km}\ gc + 2k\sqrt{2gh_0}\ - gc^2 + 4mgk}{k\ 4km - c^2} \qquad (2.45)$$

$$+\left(r_0 + \frac{mg}{k}\right)$$

Closed-Form Solution for the Single Ball Problem during Contact with Local Damping
The closed-form solution for Eq. (2.22) during Contact Interval 1, the initial contact to the equilibrium position (A-B) in Figure 2.2, with the initial condition provided in Eq. (2.23):

$$y = -\frac{1}{2}\,\frac{\exp\left(\sqrt{k/m}\,\sqrt{\alpha-1}\;t\right)\left(\sqrt{2mgk}\,\sqrt{\alpha-1}\;(y_0-r_0)+\sqrt{\alpha-1}\;mg\right)}{k\sqrt{\alpha-1}}$$

$$-\frac{1}{2}\,\frac{\exp\left(-\sqrt{k/m}\,\sqrt{\alpha-1}\;t\right)\left(-\sqrt{2mgk}\,\sqrt{\alpha-1}\;(y_0-r_0)+\sqrt{\alpha-1}\;mg\right)}{k\sqrt{\alpha-1}} \qquad \textbf{(2.46)}$$

$$+\left(r_0+\frac{mg}{k}\right)$$

For solution from Contact Interval 2 to Interval 4, a closed-form analytical solution is available but the use of numerical methods is probably more appropriate.

Appendix 2.B Analytical Solution for the Closely Stacked Two-Particle System in the Second Verification Problem

2.B.1 *Undamped Case*

The analytical solution for the closely stacked two-particle system in the absence of damping can be derived in a manner similar to Thomson (1993). The differential equation of motion for the system shown in Figure 2.4 becomes:

$$m_1\ddot{y}_1 = -m_1 g - F_{12} + F_{1w} \qquad \textbf{(2.47)}$$

$$m_2\ddot{y}_2 = -m_2 g + F_{12} - F_{2w} \qquad \textbf{(2.48)}$$

where:

$$F_{1w} = \left(r_0 - y_1\right)k_{1w} \qquad \textbf{(2.49)}$$

$$F_{2w} = \left[r_0 - \left(y_w - y_2\right)\right]k_{2w} \qquad \textbf{(2.50)}$$

$$F_{12} = \left[2r_0 - \left(y_1 - y_2\right)\right]k_{12} \qquad \textbf{(2.51)}$$

With the initial condition:

$$y_1\big|_{t=0} = 0.25\,y_{w2},\; \dot{y}_1\big|_{t=0} = 0 \qquad \textbf{(2.52)}$$

$$y_2\big|_{t=0} = 0.75\,y_{w2},\; \dot{y}_2\big|_{t=0} = 0 \qquad \textbf{(2.53)}$$

A closed-form solution is practically available if $m_1=m_2=m$:

$$y_1 = -\frac{mg}{k}+\frac{r+2y_w}{3}+\frac{mg}{k}\cos\left(\sqrt{\frac{k}{m}}\,t\right)+\left(-\frac{r}{3}+\frac{y_w}{12}\right)\cos\left(\sqrt{\frac{3k}{m}}\,t\right) \qquad \textbf{(2.54)}$$

26

$$y_2 = -\frac{mg}{k} + \frac{-r + y_w}{3} + \frac{mg}{k}\cos\left(\sqrt{\frac{k}{m}}t\right) - \left(-\frac{r}{3} + \frac{y_w}{12}\right)\cos\left(\sqrt{\frac{3k}{m}}t\right)$$ (2.55)

If m1≠m2, the solution becomes complicated. However a numerical solution using numerical methods can be obtained. The solution provided in the second verification problem was obtained via the Fehlberg fourth–fifth order Runge-Kutta method as implemented by Maple routines (Maplesoft 2005).

2.B.2 *Viscous Damping Case*
Only the differential equation of motion and the initial conditions for the stacked two particles with viscous damping will be listed here. The numerical solution method shown in Figure 2.5(b) was obtained using Maple (Maplesoft 2005):

$$m_1\ddot{y}_1 = -m_1 g - F_{12} + F_{1w} - F_{dv1w} + F_{dv12}$$ (2.56)

$$m_2\ddot{y}_2 = -m_2 g + F_{12} - F_{2w} - F_{dv2w} - F_{dv12}$$ (2.57)

where:

$$F_{dv1w} = 2\beta\sqrt{k_{1w}m_1}$$ (2.58)

$$F_{dv2w} = 2\beta\sqrt{k_{2w}m_2}$$ (2.59)

$$F_{dv12} = 2\beta\sqrt{k_{12}\frac{m_1 m_2}{m_1 + m_2}}$$ (2.60)

The term F_{1w}, F_{2w}, F_{12}, and the initial conditions are the same as presented in 2.B.1 under "Undamped Case."

2.B.3 *Local (Nonviscous) Damping Case*
As in the case of the viscous damping case, a closed-form solution for the differential equation of motion for the local damping case is complex because it involves the nonlinear term, sgn $\dot{y}$. The results shown in Figure 2.5(c) were obtained using Maple (Maplesoft 2005).

$$m_1\ddot{y}_1 = -m_1 g - F_{12} + F_{1w} + F_{dl1}$$ (2.61)

$$m_2\ddot{y}_2 = -m_2 g + F_{12} - F_{2w} + F_{dl2}$$ (2.62)

where:

$$F_{dl1} = -\alpha\left|-m_1 g - F_{12} + F_{1w}\right|\text{sgn }\dot{y}_1$$ (2.63)

$$F_{dl2} = -\alpha\left|-m_2 g + F_{12} - F_{2w}\right|\text{sgn }\dot{y}_2$$ (2.64)

The term F_{1w}, F_{2w}, F_{12}, and the initial conditions are the same as presented in 2.B.1 under "Undamped Case."

27

Appendix 2.C Comparisons of DEM Codes YADE and PFC2D

Minor differences were found in the solutions from the well known commercial 2D code PFC2D (Itasca Inc. 2004a) and the open source 3D code YADE (Galizzi and Kozicki 2005). These differences are shown not to be related to the 2D/3D correlations, but to subtle differences in the assumptions made in the time step process.

Consider the example for the free fall of a single particle without damping, with the initial parameters as listed in Table 2.1. The time step is set to $\Delta t = 2.0 \times 10^{-3}$s. The exact analytical solution for the first step where $\Delta t = 2.0 \times 10^{-3}$s is obtained from Eq. (2.4):

$$\ddot{y} = g = -9.81 \text{m/s}^2$$

$$\dot{y} = gt = -1.962 \times 10^{-2} \text{m/s}$$

$$y = y_0 + \frac{1}{2} gt^2 = 9.9998038 \times 10^{-1} \text{m}$$

The PFC2D code yields:

$$\dot{y} = g \Delta t = -1.962 \times 10^{-2} \text{m/s}$$

$$y = y_0 + \dot{y} \Delta t = 9.9996076 \times 10^{-1} \text{m}$$

whereas the open source code YADE (with the default settings) yields:

$$\dot{y} = g \frac{\Delta t}{2} = -9.81 \times 10^{-3} \text{m/s}$$

$$y = y_0 + \dot{y} \Delta t = 9.9998038 \times 10^{-1} \text{m}$$

The calculation for the initial time step is thus slightly different for the two DEM solutions. For this particular problem, and for many problems, the difference is negligible. However, when the gravity field and/or the time step are large, the differences may be greater, or more importantly, these differences may cause confusion during the solution of verification or test problems. In the case where damping is included, further investigation shows that the PFC2D code starts the first time step with only gravity and no damping force applied, regardless of the type of damping that is specified. The default settings for YADE, however, start the first time step with both gravity and damping effects which causes a subtle difference between the two numerical results. If the YADE code is forced to apply only gravitational force during the first calculation step, the results of the two DEM code agree to 11 significant digits. Note that the current version of YADE does not provide the viscous damping option. The results for viscous damping shown here were based on a custom user-written subroutine which will be submitted to the YADE open source code.

It is noted that the slight difference between the two DEM implementations identified here are not likely to result in significant differences in response for problems with many particles, typical gravitational constants, and appropriate time steps. However, for the sample problems likely to be chosen to verify code results and gain confidence in the solutions, minor differences may exist. It is for this reason that the response was investigated in detail here.

3 Discrete element simulation of particle-fluid interaction using a software coupling approach

3.1 Equations of motion for the particle and fluid field

3.1.1 Local mean values of point properties of fluid and solid phases

It is very difficult to implement the algorithm of solving the instantaneous flow field on both a small scale as relevant to distances between moving particles in the particle-flow field and on a large scale which is of interest in phenomena such as particles in the fluid. It is reasonable to make a calculation based on locally averaged quantities following Anderson and Jackson (1967). The approach in which the fluid motion is treated in macroscopic scale while the particles are treated in microscopic scale by solving the local averaged Navier-Stokes equation is used to simulate particle flow interaction. The fluid cell is taken or chosen to be large compared with the particle spacing and small compared to the scale of "macroscopic" variations from point to point in the fluid system, in other words, the fluid cell should be larger than the particle diameter but should be small compared to the whole fluid field domain. It is only in this case that local mean variables such as pressure and porosity would be expected to have an unambiguous physical significance, and hence to be useful in constructing equations of motion.

3.1.2 Equations of motion for the fluid - the averaged Navier-Stokes equation

The fluid domain is divided into cells as is common in the finite volume method. The pressure and the fluid velocity are treated as the locally averaged quantity over the fluid cell. The equation of continuity is given as follows:

$$\frac{\partial n}{\partial t} + \nabla \left(nU \right) = 0 \tag{3.1}$$

where n=porosity; U=fluid velocity; t=time. The momentum equation is given as follows:

$$\frac{\partial nU}{\partial t} + \nabla \left(nUU \right) - \nabla \cdot \left(\mu \nabla U \right) = -\frac{n}{\rho_f} \nabla \left(p \right) + f_P \tag{3.2}$$

where μ is the fluid viscosity, ρ_f is the density of fluid, f_P is the interaction force on the fluid per unit mass from the particle, p is fluid pressure.

3.1.3 Interaction term acting on fluid field from the particle

The interaction term representing the effect of a particle on the fluid, f_P, for the averaged Navier-Stokes equation (T. B. Anderson and Jackson 1967), is given by Ergun (1952):

$$f_P = \frac{\beta}{\rho_f} \left(\bar{U}_P - U \right) \tag{3.3}$$

where $\bar{U}_P$ is the average particle velocity within a fluid cell, U is the fluid velocity and β is an empirical coefficient. For porosity n≤0.8,

$$\beta = \frac{\mu\,1-n}{d^2 n}\left[150\,1-n\,+1.75\,\text{Re}\right] \tag{3.4}$$

while for n>0.8:

$$\beta = \frac{3}{4}C_D \frac{\mu\,1-n}{d^2}n^{-2.7}\,\text{Re} \tag{3.5}$$

where d is the particle diameter, and the Reynolds number *Re* is defined as:

$$Re = \frac{\left|\bar{U}_P - U\right|\rho_f n d}{\mu} \tag{3.6}$$

and the drag coefficient C_D is:

$$C_D = \begin{cases} 24\,1+0.15\,\text{Re}^{0.867}\,/\text{Re} & \text{if } \text{Re} \le 1000 \\ 0.43 & \text{if } \text{Re}>1000 \end{cases} \tag{3.7}$$

3.1.4 Equations of motion for the particles

For a particle in fluid, the equation of motion for a single particle is:

$$\ddot{y} = f_G + f_B + f_D + f_C\,/m \tag{3.8}$$

where $\ddot{y}$ =acceleration of the particle; f_G =gravity force; f_B =buoyancy force; f_D =drag force; f_C =contact force; and m=mass of the particle. The inter-particle contact force f_C is obtained from the standard DEM approach as proposed by Cundall and Strack (1979). The drag force f_D is the interaction force acting on the particle from the fluid defined below.

3.1.5 Interaction drag force on the particle from the fluid

The drag force f_D is caused by the pressure gradient within the fluid cell and is obtained from the sum of the velocity difference between the particles and fluid, and may be written as:

$$f_D = \left\{\frac{\beta}{1-n}\,U-\bar{U}_P\,+\nabla p\right\}V_P \tag{3.9}$$

where V_P is the volume of a single particle.

3.2 Solution algorithms for averaged Navier-Stokes equations

Eqs. (3.1) and (3.2) are typically discretized and solved via a pressure-correction process which is detailed in Appendix 3.A. Basic steps for two selected algorithms, which are implemented either in PFC2D or OpenFOAM are summarized below:

3.2.1 SIMPLE Solver Algorithm

The basic steps for the SIMPLE (Semi-Implicit Method for Pressure-Linked Equations) (Patankar 1980) solution algorithm may be summarized as follows:

(1) Set the initial velocity and pressure field U^o and p^o.

(2) Solve the under-relaxed discretized momentum equation Eqn. (3.A.2) to compute the tentative velocity field U^*.

(3) Solve the pressure correction equation Eqn. (3.A.10) to update the pressure field using under-relaxation factor α_p.

(4) Correct the velocity field using Eqn. (3.A.12).

(5) Return to step (1) until convergence.

3.2.2 PISO Solver Algorithm

The basic steps for the PISO (Pressure-Implicit Split-Operator) solution algorithm (Issa 1986) may be summarized as follows:

(1) Set the initial or old velocity and pressure field U^o and p^o.

(2) Solve the discretized momentum equation Eqn. (3.A.2) to compute the tentative velocity field.

(3) Corrector step 1:

   (a) Solve the pressure correction equation Eqn. (3.A.10) to update the pressure field.

   (b) Correct the velocity field using Eqn. (3.A.12).

(4) Corrector step 2:

   (a) Repeat corrector step 1 with Eqn. (3.A.21) for the pressure correction equation

   (b) Correct the velocity field using Eqn. (3.A.23).

(5) Return to step (1) until convergence.

3.2.3 General comments on SIMPLE and PISO

In order to solve the fluid field using finite volume method, the framework of SIMPLE and PISO algorithms has been illustrated in this section. Both SIMPLE and PISO are based on evaluating some initial solutions and then correcting them. Compared with the SIMPLE algorithm, which only makes 1 correction while using under-relaxation procedures for pressure and momentum equations, PISO requires more than 1 correction step, but no more than 4 (typically 2,(OpenCFD Ltd 2008)).

Tsuji (1993) and PFC2D (Itasca Inc. 2004a) used SIMPLE algorithm to calculate the fluid field while the PISO algorithm is used in this study to solve the transient fluid field. In OpenFOAM, the PISO algorithm is used for transient problems and SIMPLE for steady state.

3.3 Solving averaged Navier-Stokes equations using OpenFOAM and YADE code coupling

3.3.1 OpenFOAM: The Open Source CFD Toolbox

The OpenFOAM (Open Field Operation and Manipulation) CFD tool box can simulate various field problems from complex fluid flows involving chemical reactions, turbulence and heat transfer, to solid dynamics. Essentially, OpenFOAM is an open source suite of C++ libraries. It uses primarily the finite volume method to solve coupled sets of partial differential equations (typical of engineering problems) ascribed on any 3D unstructured mesh of cells with an arbitrary number of faces that may undergo motion and/or topological changes. OpenFOAM is

designed to be a flexible, programmable environment for simulation by having top-level code that is a direct representation of the equations being solved.

3.3.2 Code coupling between YADE and OpenFOAM

In order to couple YADE and OpenFOAM, a customized YADE routine FluidDragForceEngine was developed to wrap and incorporate the OpenFOAM IcoFoam solver into the YADE main program as shown in Figure 3.1.
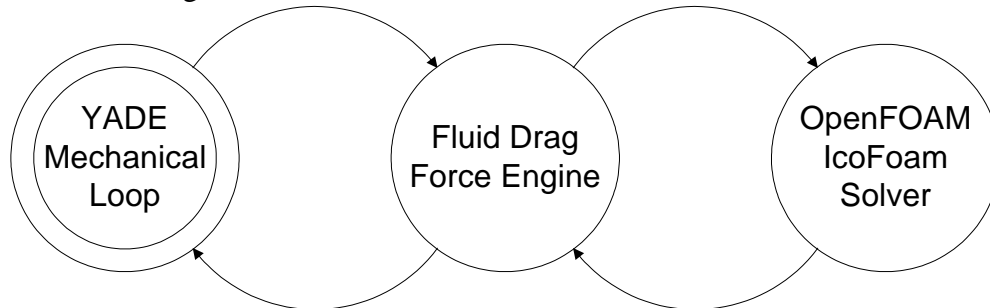
Figure 3.1 Relationship between YADE and OpenFOAM solver
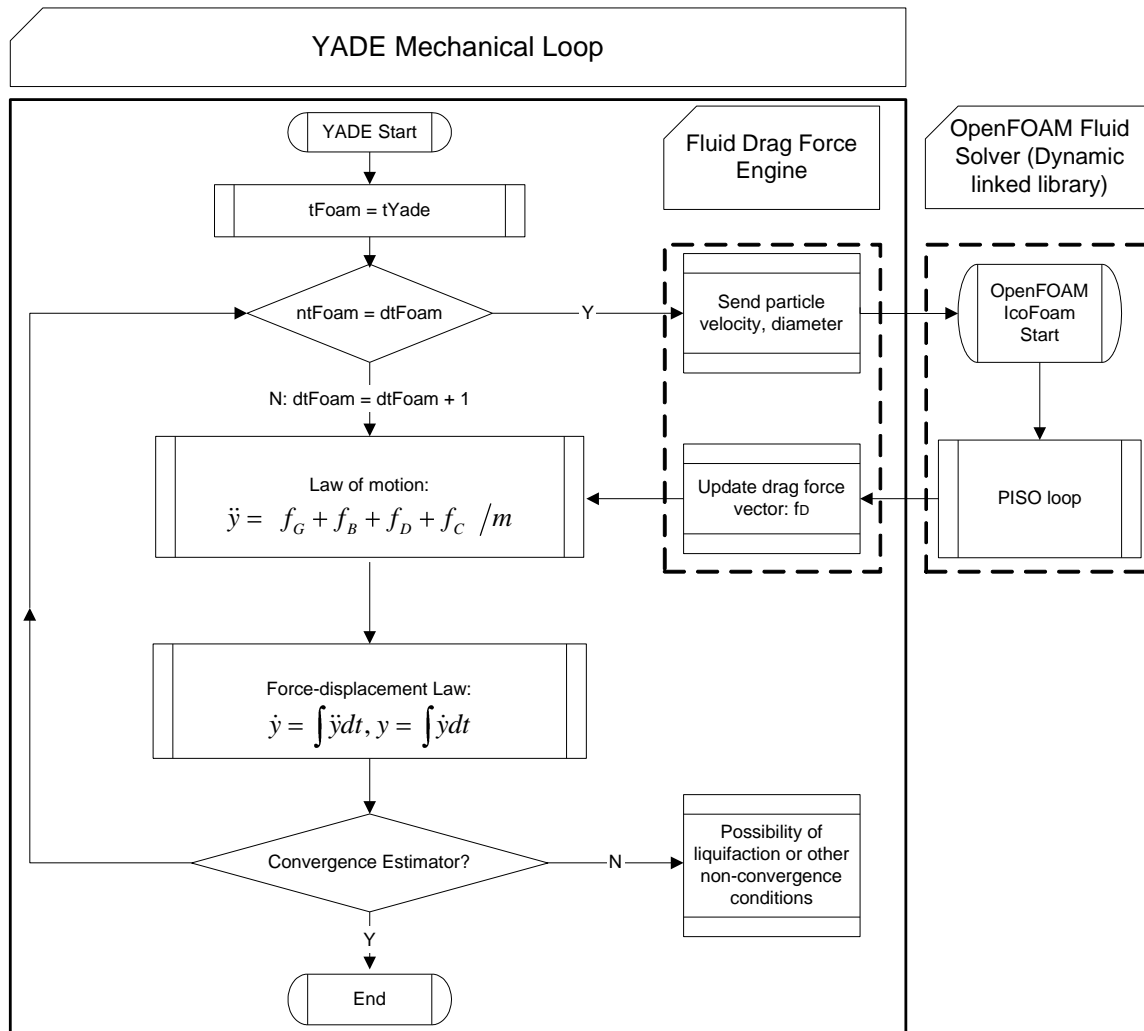
Figure 3.2 Data flow chart of YADE-OpenFOAM coupling

33

3.3.2.1 YADE Mechanical Loop

YADE mechanical loop is a stack of subroutines (called an "Engine" in YADE) which perform different calculation tasks including gravitational force, buoyancy force, contact force and damping force, for each mechanical time step (iteration).

3.3.2.2 FluidDragForceEngine

To include fluid effects on the mechanical behavior of the particles in YADE, the YADE main program requires an update of the drag force vector from the fluid field every **ntFoam** mechanical step. In the **FluidDragForceEngine** developed here, the value of **ntFoam** is determined in a manner similar to PFC2D (Itasca Inc. 2004b). The FluidDragForceEngine acts as a wrapper of the OpenFOAM solver which collects the latest information about the fluid step and mechanical step and passes the particle information (velocities and diameters) to the **IcoFoam** fluid solver and then returns the updated drag force for each particle as shown in Figure 3.2.

3.3.2.3 OpenFOAM Fluid Solver

OpenFOAM provided extensible and flexible solvers for various kinds of applications. **IcoFoam**, the standard transient solver for incompressible laminar flow of Newtonian fluids, is modified as a dynamically linked library (Richard and Rago 2005). The data flow chart of **FluidDragForceEngine** and the **IcoFoam** solver is as shown in Figure 3.2.

3.4 Closure

The basic equations of interaction terms between particle and fluid are presented in this section. The Finite Volume discretization for the averaged Navier-Stokes equation including the temporal and spatial terms with two solution algorithms: PISO and SIMPLE, are discussed and also serve as the theoretical basis for the software implementation. The framework of YADE and OpenFOAM coupling is also presented which can be used for verification problems from Chapter 6 to Chapter 8.

Appendix

Appendix 3.A Solution of the averaged Navier-Stokes equation using SIMPLE and PISO algorithm

The finite volume method (FVM) is a numerical method for representing and evaluating partial differential equations as algebraic equations. Similar to the finite difference method, values are calculated at discrete places on a meshed geometry. In contrast to the finite element method, which is an approximation to its solution, the finite difference method is an approximation to the differential equation. The calculation domain is divided into a number of non-overlapping cells such that there is one cell surrounding each grid point. The term "finite volume" (FV) or "control volume" (CV) refers to the small cell surrounding each grid point over a mesh. The FVM can solve problems with irregular geometries. Furthermore, one advantage of the finite volume method over the finite element method is that it can conserve the variables, e.g. the mass conservation, on a coarse mesh easily. This is an important characteristic for fluid problems.

Notation of variables:

n	superscript for the new iteration
o	superscript for the old iteration
ρ	fluid density
ρ_P	fluid density at an arbitrary node P
ϕ	unknown field variable for fluid
ϕ_P	unknown field variable for fluid at an arbitrary node P
ϕ_f	unknown field variable for fluid at cell face f
V	volume for a fluid cell
S	outward-pointing surface vector for a fluid cell
S_f	face area vector for a fluid cell
μ	fluid viscosity
μ_f	fluid viscosity at cell face
U	fluid velocity
U_f	fluid velocity at cell face

Most fluid dynamics codes (e.g. OpenFOAM (OpenCFD Ltd 2008)), Fluent (Fluent Inc. 2006) and StarCD (CD-adapco Group 2001)) use the Pressure-Implicit Split-Operator (PISO) or Semi-Implicit Method for Pressure-Linked Equations (SIMPLE) algorithms to solve the equations for the fluid field. These methods follow the general idea proposed by Partankar (1980). These algorithms are iterative procedures for solving equations for velocity and pressure. In this study, the derivation of equations for SIMPLE and PISO will follow the procedure of Ferziger and Peric (2001), but using a similar notation as Jasak (1996).

3.A.1 *Discretization Procedure for the Navier-Stokes System*

Discretization of the solution domain produces a computational mesh on which the governing equations a subsequently solved. The L.H.S of Eqn. (3.2) can be discretized according to the discretization procedure from OpenFOAM programmer's guide (OpenCFD Ltd 2008) as:

$$\frac{\partial}{\partial t} \int_V nU dV + \int_V \nabla \cdot \left(nUU \right) dV + \int_V \nabla \cdot \left(\mu \nabla U \right) dV$$

$$= \frac{n_P U_P V^n - n_P U_P V^o}{\Delta t} + \sum_f FU_f + \sum_f \mu_f S_f \cdot U_f \qquad \textbf{(3.A.1)}$$

The face values with the subscript f are calculated from the cell values on each side of the face, i.e. the node values U_P, and therefore Eqn. (3.A.1) produces a linear algebra equation of the unknown (new) value of U^n if the pressure gradient term is not included in the source term of the R.H.S of Eqn. (3.2):

$$A \cdot U^n = a_P U_P + \sum_N a_N U_N = f_S - n\nabla p \qquad \textbf{(3.A.2)}$$

where $A = a_P + a_N$ is the discretized momentum coefficient, which is a sparse tri-diagonal matrix, a_P is the diagonal of the matrix A, P is the index of an arbitrary node, and a_N denotes the neighbor coefficients of P that appear in the discretized momentum equation. The source term f_S, contains all of the terms that can be explicitly computed in terms of the velocity in the previous *(old)* iteration U^o, in our case, the interaction force from particle to fluid $f_P (U^o)$ from Eqn. (3.9).

3.A.2 *Pressure-Velocity coupling*

The iterations within one time step, in which the coefficients and source matrix are updated, are called outer iterations to distinguish them from the inner iterations performed on linear systems with fixed coefficients. SIMPLE and PISO are both implicit pressure-correction methods, they use a pressure (or pressure-correction) equation to enforce mass conservation at each time step or, in steady state problem, each outer iteration.

Due to non-linearity and coupling of the underlying differential equations, Eqn. (3.A.2) cannot be solved directly as the coefficient matrix A might depend on the unknown next-step solution U^n, iterative approach has to be applied. For time-dependent transient flow, iteration must be continued within each time step until the entire system of non-linear equations is satisfied to within a narrow tolerance. For a steady-state flow, the tolerance can be much more generous.

If we solve Eqn. (3.A.2) using the last known pressure p^o, we obtain a tentative velocity field U^*, back substitute into Eqn. (3.A.2), we have:

$$a_P U_P^* + \sum_N a_N U_N^* = f_S - n\nabla p^o \qquad \textbf{(3.A.3)}$$

The velocity at node P, obtained by rearranging Eqn. (3.A.3), can be expressed as:

$$U_P^* = \frac{-\sum_N a_N U_N^* + f_S}{a_P} - \frac{n\nabla p^o}{a_P} \qquad \textbf{(3.A.4)}$$

Denote:

$$H(U^*) = -\sum_N a_N U_N^* + f_S \qquad \textbf{(3.A.5)}$$

Since the pressure used in these iterations was obtained from the previous outer iteration or time step, the velocities U^* in Eqn. (3.A.3) do not normally satisfy the discretized continuity equation.

37

To enforce the continuity equation, the velocities need to be corrected, which requires the correction of the pressure field.

3.A.2.1 Derivation of SIMPLE algorithm

Assume Eqn. (3.A.2) contains the final solution of velocities U^n and pressure p^n which satisfy both the momentum Eqn. (3.2) and continuity Eqn. (3.1), the correction values for velocity and pressure can be obtained via Eqn. (3.A.2) Eqn. (3.A.3):

$$a_P U'_P + \sum_N a_N U'_N = -n\nabla p'$$
(3.A.6)

where:

$$U' = U^n - U^*$$
(a)

(3.A.7)

$$p' = p - p^o$$
(b)

From Eqn. (3.A.6) and Eqn. (3.A.7), we obtain the relation between the velocity and pressure equations:

$$U' = -\frac{\sum_N a_N U'_N}{a_P} - \frac{n\nabla p'}{a_P}$$
(3.A.8)

in order to satisfy the continuity Eqn. (3.1). Substitute Eqn. (3.A.7) to Eqn. (3.1) using Eqn. (3.A.8), the corrected velocities and pressure are linked by:

$$\frac{\partial n}{\partial t} + \nabla \cdot \left(nU \right) = 0$$

$$= \frac{\Delta n}{\Delta t} + \nabla \cdot \left[n \left(U^*_P + U'_P \right) \right]$$

$$= \frac{n^n - n^o}{\Delta t} + \nabla \cdot \left[n \left(\frac{H \left(U^* \right)}{a_P} - \frac{n\nabla p^o}{a_P} \right) + n \left(-\frac{\sum_N a_N U'_N}{a_P} - \frac{n\nabla p'}{a_P} \right) \right]$$
(3.A.9)

$$= \frac{n^n - n^o}{\Delta t} + \nabla \cdot \left[n \frac{H \left(U^* \right)}{a_P} + n \left(-\frac{\sum_N a_N U'_N}{a_P} - \frac{n\nabla p^n}{a_P} \right) \right]$$

Note that the velocity corrections containing U'_N in the R.H.S of Eqn. (3.A.8) and Eqn. (3.A.9) are unknown at this point, so it is commonly neglected. In other words, it is effectively assumed that the whole velocity error comes from the error in the pressure term (Jasak 1996), and therefore the following pressure correction equation is obtained:

$$\nabla \cdot \left(\frac{n^2 \nabla p^*}{a_P} \right) = \nabla \cdot \left[n \frac{H \left(U^* \right)}{a_P} \right] + \frac{n^n - n^o}{\Delta t}$$
(3.A.10)

38

Note that in the L.H.S of Eqn. (3.A.10), the notation p^* is used as $p^* = p^o + p'$ to distinguish it from the final pressure value p^n due to omission of the U'_N term in Eqn. (3.A.9). The velocity correction U' is calculated from Eqn. (3.A.8), but without the first U'_N term at the R.H.S:

$$U' = -\frac{n\nabla p'}{a_P} \tag{3.A.11}$$

The velocity for the new iteration, or the second corrector step U^{**} can be obtained from Eqn. (3.A.4) and Eqn. (3.A.11):

$$U^{**} = U_P^* + U'_P = \frac{H\ U^*}{a_P} - \frac{n\nabla p^*}{a_P} \tag{3.A.12}$$

Up till now we have obtained the solution of U^{**} and p^* for one (the first) corrector step, this is known as the SIMPLE algorithm (Patankar 1980).

For the SIMPLE algorithm, the pressure correction equation Eqn. (3.A.10), however, is subjected to divergence unless some under-relaxation is used (Patankar 1980). A general successful procedure is to:

1. Relax U^* using an under-relaxation factor α_U while solving the momentum equation Eqn. (3.A.3);

2. Relax p' while obtaining the corrected pressure field p^*, in other words, instead of directly using Eqn. (3.A.7)(b), we add only a portion of p':

$$p^* = p^o + \alpha_p p' \tag{3.A.13}$$

The recommended values of under-relaxation factors are (Jasak 1996):
- $\alpha_P = 0.8$ for Eqn. (3.A.13);
- $\alpha_U = 0.2$ for solving the momentum equation Eqn. (3.A.3).

3.A.2.2 Derivation of PISO algorithm

Instead of using under-relaxation factors, we start from Eqn. (3.A.12). Similar to the first corrector step in the SIMPLE algorithm, if we artificially substitute U^{**} and p^* into Eqn. (3.A.2), we then begin the second corrector step from the discretized momentum equation:

$$a_P U_P^{**} + \sum_N a_N U_N^{**} = f_S - n\nabla p^* \tag{3.A.14}$$

Rearranging Eqn. (3.A.14) gives:

$$U_P^{**} = \frac{-\sum_N a_N U_N^{**} + f_S}{a_P} - \frac{n\nabla p^*}{a_P} \tag{3.A.15}$$

Denote:

$$H(U^{**}) = -\sum_N a_N U_N^{**} + f_S \tag{3.A.16}$$

Eqn. (3.A.2) minus Eqn. (3.A.14) yields:

$$a_P U''_P + \sum_N a_N U''_N = -n\nabla p''$$

(3.A.17)

A similar definition as Eqn. (3.A.7) is made as the second correction field of velocities U'' and pressure p'':

$$U'' = U^n - U^{**}$$

(3.A.18)

$$p'' = p^n - p'$$

And we obtain the second relation between velocities and pressure:

$$U''_P = -\frac{\sum_N a_N U''_N}{a_P} - \frac{n\nabla p''}{a_P}$$

(3.A.19)

The continuity equation Eqn. (3.1) is applied the same way as the first corrector step:

$$\frac{\partial n}{\partial t} + \nabla \cdot \left(nU \right) = 0$$

$$= \frac{\Delta n}{\Delta t} + \nabla \cdot \left[n \left(U_P^{**} + U''_P \right) \right]$$

$$= \frac{n^n - n^o}{\Delta t} + \nabla \cdot \left[n \left(\frac{H\left(U^{**}\right)}{a_P} - \frac{n\nabla p^*}{a_P} \right) + n \left(-\frac{\sum_N a_N U''_N}{a_P} - \frac{n\nabla p''}{a_P} \right) \right]$$

(3.A.20)

$$= \frac{n^n - n^o}{\Delta t} + \nabla \cdot \left[n \frac{H\left(U^{**}\right)}{a_P} + n \left(-\frac{\sum_N a_N U''_N}{a_P} - \frac{n\nabla p^n}{a_P} \right) \right]$$

Again the U''_N term is neglected in Eqn. (3.A.19) and (3.A.20), which yields the second pressure correction equation:

$$\nabla \cdot \left(\frac{n^2 \nabla p^{**}}{a_P} \right) = \nabla \cdot \left[n \frac{H\left(U^{**}\right)}{a_P} \right] + \frac{n^n - n^o}{\Delta t}$$

(3.A.21)

After solving Eqn. (3.A.21) for the second corrected pressure $p^{**} = p^* + p''$, the second velocity correction U''_P can be calculated using Eqn. (3.A.19) without the first term containing U''_N:

$$U'' = -\frac{n\nabla p''}{a_P}$$

(3.A.22)

The second corrected velocity field U^{***} can be obtained from Eqn. (3.A.15) and Eqn. (3.A.22):

$$U^{***} = U_P^{**} + U''_P = \frac{H\left(U^{**}\right)}{a_P} - \frac{n\nabla p^{**}}{a_P}$$

(3.A.23)

Although further corrector steps can be performed in the same way, this is seldom done. The coefficients a_N in the "$H()$" operator of the coefficient matrix A in Eqn (3.A.5) and (3.A.16) can be reused. This procedure is an iterative method for solving Eqn. (3.A.2) with the last pressure term explicitly treated. It is known as the PISO algorithm (Issa, 1986). In addition, Eqn. (3.A.10) and Eqn. (3.A.21) indicate that the porosity of each finite volume can be considered as a constant (actually can be included in the source term f_S in Eqn. (3.A.2) within each outer iteration.

4 Simulation of Graded Rock Fill for Sinkhole Repair in Particle Flow Model

4.1 Introduction

4.1.1 Problem statement

Shallow sinkholes have been successfully repaired or stabilized by placement of graded rock fill over the exposed sinkhole. Typically, the sinkhole is excavated and large diameter (0.25 to 0.5 m) shot rock aggregate is dumped down the excavated throat of the sinkhole. Through bridging, the throat is stabilized, and subsequent layers of finer material are placed to create a graded rock fill. This fill provides stability, while still permitting the flow of surface water into the cavity below. In practice, the choice of aggregate size is strictly made based on experience. To investigate the relative particle size to throat radius necessary for stability, the distinct element method, as implemented in the PFC2D code (Itasca Inc. 2004a), is used to simulate the construction of the graded rock fill. During the filling procedure, the interaction of the rock fill and surrounding material is simulated by interacting disks.

4.1.2 Particle properties in the Discrete Element Method

The original application of Discrete Element Method (DEM), which was proposed by Cundall (1979), is a tool to investigate the behavior of granular material. The general DEM model simulates the mechanical behavior of a system comprised of a collection of arbitrarily-shaped particles, which means the particle shape can be any form such as polygonal, or circular. Here the term "particle" denotes a body that occupies a finite amount of space. The model is composed of discrete particles that displace independently from one another, and interact only at contacts or interfaces between the particles.

The 2-D particle flow model, implemented in PFC2D (Itasca Inc. 2004a), treats the 3-D rock particles as disks and incorporates the following main assumptions:

1. The particles are treated as rigid bodies;

2. The particle contacts occur over a vanishingly small area (i.e., at a point).

3. Behavior at the contacts uses a soft-contact approach, wherein the rigid particles are allowed slightly to overlap one another at contact points. The magnitude of the overlap is related to the contact force via a force-displacement law, and all overlaps are small in relation to particle sizes. A representation of the 2-D particle contact is shown in Figure 4.1.
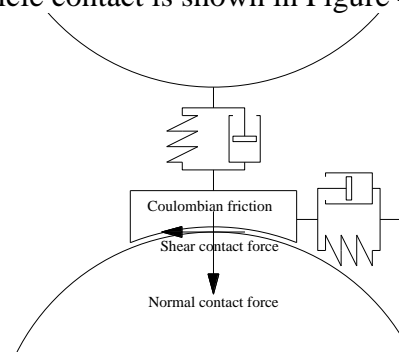
Figure 4.1 Schematic representation of Cundall's (1979) contact model for normal and shear forces between particles

4.1.3 Description of the sinkhole model

The geometry of the sinkhole throat and the surrounding overburden soil is assumed to be similar to a system of balls in a hopper (Figure 4.2). The residual soil surrounding the sinkhole is assumed to be at a slope of 1:1, and is assumed to be stiff for simplicity (analogous to the hopper with fixed right and left walls), which means zero displacement across this boundary. While the friction between the rock and sloping soil (ball-wall contact) could be assigned a value different than that between particles, for simplicity they were assigned to be equal in this parametric study. A temporary wall or horizontal support is placed across the middle of the hopper to collect the particles; the wall is then removed to allow particles to fall, simulating the dumping of the rock fill. The rock fill particles are assumed to have a minimum and maximum radius r_{min} and r_{max}, respectively. The stability of the rock fill is then investigated for a range of particle radii and sinkhole throat radii, R, which was assumed to have values of 0.15, 0.5 and 1.0 m. The particle radius used in the simulation has a Gaussian distribution with mean value $r_{mean} = \frac{1}{2}(r_{min} + r_{max})$, standard deviation $r_{max} - r_{min}$. Typical properties of the particles are shown in Table 4.1.

The analysis involves the following sequence containing two major steps:

Step 1: The assembly of particles are first randomly generated within the upper part of the hopper and subjected to gravity; the whole system of particles is cycled to a stable state. This state is as shown in Figure 4.3.

Step 2: The base wall is then removed to simulate the dumping of the rock fill, and the particles begin flowing downward by the action of gravity. If the mechanical properties of the particles and the radius of the particles and sinkhole throat are such that an arch is successfully formed as shown in Figure 4.4, the whole system will come to a stable state; otherwise the particles will continuously flow into the sinkhole throat (out of the hopper) as shown in Figure 4.5.

(a) (Drumm, 1990)　　　　　　　　　　　　　(b)
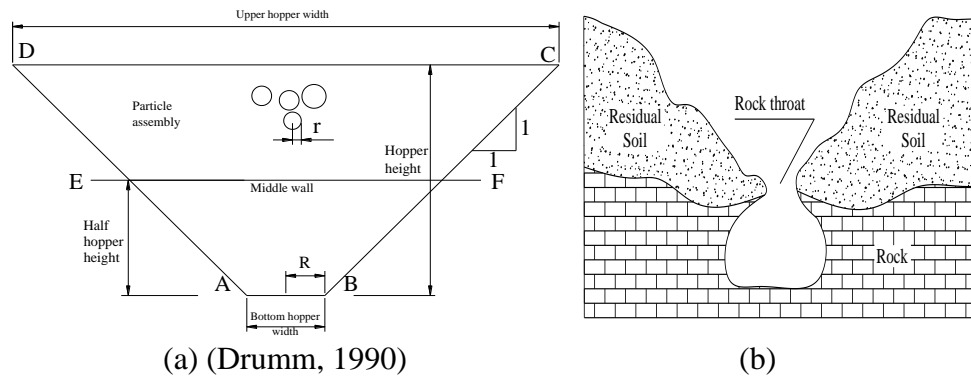
Figure 4.2 Schematic of the sinkhole (a) and idealized hopper model (b)

Table 4.1 Physical properties of the particles in the assembly

Ball Properties		Value	Unit
r_{min}		0.03 to 0.50	m
r_{max}/ r_{min}		1.1	
2-D porosity		0.16	
Bottom hopper width/radius		1.0/0.5	m
Density		2000	kg/m^3
Friction coefficient	ball-ball	1.0	
	ball-wall	1.0	
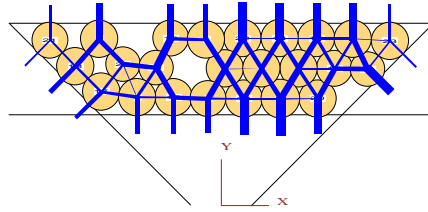
Figure 4.3 Particles holding at the upper part of the hopper, ready to dump. Heavy lines indicate the inter-particle forces, with the line width proportional to the force magnitude
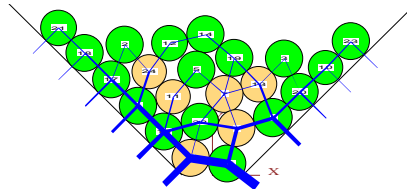
Figure 4.4 Successfully created arch within the hopper, stable state
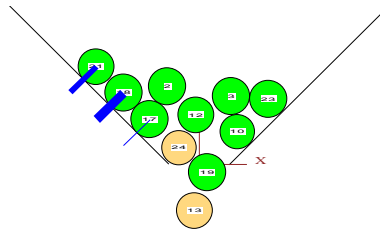
Figure 4.5 Unsuccessful arch formation

(a) $r_{min}/R=0.380$, unstable

(b) $r_{min}/R=0.404$, stable

(c) $r_{min}/R=0.412$, unstable

(d) $r_{min}/R=0.426$, unstable

(e) $r_{min}/R=0.448$, stable

(f) $r_{min}/R=0.478$, stable
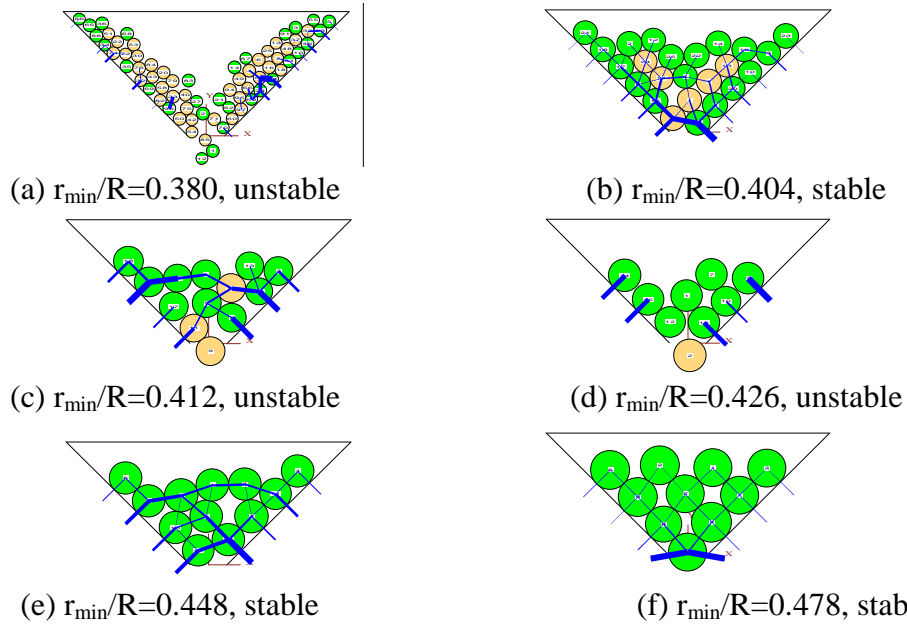
Figure 4.6 Final state of hopper with increasing minimum particle radius and throat radius R = 1.0m

4.2 Discussion of results
4.2.1   Relationship between normalized particle radius and stable arch formation

For a given sinkhole throat radius, R, the stability was investigated for a range of r_{min} from 0.03m to 0.50m, with an increment of 0.01m. Several final states are shown in Figure 4.6(a)-(f), for R = 1.0m.

Results for R = 1 and a range of r_{min} values are presented in Figure 4.7, which is typical of the analyses at other values of R. As expected, the smaller r_{min} values are unstable as arching cannot develop, while with larger particle radii arching always develops. It is observed that there is an intermediate range of r_{min} from about 0.4 to 0.5 m which may be either stable or unstable.
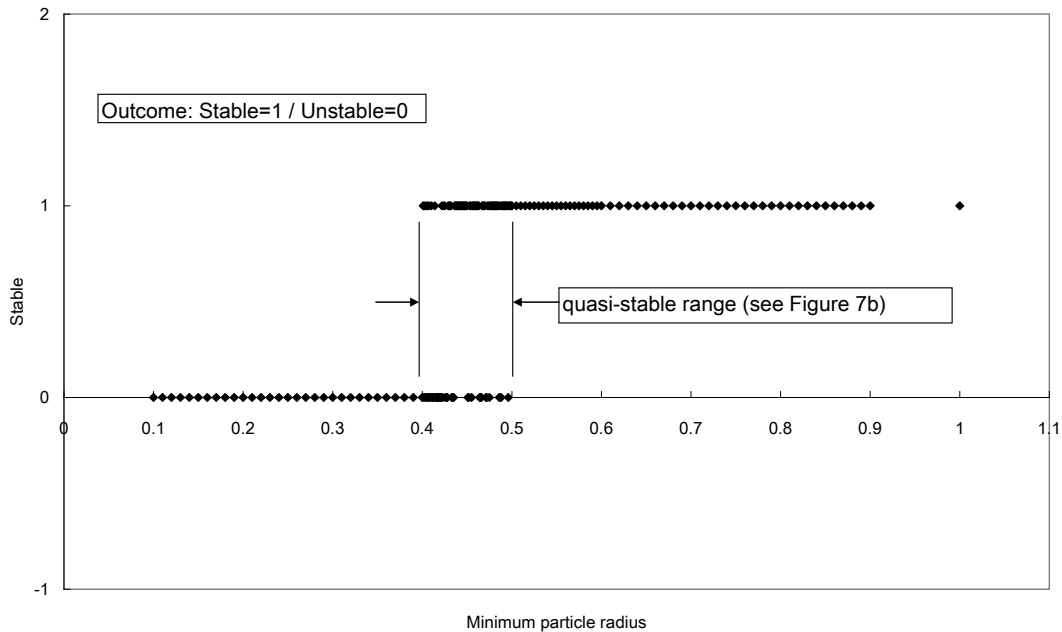
(a) Complete results for R=1.0m, data points with stable = 0 indicate failure state and data points with stable = 1 indicates stable state for minimum particle radius<0.5m
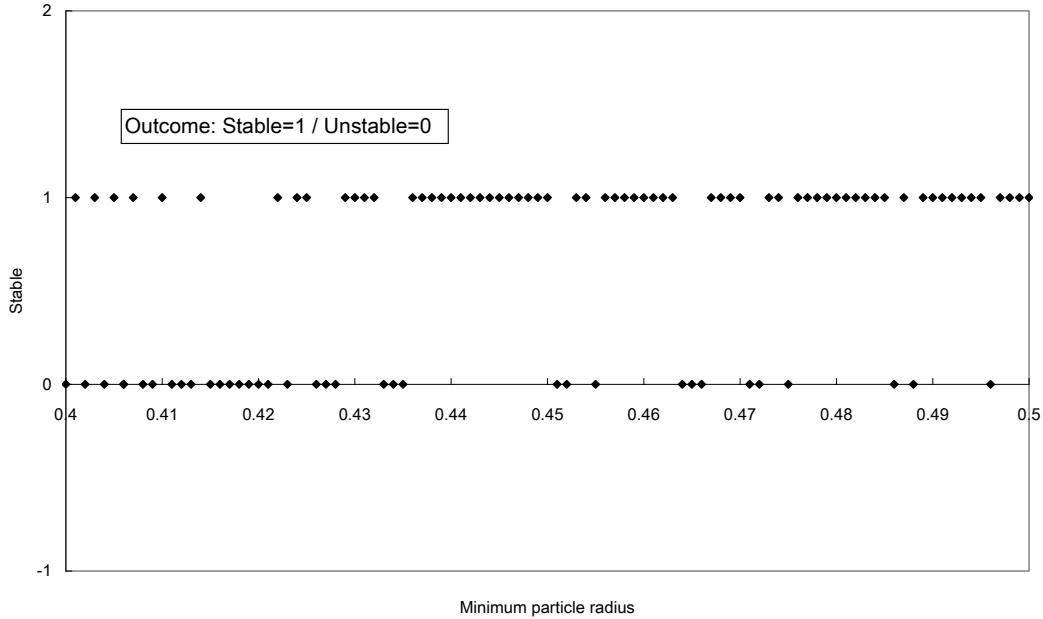
(b) Magnified results for outcome of stable state for minimum particle radius between 0.4 and 0.5m (quasi-stable state)

Figure 4.7 Analysis results for outcome of stable state

4.2.2 Probability of stability and critical particle radius

The results from Figure 4.6 and Figure 4.7 indicate that simply increasing the particle radius (relative to throat radius) does not provide a stepwise jump from unstable to stable, or that there exists a range of particle radii that may be stable or unstable, depending upon how the particles arrange or are dumped. A brief explanation is shown in Figure 4.8 , where the same three particles are shown to form both a stable state and an unstable state, depending on their initial random positions.

Increasing the relative particle radius may increase the probability of stability, but does not assure stability, suggesting that the analysis of stability should be treated on a statistical basis. A logistic regression (Kutner et al. 2004) was performed on the data provided in Figure 4.7, where π is defined as the probability of stability with respect to r_{min} /R, and the natural logarithm of the odds (which is referred to as *logit*) becomes:

$$\text{logit} = \log_e\left(\frac{\pi}{1-\pi}\right) \tag{4.1}$$

(a) Stable state   (b) Unstable state
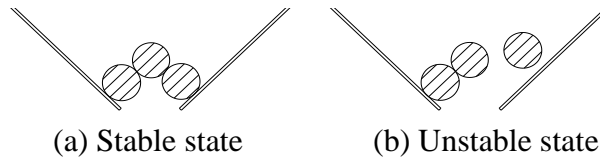
Figure 4.8 Stable and unstable particle arrangements for the same rmin /R

Probablity of forming a stable arch
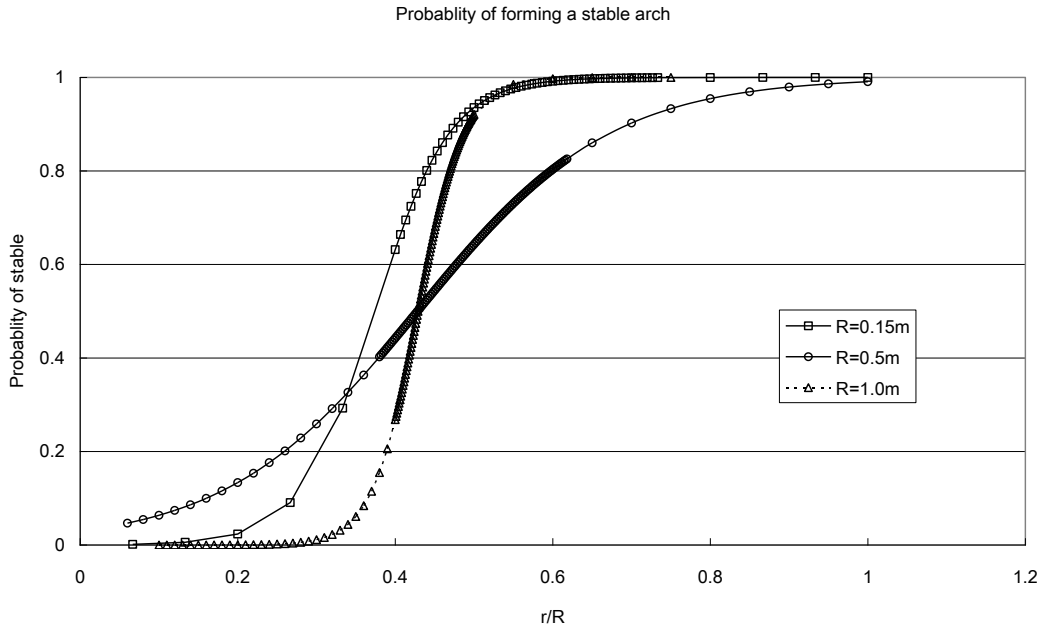
Figure 4.9 Regression curve for probability of stability

Table 4.2 Median for r_{min}/R ratios

R (m)	Median (r_{min}/R)
0.15	0.374
0.5	0.428
1.0	0.429

The resulting regression curve (Figure 4.9) shows the transition from unstable (probability = 0) to stable (probability = 1) as the normalized particle radius r_{min} /R increases. Results for three different throat radii (R = 0.15m, 0.5m, 1.0m) are shown for comparison. The medians (50% percentile) for each curve are as shown in Table 2.

For probability = 0.5, the corresponding r_{min}/R ratio for R = 0.15m is 0.374, for R=0.5m is 0.428, for R=1.0m is 0.429, which means for a given bottom hopper width of R=0.15m, 0.5m and 1.0m, it is more likely to reach a final stable state when the r_{min}/R ratio is greater than 0.374, 0.428 and 0.429, holding other parameters constant.

4.3 Closure

Based on the analysis above, the discrete element method may be a reasonable method to investigate the stability of graded rock fills for sinkhole repair. Several simplifying assumptions were made, and the relationship between the macro properties of the granular assembly and the micro properties of the particles should be examined. It is suggested that logistic regression analysis may be an appropriate method to describe the probability that a given size rock will produce a stable graded rock fill for an anticipated sinkhole throat.

5 3D DEM analysis of Graded Rock Fill Sinkhole Repair: Particle Size Effects on the Probability of Stability

5.1 Introduction
5.1.1 Problem statement

Shallow sinkholes have been successfully repaired or stabilized by placement of graded rock fill over the exposed sinkhole. Typically, the sinkhole is excavated and large diameter (0.25 to 0.5 m) shot rock aggregate is dumped down the excavated throat of the sinkhole (Kemmerly 1984; Moore 1981, 2006; Sowers 1996). Through bridging, the throat is stabilized, and subsequent layers of finer material are placed to create a graded rock fill. This fill provides stability, while still permitting the flow of surface water into the cavity below. In practice, the choice of aggregate size is strictly made based on experience, and Sowers (Sowers 1996) recommends that the diameter of the particles in the rock fill be greater than approximately 0.5 the throat width.

In many respects, the rock placement is to be similar to the classic problem of granular material flowing through a hopper or funnel. Particles above a given size will always bridge the throat, even if smaller than the throat diameter, while particles below a given size will never bridge or arch the throat. However, there is an intermediate range of particles for which stability or clogging depends on the order, timing, and how the particles arrange during the filling procedure. This intermediate range, termed the semi-stable state here, is investigated in this paper using 3D discrete element method (DEM) as formulated in the open source code YADE (Kozicki and Donzé 2008).

A preliminary study of the stability of a graded rock fill using the DEM was described by Chen et al. (Chen et al. 2006). A series of 2 dimensional DEM simulations for a range of particle diameters demonstrated that a small (relative to the throat diameter) mean particle diameter value will lead to an unstable state, while a large particle diameter will always develop a stable arch, and investigated the intermediate range of particle diameter which can be either stable or unstable depending on the initial random position and diameter of the particles. This paper further develops the approach in 3-dimensions, and has two goals:

a) Describe the three-dimensional modeling of the placement of shot rock using the Discrete Element Method, where it is demonstrated that for a given throat radius, there exists an intermediate range of particles sizes for which stability depends upon how the particles arrange during the filling procedure, and

b) Present a statistical description of this intermediate range of particle sizes for which the throat is semi-stable, using logistic regression to describe the gradual transition from the unstable to stable behavior. This provides a rational method to determine the mean particle size (relative to throat diameter) for a given probability that the repair will be stable.

It is convenient to discuss the stability in terms of a mean diameter ratio, $D_{r, mean}$, where

$$D_{r,mean} = \frac{d_m}{d_{throat}}$$

Where d_m = the mean size (diameter) of the shot rock particles
d_{throat} = the diameter of the sinkhole or funnel throat

Thus, the empirical practice of using rock fill with a mean particle size greater than about 0.5 the sinkhole throat width would correspond to a $D_{r,mean} > 0.5$.

5.1.2 Basic assumptions in the Discrete Element Method (DEM)

The Discrete Element Method is a numerical method for computing the motion of a large number of particles such as granular material, where the term "particle" denotes a body that occupies a finite amount of space. Although the DEM particle can be of various shapes, e.g. polyhedral or spherical, in this study, the rock pieces are assumed to be spherical. The DEM was originally proposed by Cundall and Strack (1979), and makes the following assumptions:

(1) All particles are rigid, but inter-particle deformation is approximated by overlapping between particles using a simple force displacement law.

(2) All overlaps occur in a vanishingly small space in relation to particle sizes.

(3) Single rigid particle motion is predicted by Newton's second law of motion.

A representation of the 2-D particle contact is shown in Figure 5.1.

5.1.3 Description of the sinkhole model

The geometry of the sinkhole throat and the surrounding overburden soil is shown schematically in Figure 5.2.
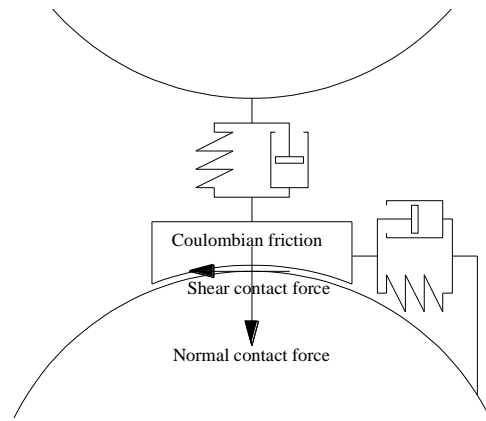
Figure 5.1 Schematic representation of the DEM contact model for normal and shear forces between particles, after (Cundall and Strack 1979)
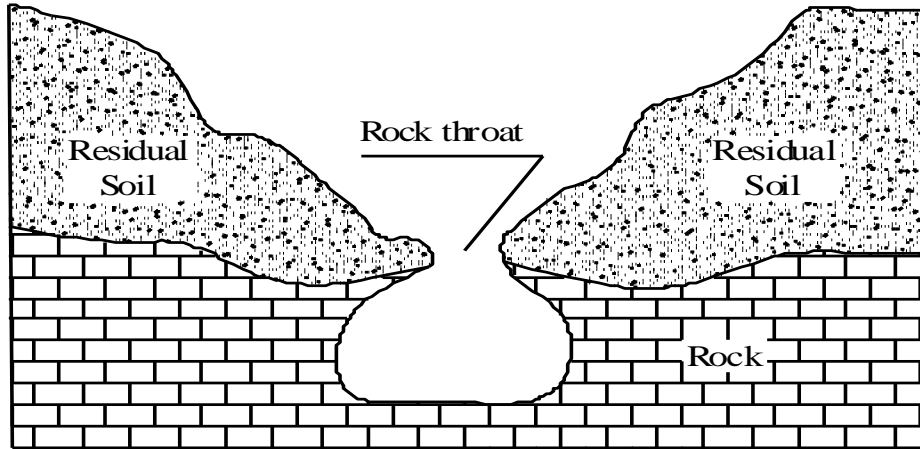
Figure 5.2 Schematic of the sinkhole (Drumm et al. 1990)

(a) 30° funnel

(b) 45° funnel
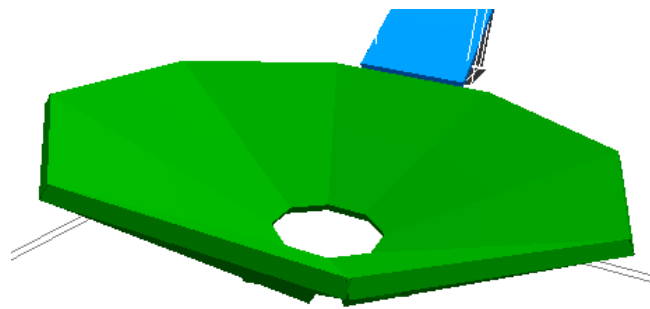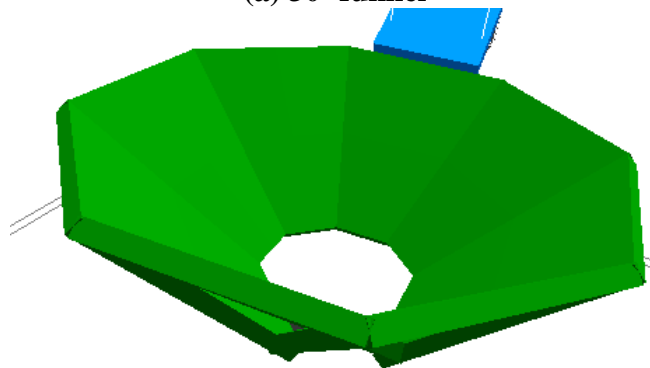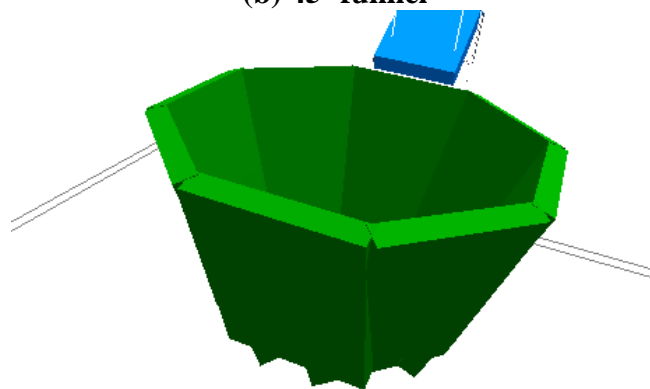
(c) 60° funnel

Figure 5.3 3D funnel with (a) 30°, (b) 45° and (c) 70° to the horizontal plane

Conceptually, the problem is similar to a system of spheres in a funnel. The shape of the funnel is approximated by a series of 8 plates (Figure 5.3), and different funnel angles characterized by plates at inclined angles of 30°, 45° and 70° with respect to the horizontal. For simplicity, the friction between surrounding soil and the rock fill is assumed to be equal, although in the real case they are rarely the same value. A dumping bin composed of four vertical walls and an inclined plate is placed beside the funnel to simulate the unloading of the rock fill from a dump truck (Figure 5.4),
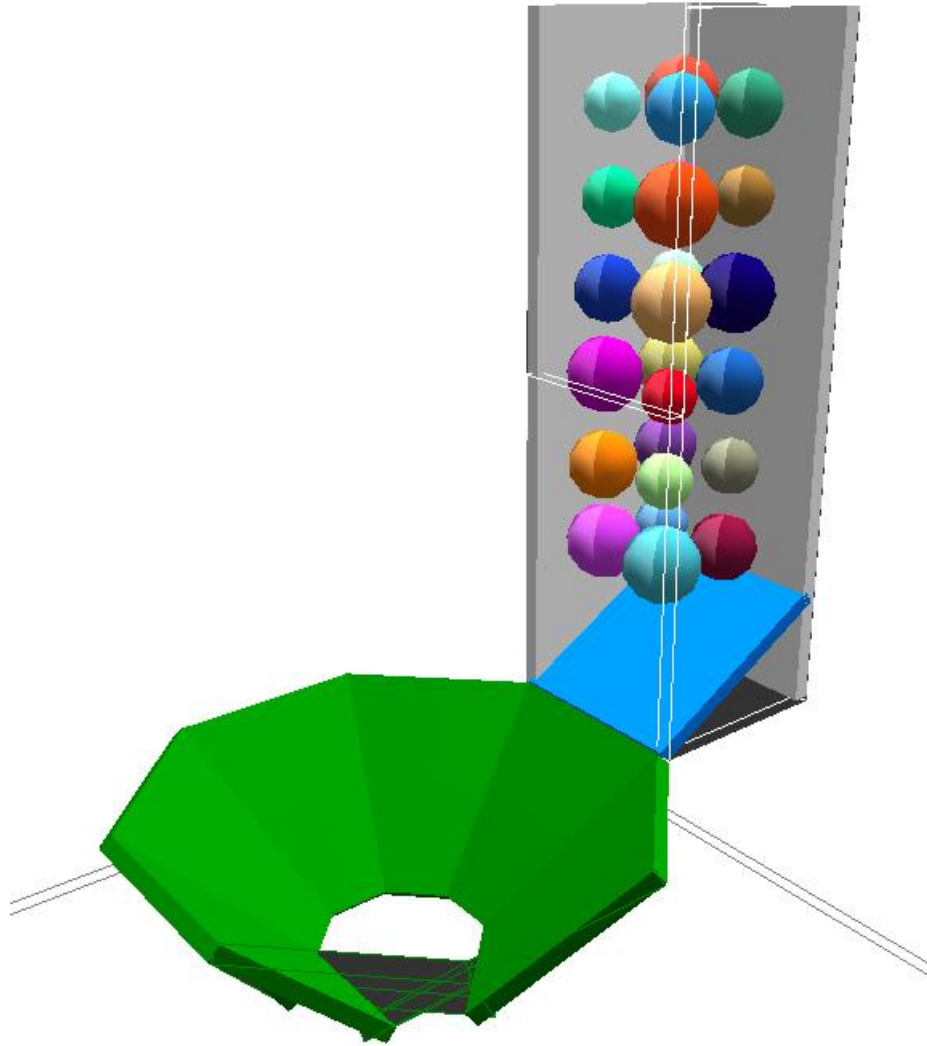
Figure 5.4 Schematic of 3D DEM simulation of the particles through a funnel

and the plate is inclined 30°. The random diameter particles are randomly placed inside the bin without overlap.

During the simulation, the particles are specified using the mean diameter d_m and the ratio of maximum diameter to minimum diameter r. Each particle diameter is then randomly generated within the maximum and minimum diameter range of $d_m/(r+1)$, $d_m \cdot r/(r+1)$. Typical physical and geometrical properties for the rock fill are listed in Table 5.1.

Table 5.1 Geometrical and Physical Properties of the Particles in the Assembly

Sphere Properties		Value	Unit
Mean diameter		0.2-0.5	m
Max diameter/Min diameter Ratio		1.5	
Bottom funnel width/radius (hole Size)		1.0/0.5	m
Density		2650	kg/m^3
Friction Angle	ball-ball	35	
	ball-wall	35	

All analyses were conducted with a throat diameter d_{throat}= 1.0, such that the diameter ratio, $D_{r,mean}$ and the mean particle diameter, d_m have the same value.

5.2 Simulation procedure

The simulation included major steps as listed below:

Step 1: Particle size is specified, and particles are randomly generated and placed inside the dumping bin.

Step 2: The dumping bin is opened and the particles are allowed to fall under gravity into the sinkhole.

Step 3: The stable/unstable condition is recorded.

The simulation process was then repeated for a different mean particle diameter and random particle packing. Depending on the particle size, either a stable state is observed such that the particles can successfully form an arch, or an unstable state is observed such that the particles will continuously flow into the funnel throat without forming a stable arch. Examples of both the stable and unstable states for the 45° funnel are as shown in Figure 5.5.
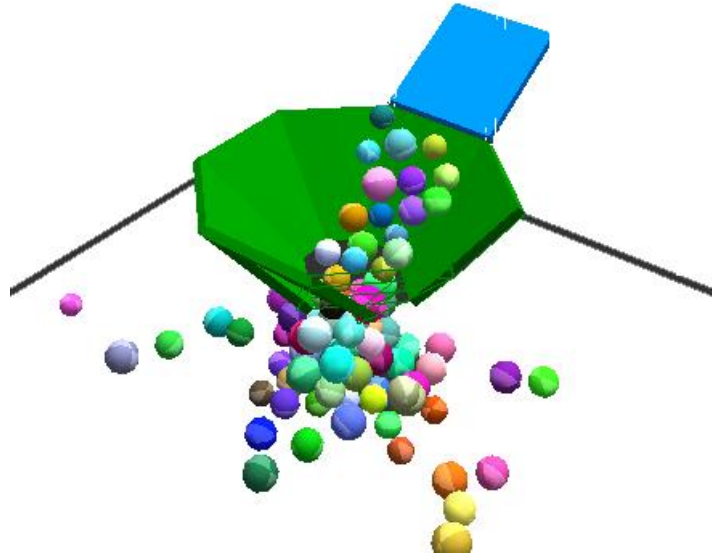
(a) Unstable state (small mean particle size relative to throat diameter)
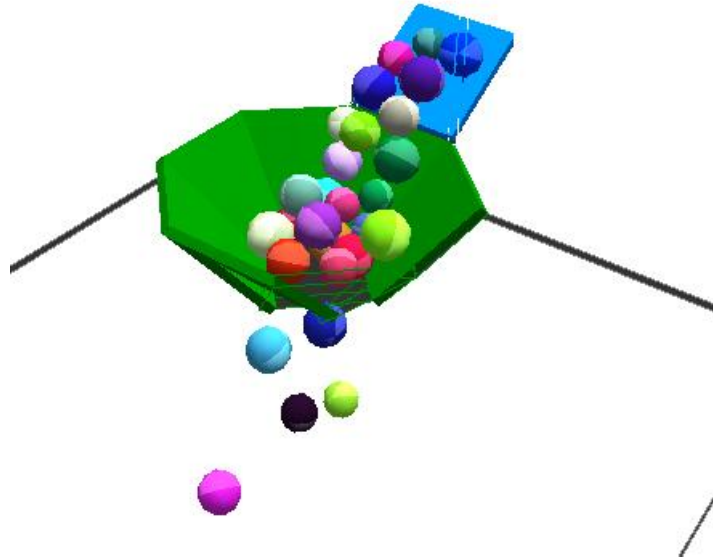
(b) Stable state (large mean particle size relative to throat diameter)
Figure 5.5 Examples of Unstable and Stable state

5.3 Discussion of results
5.3.1 Statistical definition of semi-stable state
Chen et al, (2006), observed in the 2D simulations that there is an intermediate range of d_m, within which the dumping of the particles can either be stable or unstable due to their initial random position and packing, i.e. there exists an intermediate range of particle diameters, relative to the throat diameter, for which arching may or may not develop, depending on the random nature of the particle sizes and position in the backfill. Simply increasing the particle mean diameter (relative to throat radius) does not provide a stepwise jump from unstable to stable, depending upon how the particles arrange or are dumped. A brief explanation in 2D is shown in Figure 5.6, where the same three particles are shown to form both a stable state and an unstable state, depending on their initial random positions. Such phenomena dictate that the prediction of the final stable/unstable state must be based on a statistical analysis, i.e. the outcome of the state should be described using a probability function. In structural engineering, a 5-percentile value is often used for the acceptance of material properties (Zureick et al. 2006), which would correspond for a 95-percentile value for stable sinkhole repair. The mean particle diameter for a 95% probability of stability is investigated here.
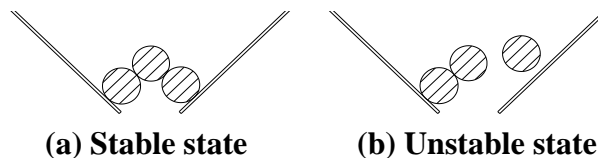
(a) Stable state   (b) Unstable state
Figure 5.6 Random stable and unstable particle arrangements for the same radius

5.3.2 Determine the semi-stable mean diameter using binary search method

Chen et al. (2006) performed a similar stability analysis in 2D, and used a constant value step of mean diameter Δd_m for the next calculation. Such step-by-step or "brute force" method is a time consuming approach to investigate the semi-stable range. In this paper, a binary search method (Knuth 1997) is applied during the process listed as follows:

Find a mean diameter value which can guarantee absolute stability, dm1, and a value which is absolute unstable, d_{m2};

(1)Start with the average of $d_{mi}=(d_{m1}+d_{m2})/2$, if d_{mi} value leads to unstable condition, then $d_{m1}=d_{mi}$, if d_{mi} value leads to stable, then $d_{m2}=d_{mi}$;

(2)Repeat Step (2) until the search approximately (see criterion below) where d_{mi} value cannot guarantee either stable or unstable.

The criterion for determining statistically stable/unstable:

For a calculated mean diameter d_{mi}, run the simulation with different random position/diameter N (e.g. 6) times, if most simulations (e.g. 5 out of 6) are stable, then the d_{mi} value is considered stable, if most simulations (e.g. 5 out of 6) are unstable, then the d_{mi} is considered unstable. When around half of the simulations are either stable or unstable, it is indicating d_{mi} is entering the semi-stable range.

The above binary search method greatly speeds up the search approach. As shown in Table 5.2, it only takes 7 trials of d_{mi} to find the semi-stable d_m value around 0.41. The results in Table 5.2 also demonstrate how the random nature of the particle assembly and filling process produces both stable and unstable configurations for the same value of d_m.

5.3.3 Regression analysis of the probability of the critical particle diameter

A logistic regression (Kutner et al. 2004) was performed based on the data obtained using the binary search as described in Section 8.1 using JMP (SAS Institute Inc. 2006), where π is defined as the probability of stability with respect to d_m, and the natural logarithm of the odds (which is referred to as logit) becomes:

$$logit = ln\left(\frac{\pi}{1-\pi}\right)$$

The resulting regression curves in Figure 5.7

Table 5.2 Example of running cases for stable/unstable for funnel inclined angle 70° (Stable=1, Unstable =0, each diameter value d_{mi} with 6 runs)

Trial	Mean Diameter (d_{mi})	Run No.					
		1	2	3	4	5	6
1	0.2	0	0	0	0	0	0
2	0.5	1	1	1	1	1	1
3	0.35	0	0	0	0	0	0
4	0.425	1	1	0	0	1	0
5	0.4625	1	1	1	1	1	1
6	0.44375	1	0	1	0	1	1
7	0.453125	1	1	1	0	0	1
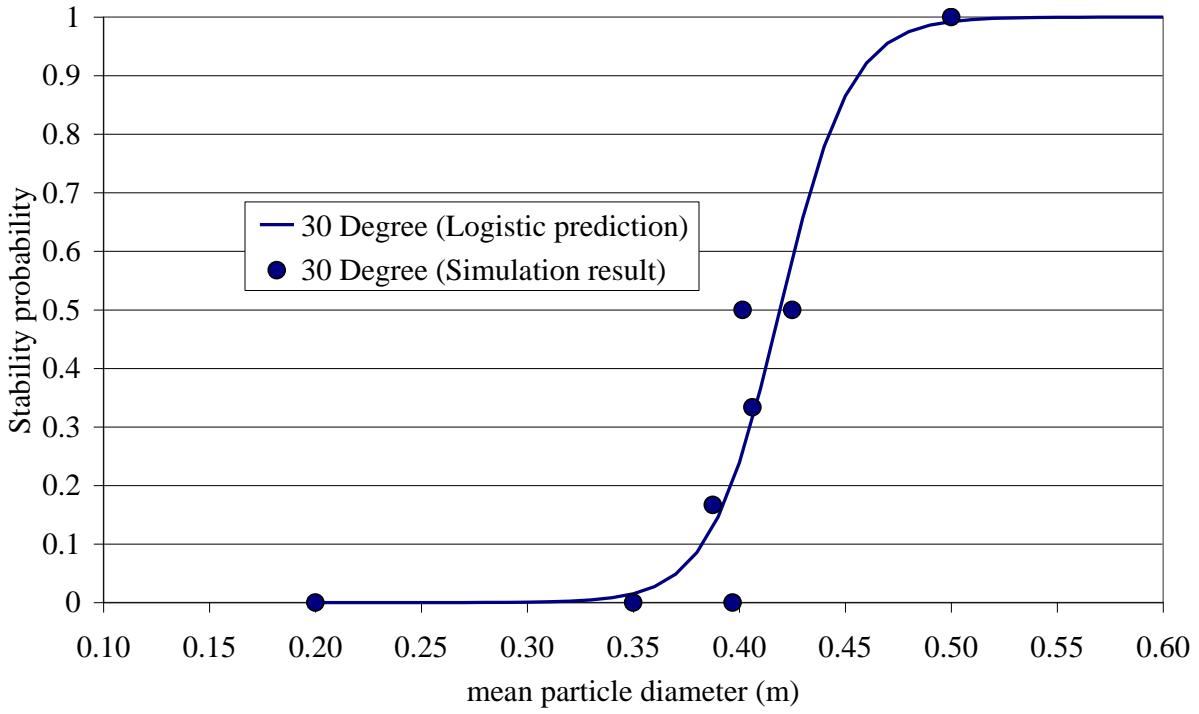
(a) Funnel Angle 30°
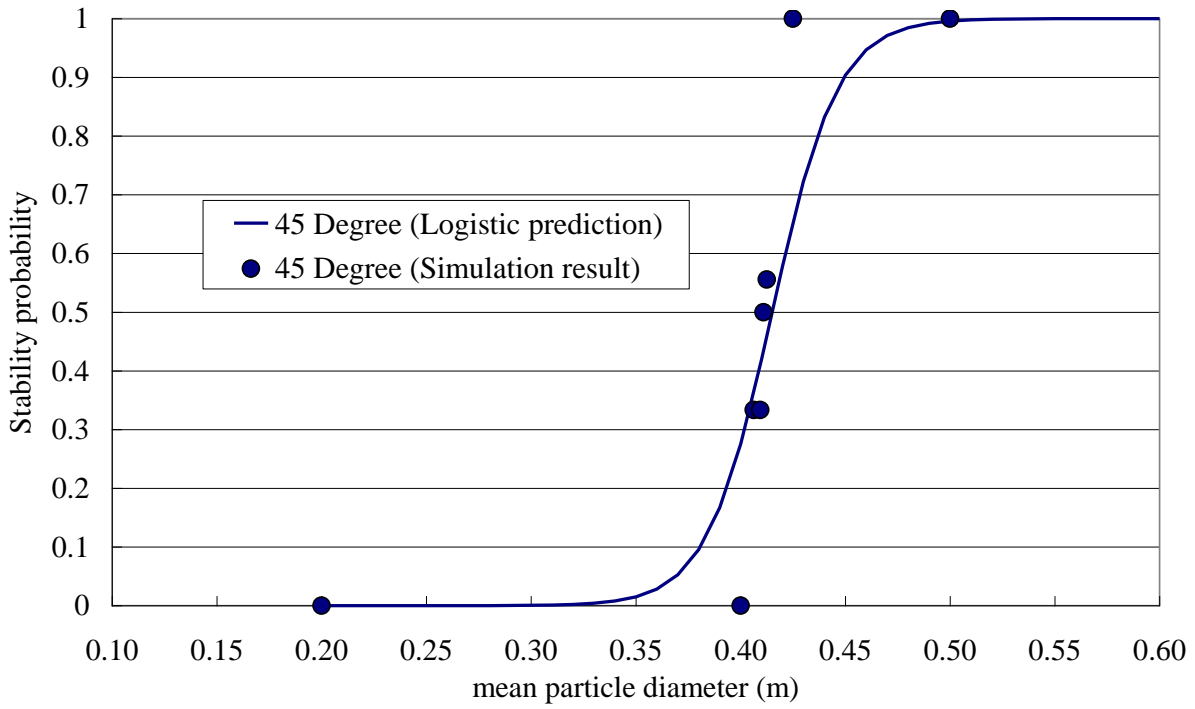
(b) Funnel Angle 45°
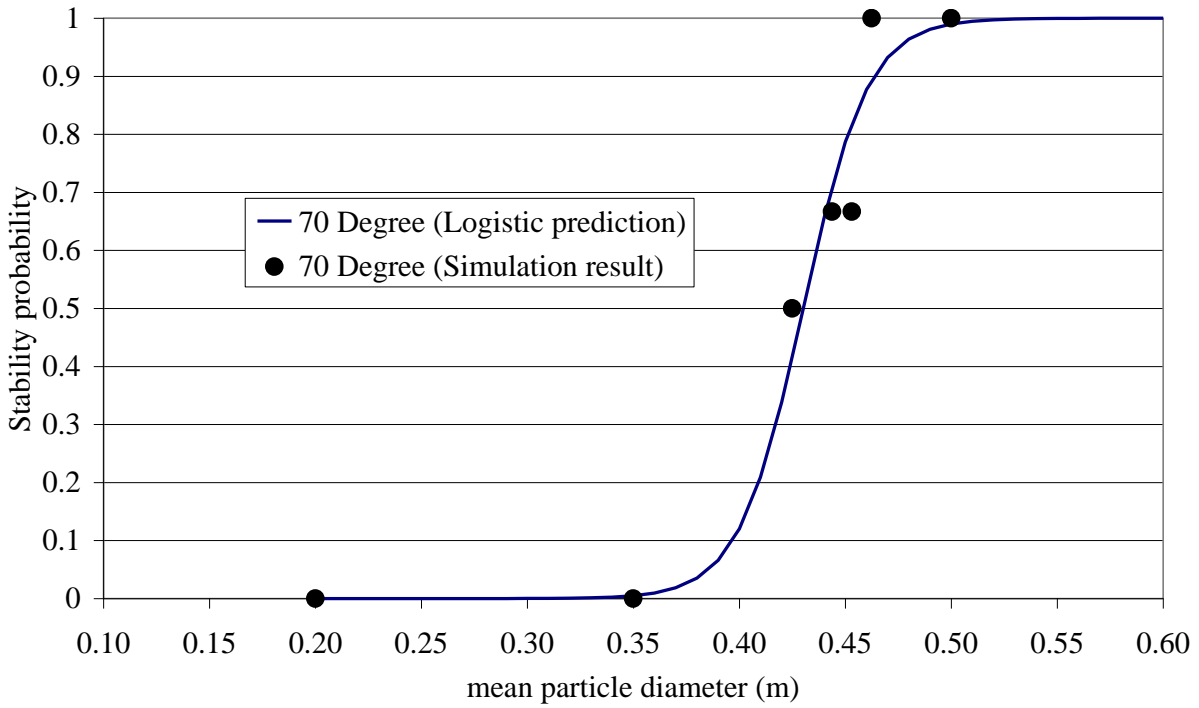
(c) Funnel Angle 70°

Figure 5.7 Logistic regression plot for simulation results from various funnel inclined angles (a) 30° (b) 45° (c) 70°
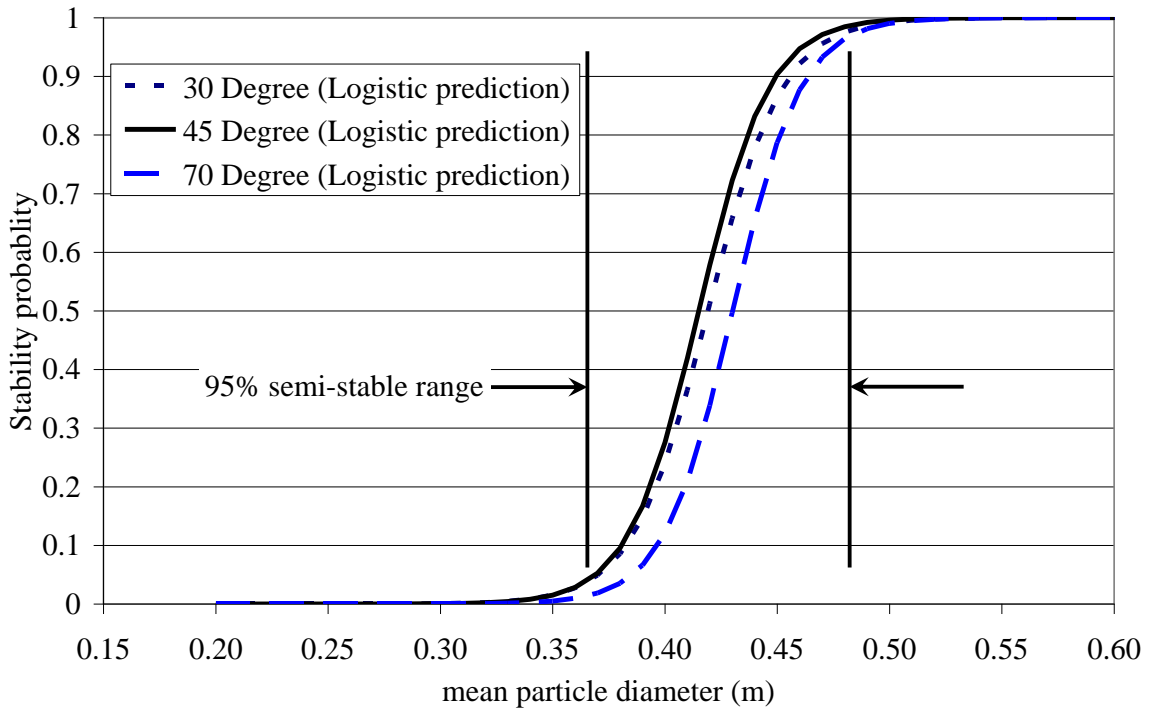
Figure 5.8 Comparisons of the stable probability curve for three funnel angles

show the transition from unstable to stable as the mean particle diameter increases, for funnel angles of 30°, 45° and 70°. The smooth curve is the predicted probability from the logistic regression, while the circle symbols are the probability of stability from the simulation for a given mean radius, e. g, From Table 5.2 for d_{mi}=0.44375, there are 4 success runs and 2 failure runs for the mean diameter 0.44375, thus the probability for stability is then 4/6=0.667. This regression suggests that for a 95% probability of a stable sinkhole repair, the mean particle diameter should be 0.468 for the 30° funnel, 0.461 for the 45° funnel and 0.475 for the 70° funnel. The mean diameter ratios for the 3 funnel angle are compared in Figure 5.8.

While additional runs could be performed to better determine the mean diameter as a function of the funnel angle, from a practical perspective the stability can be assumed to be independent of funnel angle. It can be concluded from Figure 5.8 that to obtain a 95% probability of stable arch, the mean particle diameter or diameter ratio for the 3 funnel angles is about 0.47. This relationship supports the empirical recommendation by Sowers (Sowers 1996) of using a diameter ratio greater than 0.5.

5.4 Closure

A series of discrete element simulations of the idealized placement of graded rock fill for sinkhole repair were conducted, and the stability was investigated for a range of mean particle diameters relative to the sinkhole throat diameter. The rock particles were idealized as spheres, with a ratio of maximum diameter to minimum diameter of 1.5, with each simulation using a new random assembly of particles. It is shown that there is a large (relative to the throat diameter) mean particle diameter that, although smaller than the throat size, will clog the throat or produce a stable plug. There is a small mean particle diameter which will not lead the formation of a stable plug. The investigation focused on the intermediate range of mean particle diameters between these two values which can be either stable or unstable depending on the initial random position and particle diameters.

Six simulations were performed at each mean particle size and the probability of producing a stable plug was determined. Three different funnel angles were investigated, and it was determined that the mean particle size for a 95% probability of stability was independent of funnel angle, and was about 0.47 times the sinkhole throat diameter, which compares favorably with the empirical value of 0.5.

The discrete element method appears to be a reasonable method to investigate the sinkhole repair procedure. Since the transition in mean particle size from a stable to an unstable assembly of particles is a continuous smooth function rather than a step function, the logistic regression is demonstrated as an appropriate means to estimate the mean size such that a stable repair can be determined with a 95% probability.

6 Coupled Discrete Element and Finite Volume Solution of Two Classical Soil Mechanics Problems

6.1 Introduction

The seepage flow through an assembly of saturated particles over a range of velocities or hydraulic gradients leading to a quick condition is a classic problem with application in soil mechanics, powder technology, and liquid chromatography. The one dimensional time rate dissipation of pore water pressure in a saturated layer of soil is a classic problem in soil mechanics, with a well-known analytical solution. When using numerical methods for problems of practical interest, it is helpful to have verification problems such as these for the investigation of parameter and mesh sensitivity. This is especially true when using methods such as the discrete element method (DEM), where many of the input parameters may not be well related to physical constants.

The discrete element method is an effective tool to simulate the behavior of granular soil particles while computational fluid dynamics provides a rational method to describe the fluid flow. Commercial codes are available for the analysis of coupled flow problems, however there are a number of advantages to open source software. In this paper, solutions are provided using a coupled pair of open source codes, YADE-OpenDEM for the discrete element method (Kozicki and Donzé 2008) and OpenFOAM for the computational fluid dynamics (OpenCFD Ltd 2008).

6.2 Theoretical background

In the solution of the coupled fluid flow and particle interaction, the fluid motion is treated on a macroscopic scale, while the particle motion is described on the microscopic scale, as suggested by Anderson and Jackson (T. B. Anderson and Jackson 1967).

6.2.1 Equations of motion for the fluid - the averaged Navier-Stokes equation

The fluid domain is divided into cells as is common in the finite volume method. The pressure and the fluid velocity are treated as the locally averaged quantity over the fluid cell. The equation of continuity is given as follows:

$$\frac{\partial n}{\partial t} + \nabla \left(nU \right) = 0 \tag{6.1}$$

where n=porosity; U=fluid velocity; t=time. The momentum equation is given as follows:

$$\frac{\partial nU}{\partial t} + \nabla \left(nUU \right) - \nabla \cdot \left(\mu \nabla U \right) = -\frac{n}{\rho_f} \nabla \left(p \right) + Q + f_P \tag{6.2}$$

where μ is the fluid viscosity, ρ_f is the density of fluid, f_P is the interaction force on the fluid per unit mass from the particle, p is fluid pressure and Q is an artificial viscosity term which is investigated subsequently and discussed in Appendix 6.A.

6.2.1.1 Interaction term acting on fluid field from the particle

The interaction term representing the effect of a particle on the fluid, f_P, for the averaged Navier-Stokes equation (T. B. Anderson and Jackson 1967), is given by Ergun (1952):

$$f_P = \frac{\beta}{\rho_f} \left(\bar{U}_P - U \right) \tag{6.3}$$

where $\bar{U}_P$ is the average particle velocity within a fluid cell, U is the fluid velocity and β is an empirical coefficient. For porosity n≤0.8,

$$\beta = \frac{\mu\,(1-n)}{d^2 n}\left[150\,(1-n) + 1.75\,\mathrm{Re}\right] \qquad (6.4)$$

while for n>0.8:

$$\beta = \frac{3}{4}C_D \frac{\mu\,(1-n)}{d^2}n^{-2.7}\,\mathrm{Re} \qquad (6.5)$$

where d is the particle diameter, and the Reynolds number Re is defined as:

$$Re = \frac{\left|\bar{U}_P - U\right|\rho_f nd}{\mu} \qquad (6.6)$$

and the drag coefficient C_D is:

$$C_D = \begin{cases} 24\left(1+0.15\,\mathrm{Re}^{0.867}\right)/\mathrm{Re} & \text{if } \mathrm{Re} \le 1000 \\ 0.43 & \text{if } \mathrm{Re} > 1000 \end{cases} \qquad (6.7)$$

6.2.2 Equations of motion for the particles:

For a particle in fluid, the equation of motion for a single particle is:

$$\ddot{y} = \left(f_G + f_B + f_D + f_C\right)/m \qquad (6.8)$$

where $\ddot{y}$ =acceleration of the particle; f_G =gravity force; f_B =buoyancy force; f_D =drag force; f_C =contact force; and m=mass of the particle. The inter-particle contact force f_C is obtained from the standard DEM approach as proposed by Cundall and Strack (1979). The drag force f_D is the interaction force acting on the particle from the fluid defined below.

6.2.2.1 Interaction drag force on the particle from the fluid

The drag force f_D is caused by the pressure gradient within the fluid cell and is obtained from the sum of the velocity difference between the particles and fluid, and may be written as:

$$f_D = \left\{\frac{\beta}{1-n}\left(U - \bar{U}_P\right) + \nabla p\right\}V_P \qquad (6.9)$$

where V_P is the volume of a single particle.

6.3 Coupling between YADE (DEM) and OpenFOAM (FVM) codes

Following the theory above, the particle phase is solved using the Discrete Element Method while the fluid phase is solved using the Finite Volume Method (FVM). The numerical solution was obtained by coupling two open source codes: the DEM code YADE (Kozicki and Donzé 2008) and the FVM computational fluid dynamics code OpenFOAM (OpenCFD Ltd 2008). In order to couple YADE and OpenFOAM, a customized YADE routine FluidDragForceEngine was written to wrap and incorporate the OpenFOAM fluid solver into the YADE main program as depicted in Figure 6.1.
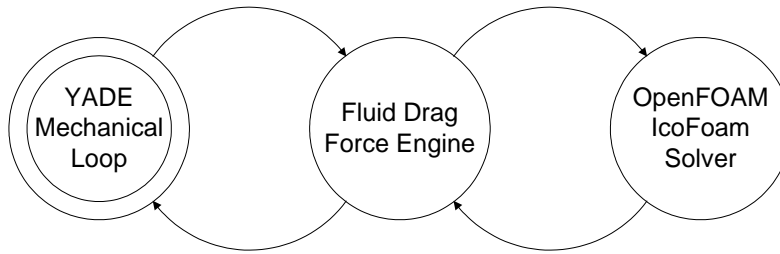
Figure 6.1 Framework of YADE and OpenFOAM coupling
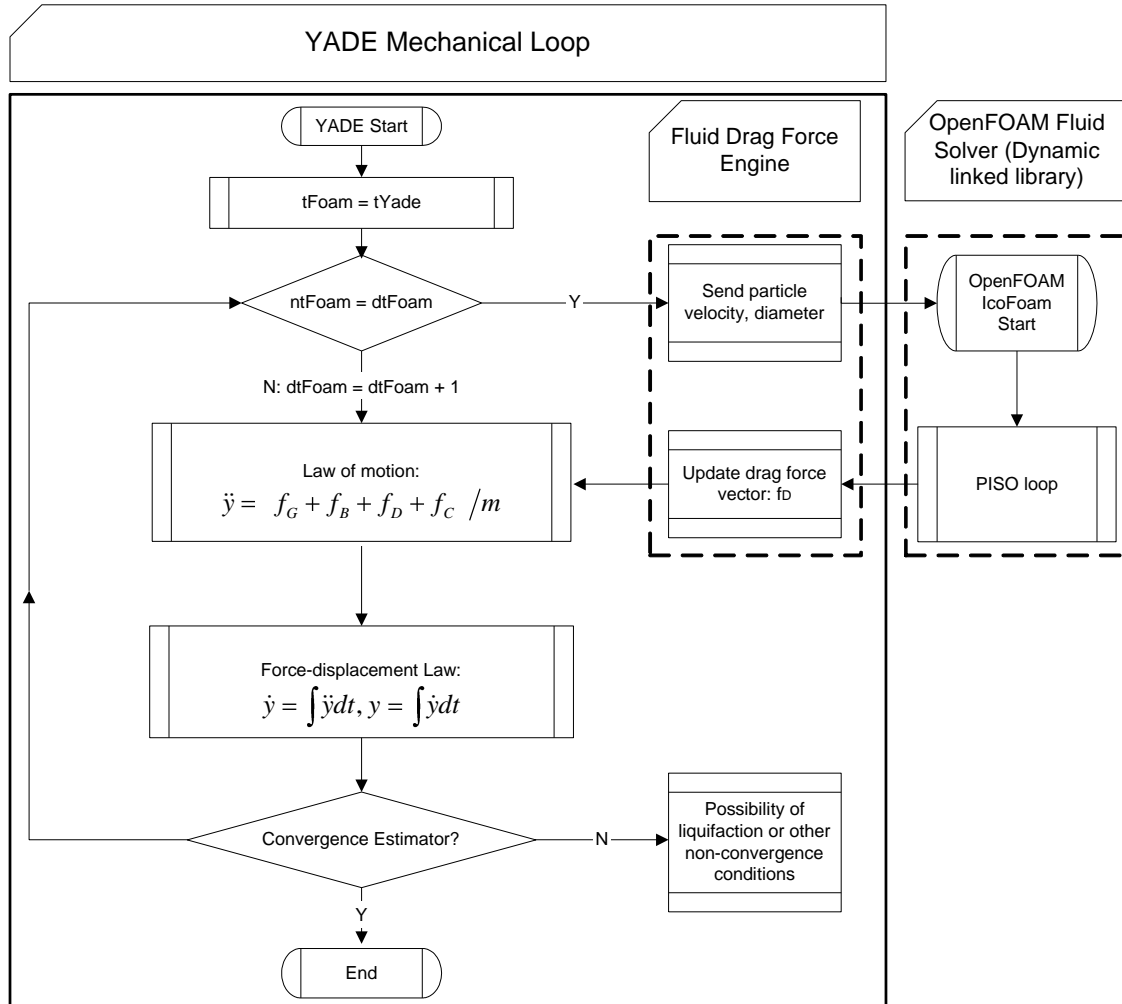
Figure 6.2 Detailed relationship of YADE-OpenFOAM algorithm

Details of the data transfer algorithm are as shown in Figure 6.2. The IcoFoam solver from OpenFOAM solves the incompressible laminar Navier-Stokes equations using the PISO algorithm (Issa 1986). A routine to check the maximum particle contact forces is added inside the convergence estimator. When the contact forces between particles are zero, a quick condition is reached within the particle assembly.

6.4 One dimensional fluid-particle model and two verification problems
6.4.1 Material and geometric properties of the one dimensional model
Two classical problems are investigated with the coupled DEM-FVM algorithm. Both problems are investigated using the same material properties and geometry, which is taken from the critical seepage flow problem investigated by Suzuki et al. (2007). The geometrical and physical particle properties are as listed in Table 6.1, and the boundary conditions are adjusted to investigate the two verification problems.

According to Terzaghi's one dimensional consolidation theory, the following assumptions are made:
(1) The soil is homogeneous, isotropic and fully saturated;
(2) The soil particles and the fluid are incompressible.
(3) The fluid flow is one dimensional.

Furthermore, it is assumed that the system can be represented by a series of equal radius spherical particles in a column of square cross section. A schematic of the one dimensional model configuration is as shown in Figure 6.3. Note that an extra fluid cell which does not contain particles is added at the top and bottom of the particle column to ensure continuity at the boundaries.

(a)   (b)
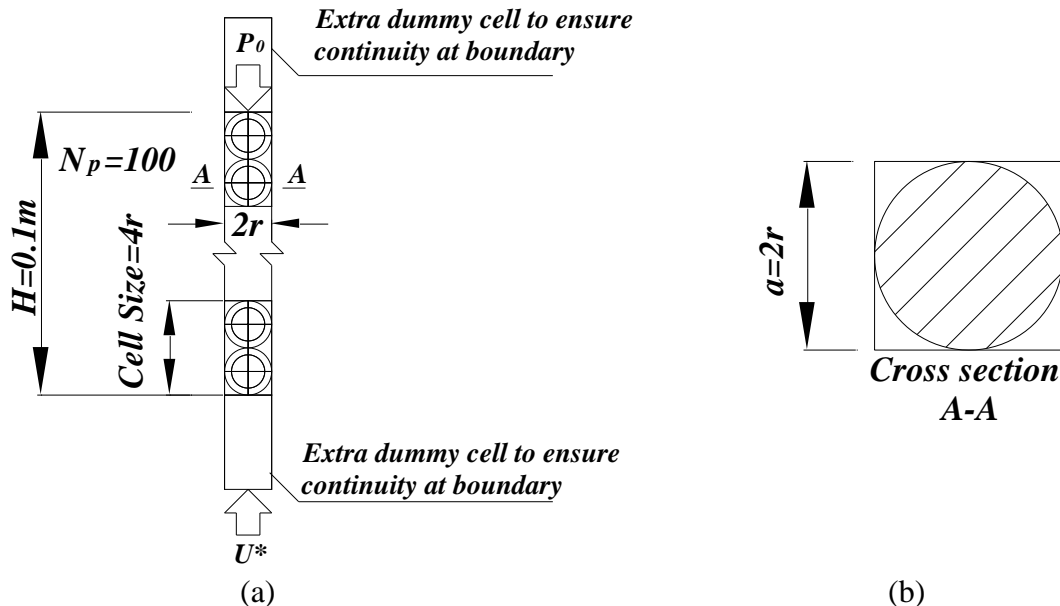
Figure 6.3 One dimensional particle column configuration, where Np = 100 = number of particles of radius r = 0.5 mm (a) elevation (b) cross section

Table 6.1 Physical and geometrical parameters for the 1D column. (Suzuki et al., 2007).

Parameter	Value	Unit
Solid (particle)		
Number, N_p	100	
Radius, r	5.0×10^{-4}	m
Density, ρ_s	2650	kg/m^3
Contact stiffness, k_n	100	N/m
Fluid (Water at 20°C, 1atm)		
Density, ρ_w	1000	kg/m^3
Viscosity, μ	0.984×10^{-3}	Pa-s
1D column configuration		
Width	1.0×10^{-3}	m
Height	0.1	m
Fluid cell size Δz	2.0×10^{-3}	m
Gravity constant	9.80665	m/s^2

Before the boundary velocity conditions are applied, the column undergoes a settling procedure so that the hydrostatic state is reached. The initial conditions are established in 2 steps:

(1) The 100 equal diameter particles are packed sequentially with no space or overlap in the vertical (or z) direction, with the water level above the topmost particle.

(2) The particles then settle to the hydrostatic state under influence of gravity and buoyancy forces, i.e. the consolidation under gravity and buoyancy force is completed.

The simulation will take the state after step (2) as the initial condition for the simulation.

6.4.2 Analytical solution for the two verification problems

Using the consolidation theory proposed by Terzaghi (1943), the one dimensional consolidation is expressed as:

$$\frac{\partial p}{\partial t} = C_v \frac{\partial^2 p}{\partial y^2} \tag{6.10}$$

where p=excess pore pressure and C_v=coefficient of consolidation which can be determined as described below.

The key parameter to estimate the dissipation of pore pressure lies in the determination of C_v. It can be derived using Ergun's empirical equation (Ergun 1952) in a packed column of height H:

$$\frac{\Delta p}{H} = \frac{1-n}{dn^3}\left\{150\frac{1-n}{d}\mu u^* + 1.75\rho_w u^{*2}\right\} \tag{6.11}$$

where u^* is the superficial velocity and ρ_w is the density of water which now replaces the fluid density ρ_f in Eq. (6.2).

The hydraulic gradient is:

$$i = \frac{\Delta h}{H} = \frac{\Delta p}{\rho_w g H} = \frac{1-n}{\rho_w g dn^3}\left\{150\frac{1-n}{d}\mu u^* + 1.75\rho_w u^{*2}\right\} \tag{6.12}$$

The permeability k_p can be obtained as:

$$k_p = \frac{u^*}{i} = \frac{\rho_w g u^*}{\frac{1-n}{dn^3}\left\{150\frac{1-n}{d}\mu u^* + 1.75\rho_w u^{*2}\right\}} = \frac{d^2 n^3 \rho_w g}{150\mu\,(1-n)^2 + 1.75d\,(1-n)\,\rho_w u^*} \quad \textbf{(6.13)}$$

For the consolidation model, the final superficial velocity for the consolidation model is zero and Eq. (6.13) reduces to the Kozeny–Carman equation (Warren et al. 2005) Eq. (6.14):

$$k_p = \frac{d^2 n^3 \rho_w g}{150\mu\,(1-n)^2} \tag{6.14}$$

Using the particle and fluid parameters listed in Table 3, due to the slightly different porosity values in the two problems, the permeability coefficient k_p is found to be 0.0248m/s for the consolidation model and 0.0224m/s for the upward seepage model (for u*=0.005m/s). The coefficient of consolidation is:

$$C_v = \frac{k_p}{\rho_w g m_v} \tag{6.15}$$

Where m_v is the coefficient of volume change:

$$m_v = \frac{\Delta\varepsilon_v}{\Delta\sigma_v} \tag{6.16}$$

The m_v can be determined using the contact spring constant k during the settlement stage for gravity and buoyancy force, the vertical strain:

$$\Delta\varepsilon_v = \frac{\delta}{H_0} = \frac{N\,(N+1)}{2H_0}\frac{f_G - f_B}{k} \tag{6.17}$$

where δ is the displacement of the topmost particle, N = the number of particles, and H_0 is the initial length of the column prior to the application of gravity and buoyant forces.
The vertical stress:

$$\Delta\sigma = (1-n)\,(\rho_s - \rho_w)\,g\frac{H_0}{2} \tag{6.18}$$

where ρ_s is the density of the particles. The coefficient of volume change is then determined as 1.01×10^{-5}m^2/N. The coefficient of consolidation is then 0.25 for the consolidation model and 0.224 for the upward seepage model (u*=0.005m/s).

6.4.3 Analytical solution for ground surface (topmost particle) movement
It is convenient to define the non-dimensional time factor T_v as from Lambe and Whitman (1969):

$$T_v = \frac{C_v t}{H^2} \tag{6.19}$$

The solution for Eq. (6.10) is then taken from literature as listed below:
 (a) Upward seepage flow:
The swelling from the ground surface (uplift of the topmost particle for the column assembly) is taken from Suzuki (2007):

$$S_{ct} = \frac{u^*}{C_v} \frac{H^2}{2} \left(1 - \frac{32}{\pi^3} \sum_{m=0}^{\infty} \frac{-1^m}{2m+1^3} \exp\left(\frac{-2m+1^2 \pi^2}{4} T_v \right) \right)$$ **(6.20)**

(b) Consolidation:

The consolidation settlement due to the applied loading corresponds to the displacement of the top particle in the column. The analytical solution for consolidation ratio U_z is (Taylor 1948):

$$U_z = \frac{S_{ct}}{S_c} = 1 - \frac{P_t}{P_0} = 1 - \frac{8}{\pi^2} \sum_{m=1,3,5,...}^{\infty} \frac{1}{m^2} \exp\left(-\frac{m^2 \pi^2}{4} T_v \right)$$ **(6.21)**

where: U_z is the consolidation ratio, P_t is the excess pore pressure at time t, P_0 is the initial excess pore pressure, S_{ct} is the surface settlement at time t, S_c is the final settlement.

6.4.4 Initial and boundary conditions for the two verification problems

(a) Upward seepage flow:

For the upward seepage flow problem, the initial conditions for p:

$$p \ z,0 \ = 0$$ **(6.22)**

The boundary condition at the top of the column ($z = 0$) for arbitrary time t:

$$p \ 0,t \ = 0, \ \left. \frac{\partial p}{\partial z} \right|_{z=H} = \gamma_w \frac{u^*}{k}$$ **(6.23)**

(b) Consolidation:

For the consolidation problem, the initial conditions for p corresponding to single drainage from the top of the layer are:

$$p \ z,0 \ = P_0$$ **(6.24)**

The boundary condition for arbitrary time t:

$$p \ 0,t \ = 0, \ \left. \frac{\partial p}{\partial z} \right|_{z=H} = 0$$ **(6.25)**

Solution for Eq. (6.10) can be obtained through a numerical approximation such as the Crank-Nicolson method (J. Anderson 1995).

6.5 Numerical Solutions to the Two Verification Problems

6.5.1 Upward seepage flow problem

Starting from the initial condition as shown in Figure 6.3, Suzuki et al. (2007) investigated three different values of the upward superficial velocity at the bottom of the column: u*=0.005m/s, 0.01m/sec, and 0.018 m/s (the velocity leading to the quick condition). The displacement of the topmost particle for the three velocities and the excess pore water distribution are then determined and compared. Below the critical hydraulic gradient, the particle assembly will reach a convergent state or steady state. When the critical gradient is reached, although a solution for pressure or displacement can be obtained, the particle system will not reach a steady-state.
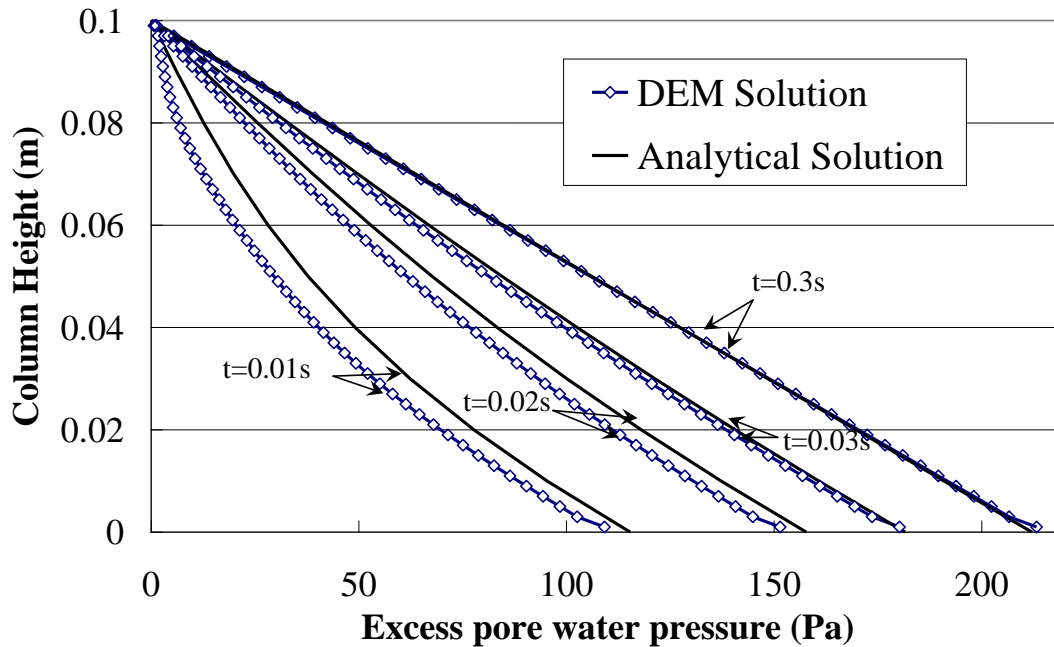
Figure 6.4 Excess pore water pressure distribution for input velocity of 0.005m/s

6.5.1.1 Early stage excess pore water pressure distribution

Figure 6.4 shows the excess pore water pressure distribution along the column for various times leading to the steady state pressure at t = 0.3 seconds. Both the analytical solution and the simulation are shown and are in close agreement. The simulation results were obtained with the addition of an artificial viscosity correction to the momentum equation, which is needed to stabilize the early stage pressure solution, as described in Appendix 6.A.

6.5.1.2 Upward displacement of the uppermost particle

The comparison between the analytical solution and the DEM solution with an input velocity of u*=0.005 m/s for times t=0.01s, 0.02s, 0.03s, 0.06s, 0.1s is shown in Figure 6.5. The DEM solutions agree well with the analytical solution.
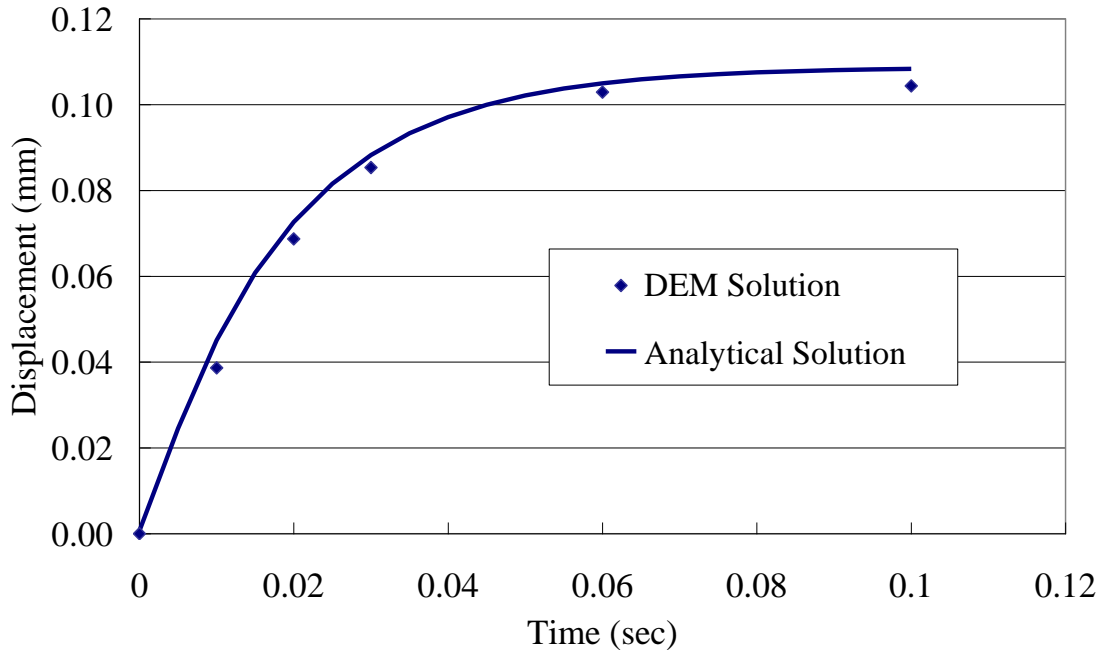
Figure 6.5 Comparison of the analytical and DEM solutions for upward displacement versus time in the seepage flow problem, input velocity = 0.005 m/s

6.5.1.3   Steady state displacement of the uppermost particle in the column

The surface displacement of the top of the column, or uplift of the uppermost particle due to the upward flow, is taken as the change in displacement of the uppermost particle between the initial hydrostatic conditions and the steady state displacement. Table 6.2 compares the analytical and numerical results given by Suzuki et al. (2007), with the numerical results from the coupled open source YADE-OpenFOAM for the three levels of input velocity, 0.005m/s, 0.010m/s and 0.018m/s (critical value). Also shown for comparison are the results from the commercial code PFC2D (Itasca Inc. 2004b). The computed excess pore pressures at the bottom of the column are also shown. It can be concluded that the three numerical solutions yield very similar results and all agree well with the analytical solutions. Note that the input velocity 0.018m/s is the critical value leading to a quick condition and therefore the analytical solution for the surface displacement is not valid and the DEM solution for bottom excess pore water pressure is just an approximation.

Table 6.2 Comparison of surface displacement and bottom pressure for analytical and numerical solutions

Inlet velocity (m/s)	Surface displacement (10^{-3}m)				Bottom excess pore water pressure (Pa)			
	Analytical	YADE-OpenFOAM	PFC2D	Suzuki et al. (2007)	Analytical	YADE-OpenFOAM	PFC2D	Suzuki et al. (2007)
0.005	0.1087	0.1070	0.1061	0.1050	217.0	213.2	210.3	212.2
0.010	0.2381	0.2352	0.2336	0.2320	476.1	465.3	461.5	460.8
0.018*	0.4870	2.8966	3.1779	3.5300	847.6	898.3	841.6	838.3

* Critical velocity at which the system becomes quick, computed values may not be valid.

6.5.2 Consolidation problem

6.5.2.1 Early stage excess pore water pressure distribution

Starting from the same initial hydrostatic conditions as in the first problem, a surcharge load P0=200Pa is applied at the top of the column (Note the load is applied to the topmost particle with a downward force of $F=P_0 \times CrossSectionalArea=2\times10^{-4}N$). The column settles under this surcharge load and the pore water pressure distributions are computed for various times. Figure 6.6 compares the YADE-OpenFOAM and analytical (Eq. (10)) solutions for the excess pore water pressure distribution during the consolidation process. Results are shown for times of t=0.0055, 0.0155, 0.0255, 0.0355 seconds, which correspond to values of T_v and U_z as shown in Table 6.3. The computed results for t = 0.0055 seconds are very early in the solution process and are assumed to correspond to conditions at time T_v=0 in the classical solution. The coupled DEM solution reflects the general time rate dissipation of pore water pressure very well over the entire consolidation process.

Table 6.3 Selected intermediate consolidation times and consolidation ratios

Time (sec)	T_v	U_z
0.0055	0	0
0.0155	0.25	0.56
0.0255	0.5	0.76
0.0355	0.75	0.87
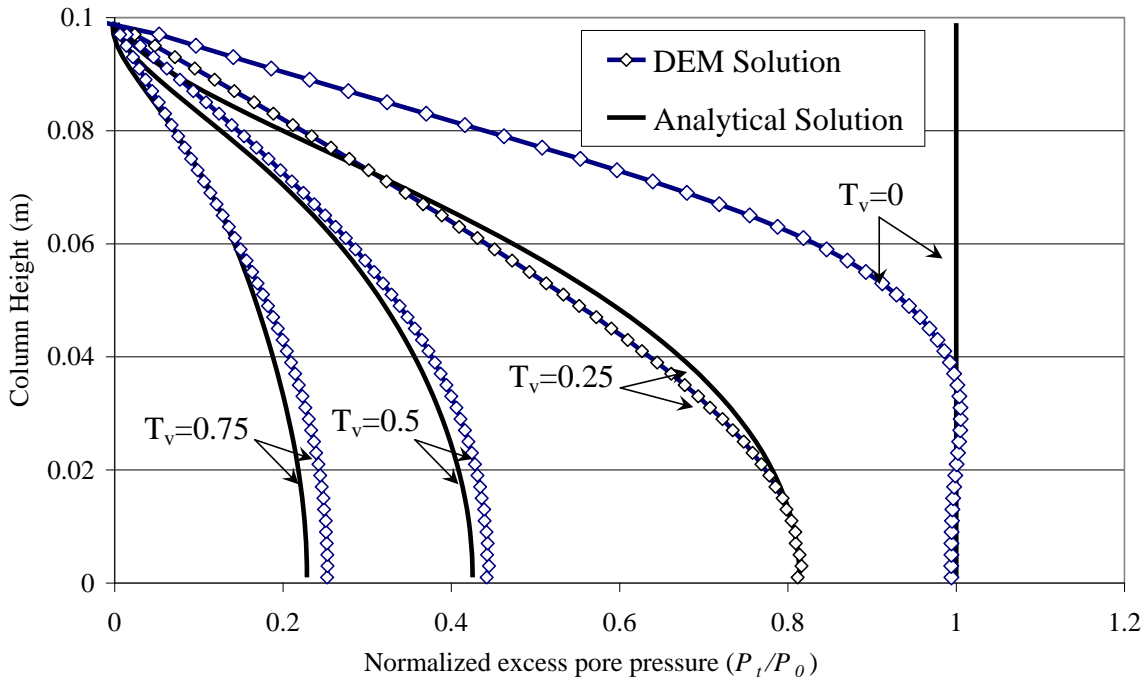
Figure 6.6 Comparison of DEM and analytical solutions for excess pore water pressure dissipation during consolidation for time of 0.0055, 0.0155, 0.0255, 0.0355 seconds, corresponding to T_v=0, 0.25, 0.5, 0.75, respectively. The excess pore water pressure normalized with respect to the initial pore water pressure, P₀=200Pa
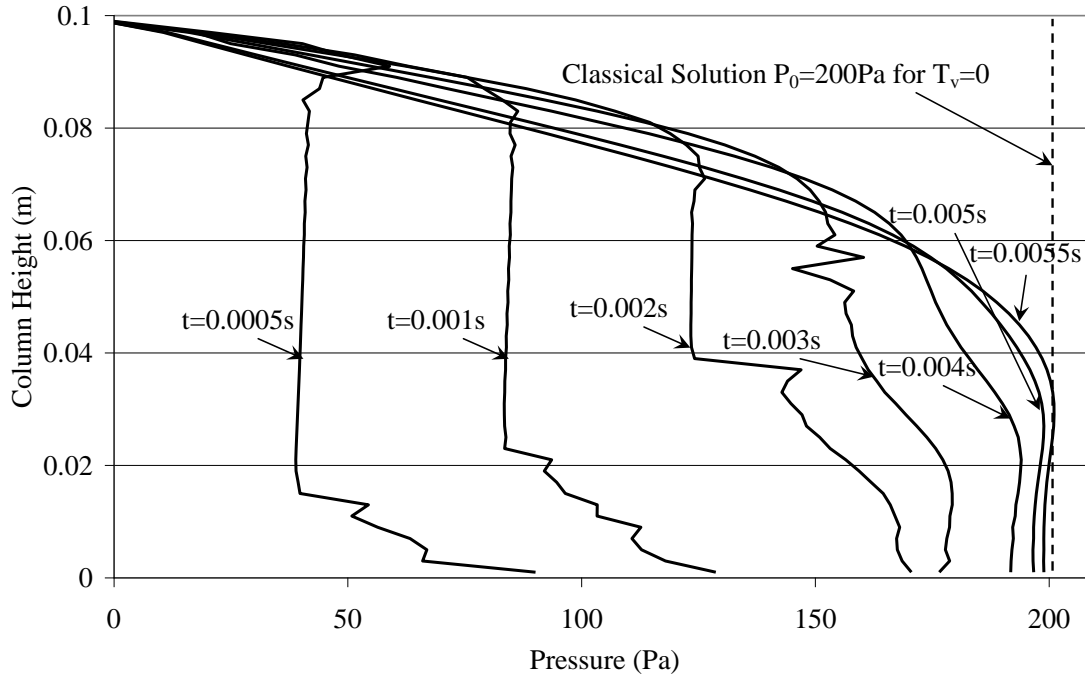
Figure 6.7 Development of excess pore pressure immediately after application of load

In the classical solution, it is typically assumed that the pore pressure instantaneously increases throughout the layer to the value equal to the applied stress in the porous layer. Thus for the verification problem, the classical solution would suggest a uniform value of excess pore pressure equal to P_0=200Pa at all points in the layer, as shown in Figure 6.6 by a normalized excess pore pressure equal to 1.0. While not of practical interest, the numerical simulation allows the prediction of the pore pressure buildup at very early times to be observed. Figure 6.7 shows the computed pore pressure distributions at times of t=0.0005 seconds through 0.0055 seconds, where 0.0055 seconds is the earliest time for which results were shown in Figure 6 (corresponding to T_v=0). The computed results at these early times show the nearly uniform build up of pore pressure at the internal portions of the layer, while the pore pressures remain zero at the upper edge consistent with the imposed boundary conditions.

6.5.2.2 Consolidation settlement calculation

The comparison between the analytical solution and the DEM solution for the settlement versus time is shown in Figure 6.8. The DEM solutions agree well with the analytical solution. Note that the DEM solution for "Time=0" seconds in Figure 6.8 corresponds to the T_v=0 in Figure 6.6 and Figure 6.7, indicating that there is some computed settlement that takes place during the development of the initial excess pore pressure.
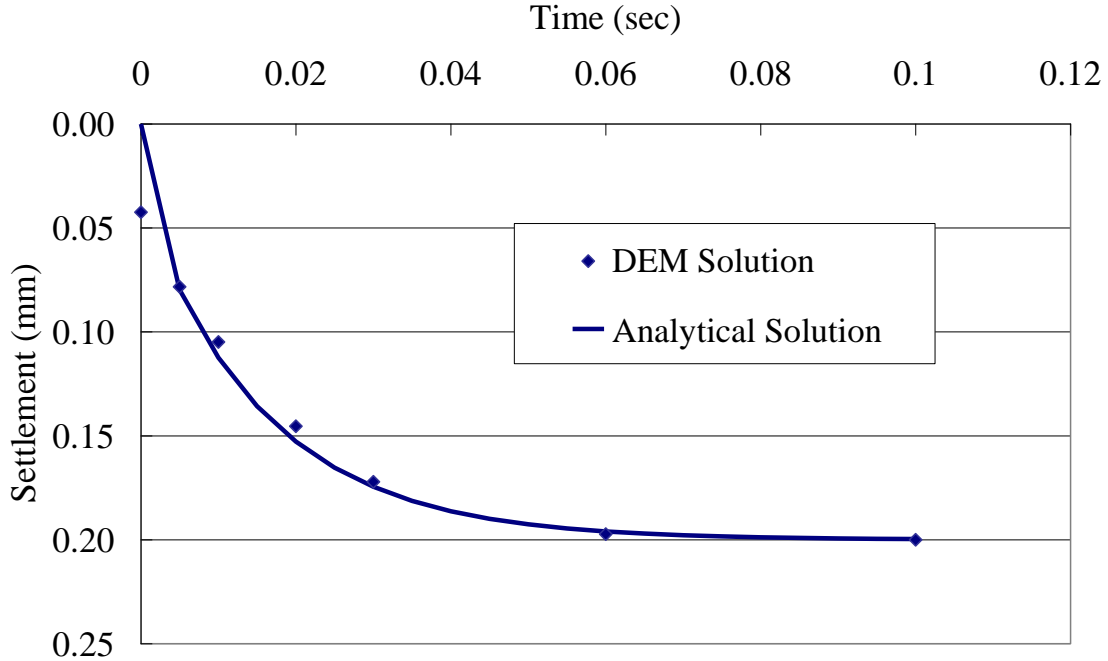
Figure 6.8 Comparison of consolidation time-settlement plot between analytical and DEM solution

6.6 Parametric effects on the results

Several parameters are significant to the transient behavior of the column during the early stages of the solution (prior to reaching the final steady state), including:

(1) Viscous damping coefficient;

(2) Number of DEM mechanical time step per FVM fluid time step;

These are discussed below.

6.6.1 Damping effects

Damping does not affect the final steady state of the particle assembly. However, it can greatly affect the early transient behavior of the fluid-particle system prior to reaching the steady state. There are two basic types of damping considered in most DEM formulations (Itasca Inc. 2004a): local damping and viscous damping. Local damping is not relevant for the two problems investigated here since the particles are in motion under gravity and particle impact. Viscous damping is present whenever particles contact (with or without the presence of the fluid). The equation of motion for a vibrating system with a viscous dashpot can be expressed as (Tsuji et al. 1993):

$$my'' + \eta y' + k_n y = 0 \tag{6.26}$$

Where y, y', y'' are the displacement, velocity and acceleration of the particle, m=particle mass, η= viscous damping coefficient, k_n = spring stiffness. From the theory of vibrations (Thomson 1993), the critical damping coefficient is:

$$\eta_{crit} = 2\sqrt{k_n m} \tag{6.27}$$

70
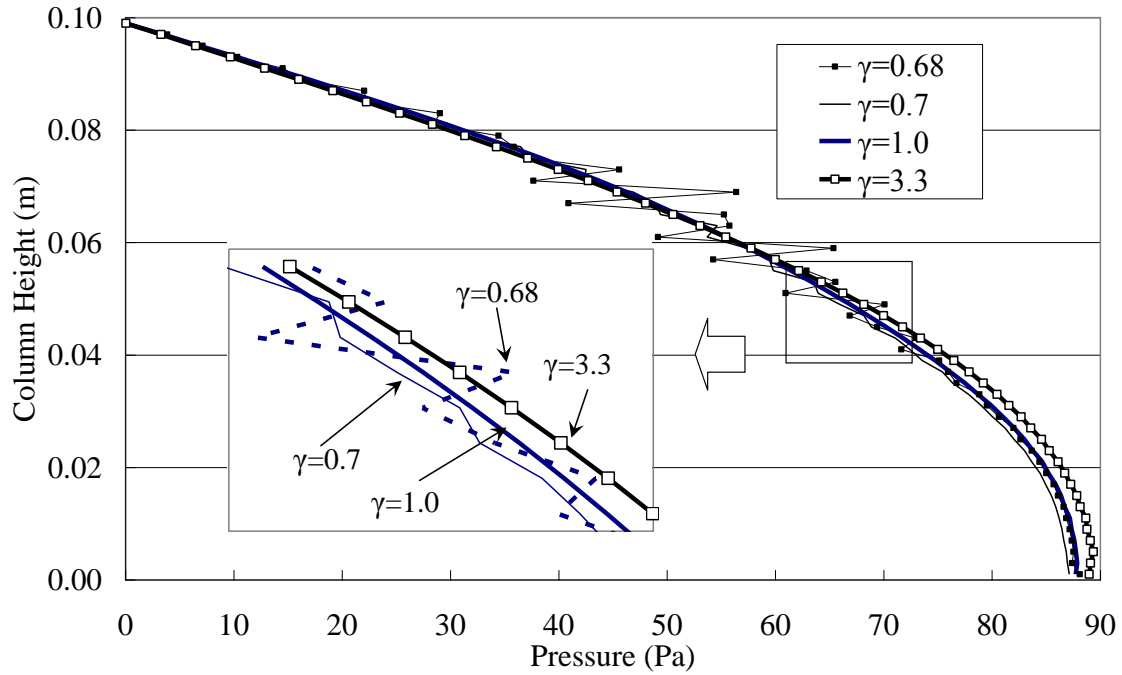
Figure 6.9 Effect of viscous damping coefficient γ on pressure curve for the consolidation problem, t = 0.0255s

The viscous damping coefficient γ is the ratio of the system damping to the critical damping coefficient:

$$\eta = \gamma \eta_{crit} \tag{6.28}$$

While $\gamma=1$ indicates the critical damping, $\gamma<1$ indicates the system is under damped, and $\gamma>1$ indicates the system is over damped.

Figure 6.9 compares the pressure distribution along the column in the consolidation problem for three values of viscous damping coefficient γ for t=0.0255 ($T_v=0.5$) seconds. From this graph, it can be concluded that a reasonable pressure curve is obtained provided that γ is greater than 1.0.

Figure 6.10 compares the effect of viscous damping coefficient γ on the pressure curve for the upward seepage problem ($t=0.01s$, $u^*=0.005m/s$). It is observed that $\gamma=3.3$ yields a more reasonable pressure profile than $\gamma=1.0$. To ensure good agreement with the classical solution, a large viscous damping coefficient is required. For both verification problems, a value of $\gamma= 3.3$ was used, which means the motion of the particles is non-periodic and will quickly reach its equilibrium state, which is probably appropriate in most geomechanical problems. A damping coefficient of $\gamma=3.3$ was chosen because that was the greatest damping that could be applied without the solution diverging.
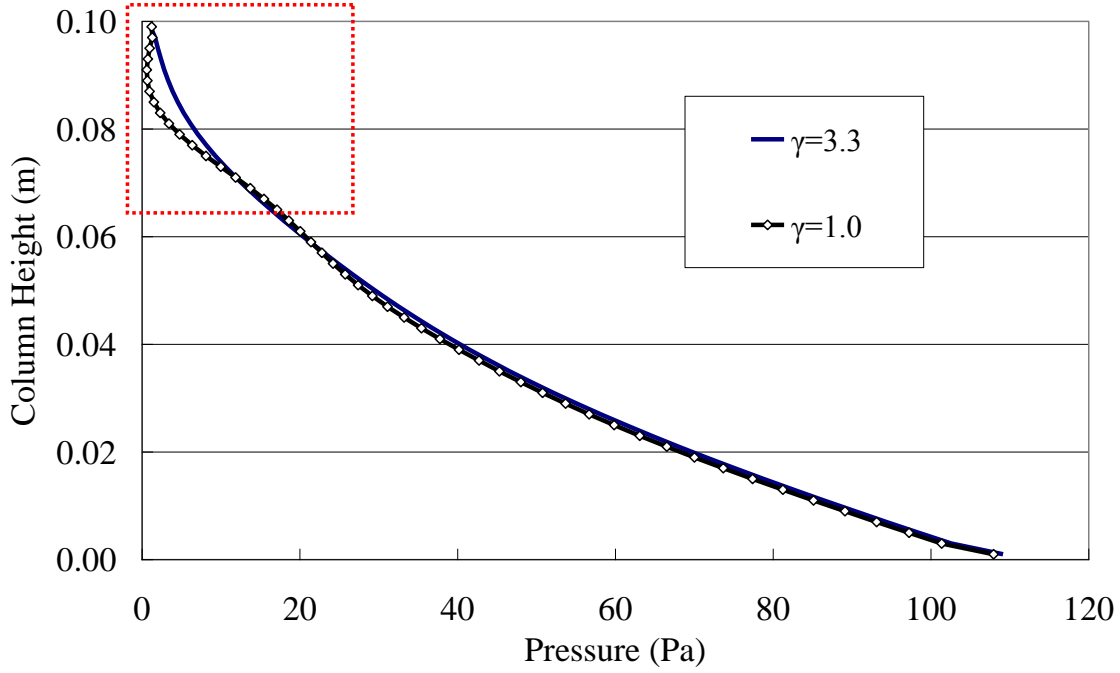
Figure 6.10 Effect of viscous damping coefficient γ on pressure curve for the upward seepage problem, t=0.01s, u*=0.005m/s

6.6.2 Effect of Number of DEM steps per Fluid step

For each computational fluid step, there should be a certain number of mechanical time steps to ensure the solid phase is relatively "stable" with respect to the fluid phase. The number of time steps in the DEM solution relative to the number of time steps in the FVM solution process, is abbreviated as NDF. The appropriate NDF value will be dependent upon characteristics of both the solid phase and the fluid phase.

For the solid phase, the DEM method requires a time step no greater than the critical time step (Itasca 2004):

$$t_{crit\_DEM} = \sqrt{\frac{m}{k}} \qquad (6.29)$$

Any time step larger than the critical time step will quickly lead to numerical instability and the particles will "explode" (fly into space).

For the fluid phase, the time step is restricted by the Courant number, Co:

$$Co = \frac{\delta t |U|}{\delta x} < 1 \qquad (6.30)$$

Therefore, the critical time step from FVM can be derived as:

$$t_{crit\_FVM} = \delta t < \frac{\delta x}{|U|} \qquad (6.31)$$
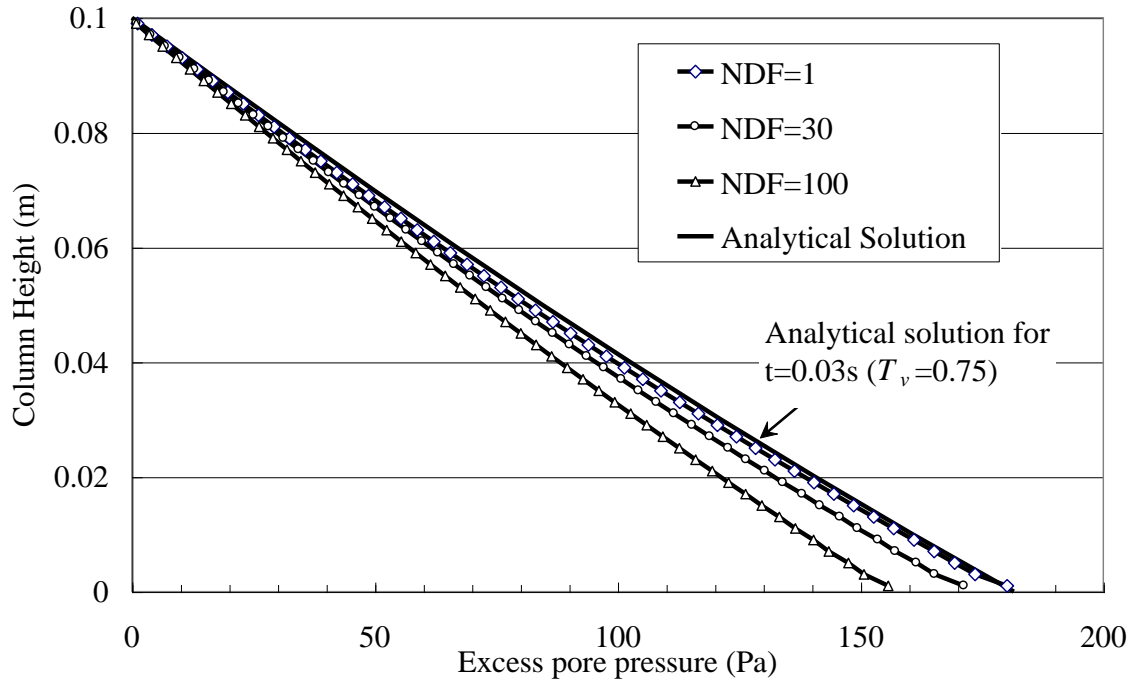
Figure 6.11 Comparison of different NDF value of pressure profile for t=0.03s corresponding to Tv=0.75 for the upward seepage problem with input velocity of velocity of 0.005m/s

For most problems this will lead to a value of NDF $\geq$ 1, which can also provide some computational efficiency. For the solutions presented above, a value of NDF = 1 was used. In general, small values of NDF (such as the value of NDF = 1 used here) produce oscillations in the computed pressure and require the use of the artificial viscosity term as discussed in Appendix 6.A. Large values of NDF (e.g. NDF =100 for the problems investigated here) reduces these pressure oscillations but tends towards a solution which may not be accurate.

Figure 6.11 shows a comparison of the computed pressure profile using different NDF values for t=0.03s in the upward seepage problem with an input velocity of 0.005m/second. As NDF increases above 1, the solution is found to deviate from the result with NDF=1, which agrees well with the analytical solution.

6.6.3 Discussion of different fluid properties

In this section, the pore water pressure distribution and the particle displacements corresponding to the steady state are investigated for different fluid properties. Keeping other parameters constant, 12 different fluids (Table 6.4) with a wide range of viscosity are selected for simulation. The bottom inlet velocity is fixed at 0.005m/s, and the bottom pressure values and the top particle displacement with respect to the hydrostatic position are determined and compared in Table 6.5. Note that with the exception of sulfuric acid, which has a density of 1840kg/m^3, the selected fluids all have similar density (ranging from 780-1100kg/m^3) such that differences in the particle displacements and pressures are primarily due to the influence of fluid viscosity.

Table 6.4 Selected fluid properties in order of increasing viscosity (after (Lide 1992)).

Type of fluid	Density (kg/m^3)	Viscosity @25°C (Pa-s)
acetone	790.0	0.306×10^{-3}
methanol	791.8	0.544×10^{-3}
benzene	878.6	0.604×10^{-3}
water	1000.0	0.894×10^{-3}
ethanol	789.0	1.074×10^{-3}
nitrobenzene	1199.0	1.863×10^{-3}
propanol	803.4	1.945×10^{-3}
blood*	1060.0	4.000×10^{-3}
ethylene glycol	1113.2	1.610×10^{-2}
sulfuric acid	1840.0	2.420×10^{-2}
cyclohexanol	968.0	4.107×10^{-2}
olive oil	920.0	8.100×10^{-2}

Table 6.5 Top particle displacement (m) and bottom pressure of different type of fluids (Pa)

Type of fluid	Top particle displacement (m)			Bottom pressure (Pa)		
	Analytical	PFC2D	YADE-OpenFOAM	Analytical	PFC2D	YADE-OpenFOAM
acetone	3.8494×10^{-5}	3.7241×10^{-5}	3.8421×10^{-5}	76.55	73.80	76.34
methanol	6.1787×10^{-5}	6.0021×10^{-5}	6.1676×10^{-5}	122.86	119.40	122.51
benzene	6.8596×10^{-5}	6.6189×10^{-5}	6.8482×10^{-5}	136.40	131.01	136.01
water	1.0867×10^{-4}	1.0609×10^{-4}	1.0886×10^{-4}	216.81	210.27	216.17
ethanol	1.1358×10^{-4}	1.0947×10^{-4}	1.1339×10^{-4}	225.87	216.61	225.10
nitrobenzene	1.9519×10^{-4}	1.8680×10^{-4}	1.9494×10^{-4}	388.13	368.20	386.93
propanol	1.9891×10^{-4}	1.9099×10^{-4}	1.9859×10^{-4}	395.55	377.18	393.95
blood	4.0265×10^{-4}	3.8406×10^{-4}	4.0213×10^{-4}	800.69	756.01	797.20
ethylene glycol	1.5865×10^{-3}	3.2198×10^{-3}	4.0440×10^{-3}	3154.73	778.41	805.67
sulfuric acid	2.3864×10^{-3}	3.8145×10^{-3}	6.1443×10^{-3}	4745.49	414.86	416.22
cyclohexanol	4.0267×10^{-3}	3.8396×10^{-3}	4.8331×10^{-3}	8007.13	871.98	890.08
olive oil	7.9308×10^{-3}	4.0244×10^{-3}	5.0906×10^{-3}	15770.65	915.43	916.57
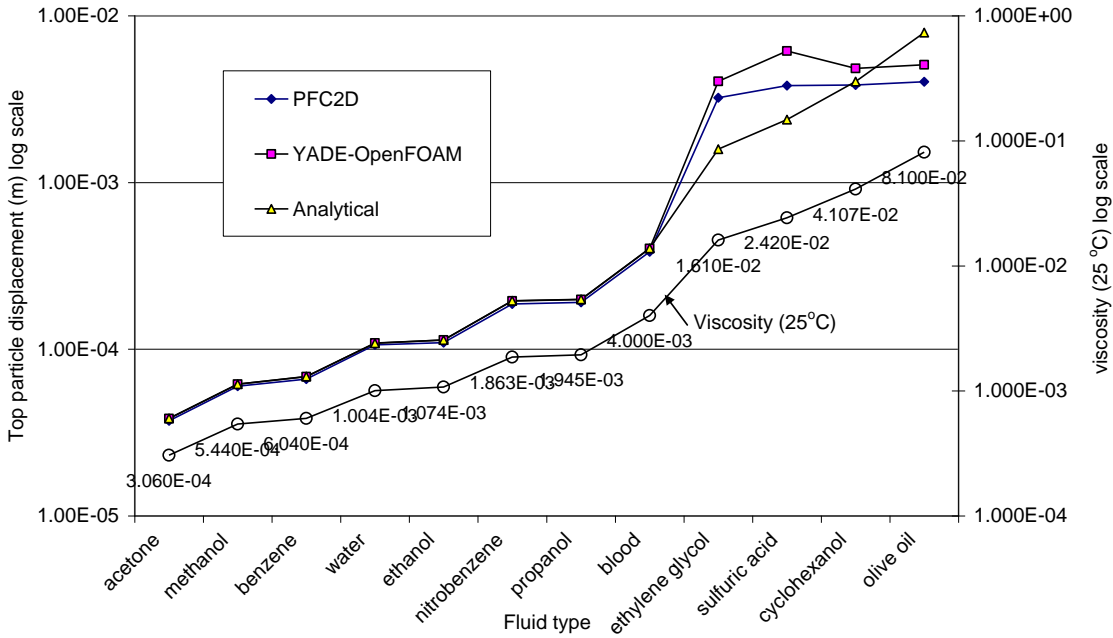
(a) Comparison of top particle displacement
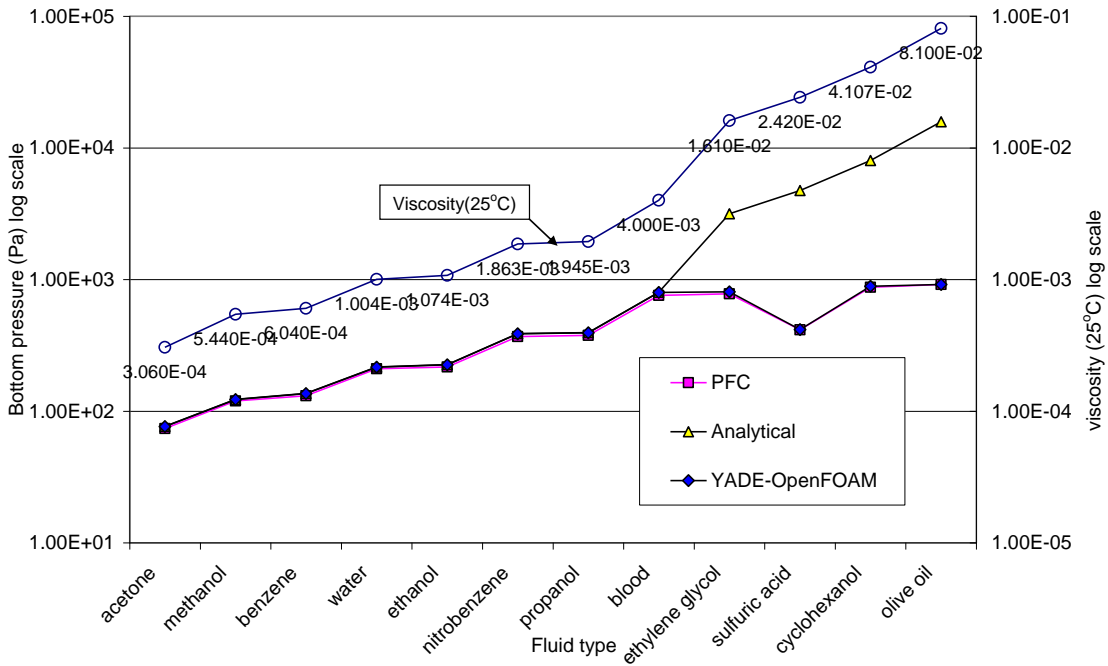
(b) Comparison of Bottom pressure.
Figure 6.12 Comparison between analytical and numerical solutions (DEM)

75

As shown from the comparison in Figure 6.12, the numerical (DEM) solutions agree well with the analytical solutions provided the viscosity is less than about 4.0×10^{-3} Pa-s (from acetone to blood). Above this value, (corresponding to sulfuric acid, ethylene glycol, cyclohexanol and olive oil) the numerical solutions differ significantly from the analytical solution. Such behavior can be explained from Eqn. (6.32), where the drag forces increase with increasing viscosity, reducing the particle contact forces. When the contact forces f_C approach zero, a quick condition results, and the equilibrium state from Eqs (6.8) yields:

$$f_D + f_B = f_G, \text{ or, } f_D = f_G - f_B \tag{6.32}$$

Substituting Eqn. (6.9) (the drag force at steady state) into Eqn. (6.32) written per particle volume, we have:

$$\frac{f_D}{V_P} = \frac{f_G - f_B}{V_P} = \frac{\mu\left[150\ 1-n\ +\dfrac{1.75u\rho_f nd}{\mu}\right]u^*}{d^2 n} + \frac{1-n\ \left[\dfrac{150\ 1-n\ \mu u^*}{d}+1.75\rho_f u^{*2}\right]}{dn^3} \tag{6.33}$$

The above equation can be simplified into the following relationship:

$$\frac{150\mu\ 1-n\ u^*}{d^2 n^3} + \frac{1.75\rho_f u^{*2}}{dn^3} = \ \rho_s - \rho_f\ g \tag{6.34}$$

Eqn. (6.34) indicates that for the single column particle assembly, for a fixed apparent velocity u*, when the relationship between fluid density and viscosity satisfies Eqn. (6.34), i.e., the sum of fluid drag force and buoyancy force equal the particle gravity force, the particle contact forces are zero. Therefore, with the inlet velocity of 0.005m/s, and a fluid density around 1000kg/m^3, when the viscosity exceeds about 0.001058 Pa-s, a quick condition exists.

6.7 Closure

A two phase flow system composed of fluid and solid particles was simulated using open source routines for the finite volume method and discrete element method. The two codes have been coupled and the solution process verified through the solution of simple one dimensional idealizations of the classical upward seepage flow and the time rate of consolidation problems. It is shown that the coupled DEM solution can produce results very similar to the well known analytical solutions for both problems. The results for both problems were obtained without the assumption of Darcy's law but are based on the basic Navier-Stokes equation for fluid phase and on the particle motion equation for the solid phase.

In the case of the upward seepage flow problem, the numerical solution yields results for the transient pore water pressure distribution, and the displacement of the uppermost particle in the column, and the results were shown to agree well with those from the analytical solution and two other DEM solutions.

For the consolidation problem, the solutions for pressure and particle displacement were provided with a range of consolidation times that are typically of interest in practice.

The DEM was also shown to be able to simulate the development of the excess pore water pressure distribution at very early solution times, where the classical solution would assume a uniform pore pressure equal to the applied stress P_0.

In addition to the solution of the two classical verification problems, two key issues in the numerical solution of coupled fluid/solid systems were discussed: the dependence on time step size for both the fluid and mechanical solution processes and the choice of viscous damping coefficients. The effects of these parameters on the solution was investigated, and while these effects are expected to be problem dependent, the paper provides some insight into how sensitive the results may be to the choice of these parameters.

With respect to time step size, it was shown that the number of time steps in the DEM solution relative to the number of time steps in the FVM solution process, termed NDF, can affect the solution. While smaller NDF leads to greater computational times, it provides better results. However, artificial viscosity may be required to reduce spurious oscillations which do not occur at larger values of NDF.

Appendix

Appendix 6.A Artificial Viscosity and Upwind Interpolation

When the central difference method is used for the time integration, the 1D upward seepage flow problem may develop a shock condition (Courant and Friedrichs 1948). This is exhibited by oscillation in the calculated pressure profiles due to the sudden change of the column density/porosity producing results as shown in Figure 6.14 (a). To correct this oscillation, the upwind scheme (Patankar 1980) and artificial diffusion (von Neumann and Richtmyer 1950)have both been used in the fluid solver to eliminate the oscillation.

The upwind interpolation or upwind differencing (UD) scheme determines the face flux   from the direction of flow:

$$\phi_f = \begin{cases} \phi_P, \text{ for } F \geq 0 \\ \phi_N, \text{ for } F < 0 \end{cases}$$

(6.35)

where $F=\rho_f U$, and ϕ_P, ϕ_N are the face fluxes at the finite volume node P, N, ϕ_f is the face flux at the finite volume surface f as shown in Figure 6.13.

The upwind scheme alone cannot completely remove the pressure oscillation as shown in Figure 6.14(b). In order to obtain a smooth pressure profile, the tensor artificial viscosity term Q is added to the momentum equation as in Eq. (6.10), where Q has a form similar to Stone and Norman (1992):

$$Q = \begin{cases} l^2 \rho \nabla \cdot U \left[\nabla U - \frac{1}{3} \nabla \cdot U \ I \right] & \text{if } \nabla \cdot U < 0 \\ 0 & \text{otherwise} \end{cases}$$

(6.36)

where I is the unit tensor and l^2 is a constant. The determination for l^2 is through trial and error. For the particular 1D upward seepage problem in our study, l^2 is found to be 0.0022.

Typically, artificial viscosity is expressed in explicit form as in Eq (6.36). However, an implicit form of the artificial viscosity may be expressed (the in implicit form) as:

$$n\nabla \cdot Q = c \cdot \nabla \cdot U \ \nabla^2 U$$

(6.37)

where the constant c is determined by trial and error. This implicit artificial viscosity may display better performance than the explicit form as shown in Figure 6.14(c). Figure 6.14(d) shows the comparison of pressure profile using $c=0$, $c=0.04$ and $c=0.08$. The results shown in Figure 6.5 and Figure 6.6 were both obtained using the implicit artificial viscosity with the form in Eq. (6.37), but the selection of artificial viscosity might be problem dependent and not be important in other problems.

A parametric study of the effect of fluid viscosity solution was provided. A constant inlet velocity was applied for a range of fluid viscosities and the response compared. The boundary conditions were chosen such that the higher viscosity fluids reached a critical gradient or quick condition, at which point the results diverged from the analytical solution. For a given inlet velocity, a higher viscosity fluid will more likely lead to the quick condition due to the greater drag effect produced by the upward fluid, and varying the viscosity is a convenient way to investigate the conditions leading to a quick condition.
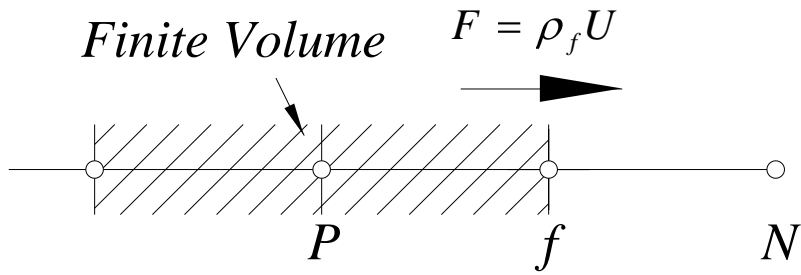
Figure 6.13 Upwind differencing scheme (Partankar 1980)

(a)
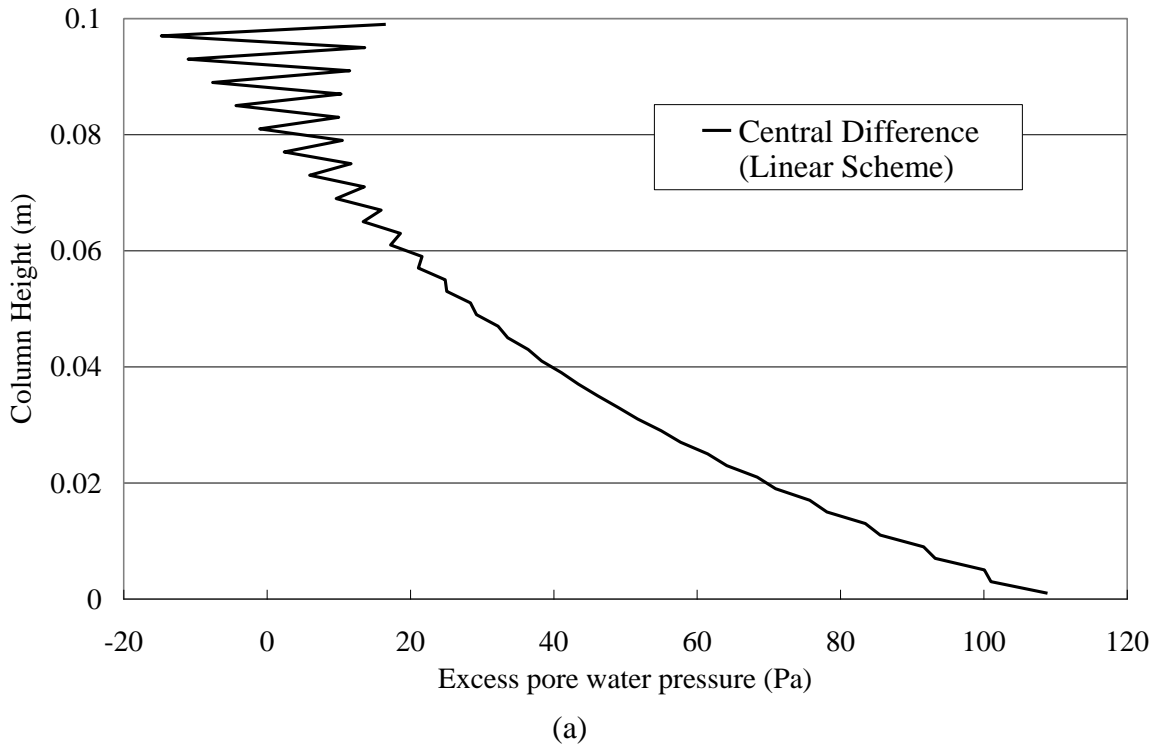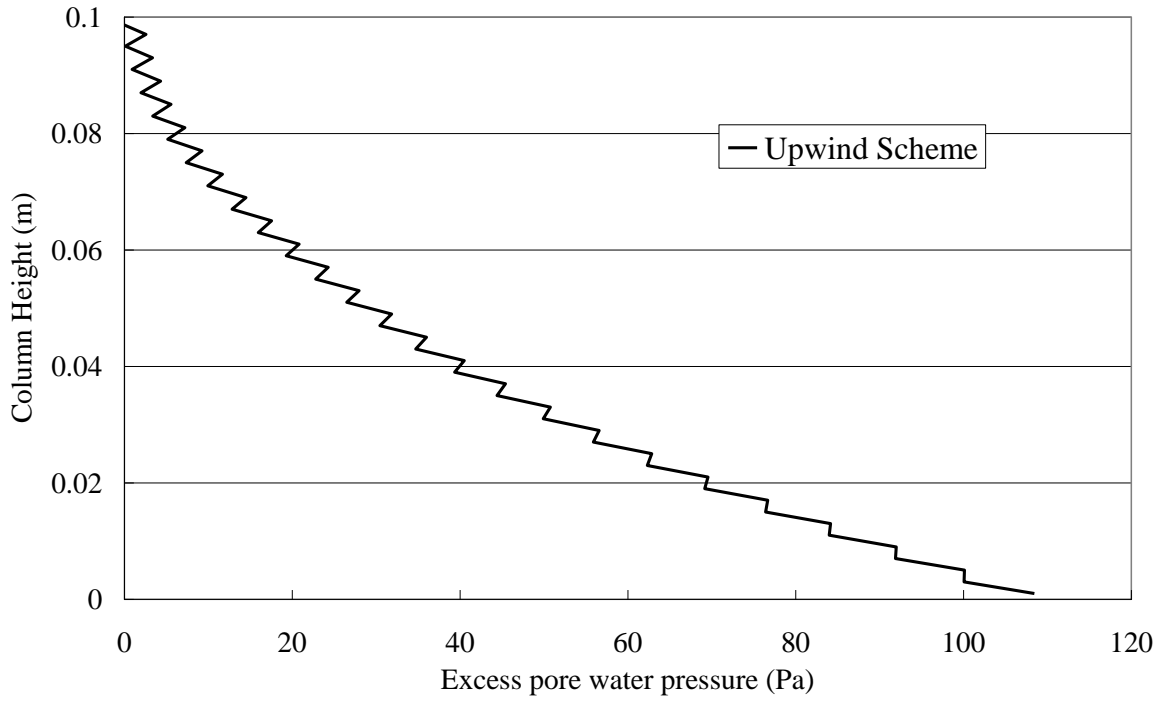
(b)
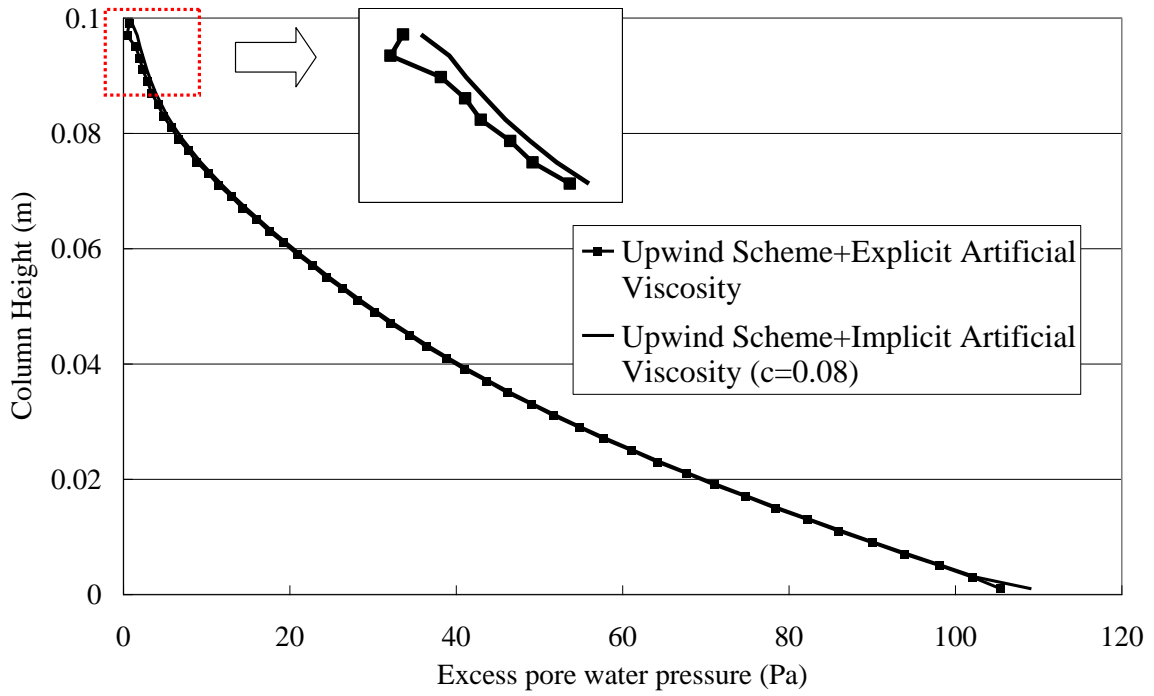
(c)
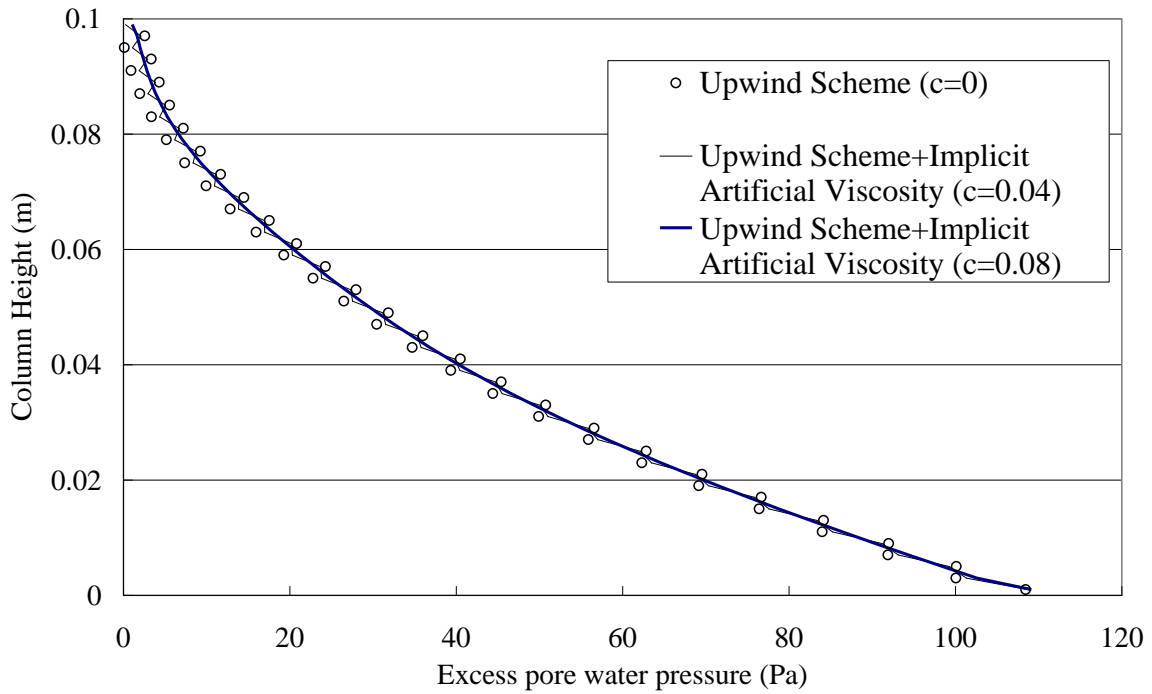
(d)

Figure 6.14 Results using the upwind scheme and artificial diffusion to reduce effects of shock on early stage pressure profile (t=0.01s for the upward seepage problem with u*=0.005m/s) (a) Central Difference scheme; (b) Upward scheme; (c) Comparison of implicit and explicit artificial viscosity; (d) Artificial viscosity constant c=0, c=0.04, c=0.08

7 Coupled Discrete Element and Finite Volume Solution for 2D Fluid Flow in Soil Mechanics

7.1 2D seepage sheet pile problem description

The classical sheet pile problem is investigated with the coupled DEM-CFD algorithm. The geometry of the sheet pile model is taken from Lambe and Whitman (1969) as depicted in Figure 7.1. The seepage under the sheet pile wall, pore water pressure, and pressure gradient in the subsoil can be obtained from the well established approach based on the flow net.

7.2 Analytical solution for the sheet pile model

The flow net is a graphical solution to the Laplace equation describing the total head at any point in the flow domain. The solution for the quantity of flow under the sheet pile wall and the hydraulic gradient at any portion of the flow domain can be obtained directly from the flow net as described in Lambe and Whitman (1969).

The seepage or quantity of flow under sheet pile wall is:

$$\frac{Q}{L} = k_p h_L \frac{n_f}{n_d} \tag{7.1}$$

Where k_p is the permeability coefficient, h_L is the head loss, and n_f/n_d is the shape factor of the flow net.

The exit gradient is:

$$i = \frac{\Delta h}{l} \tag{7.2}$$

Where Δh is the total head loss across any pair of equipotential lines which is equal to H/n_d and l is the distance between the equipotential lines in the region of interest.

7.3 Coupled DEM-CFD sheet pile model

7.3.1 Scaling law for the sheet pile model

The computational time for a DEM solution can be significant for coupled flow problems with a large number of particles. Assuming the particle diameter $d=1$mm, the number of soil particles in the horizontal direction of the above model is $N_x = 1$ mm x 39 m and is $N_y = 1$ mm x 18 m in the vertical direction, or about $Nx \times N_y = 39000 \times 18000 = 7.02 \times 10^8$ total particles. The computation demands for this many particles can be significant for even a rather simple problem such as this. An alternative approach is to adopt a reduced scale model of the prototype shown in Figure 7.1 so that the DEM model can contain an acceptable number of particles, yet preserve the desired permeability. The dimension for the reduced scale sheet pile model is $1/N=1/660$ of the dimensions of the prototype as listed in Table 7.1.
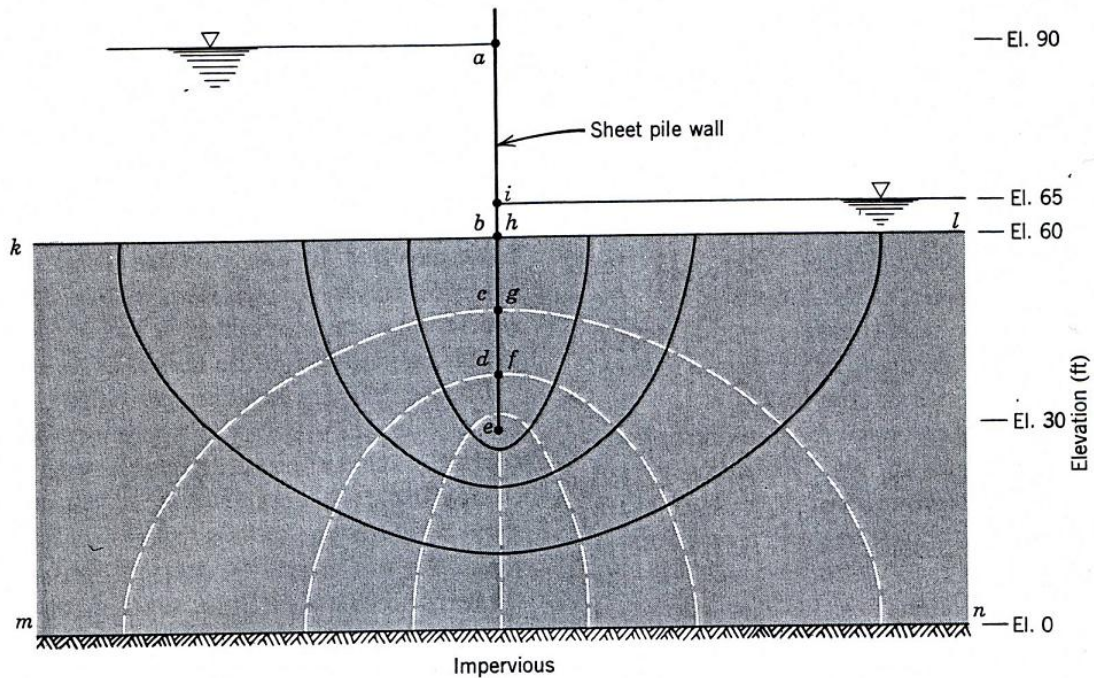
Figure 7.1 Flow under sheet pile wall (Lambe and Whitman 1969)

Table 7.1 Scaled dimensions for the sheet pile prototype in Figure 7.1 and the DEM/FVM model.

Length(Figure 7.1)	Prototype (ft)	Prototype (m)	Model (m)
km	60	18.29	0.028
mn	130	39.62	0.060
be	30	9.14	0.014

7.3.1.1 Equal vertical stress scaling

From geotechnical centrifuge theory, the basic scaling law derives from the need to ensure stress similarity between the model and the prototype, i.e. the vertical stress σ_{vm} at an arbitrary depth for the model h_m should be equal to the vertical stress σ_{vp} at the corresponding depth h_p for the prototype. Therefore:

$$\sigma_{vm} = \sigma_{vp} = \rho g' h_m = \rho g h_p \qquad \textbf{(7.3)}$$

Where ρ is the soil density, g is the Earth's gravity and g' is the scaled gravity value, and therefore from Eq. (7.3) the scaled gravity should be N times the value in the prototype:

$$g' = Ng \qquad \textbf{(7.4)}$$

Darcy's permeability constant is treated as a material parameter for both the model and prototype which implies:

$$k_{pm} = k_{pp} \qquad \textbf{(7.5)}$$

Where k_{pm} is the permeability of the model and k_{pp} is the permeability of the prototype. In the DEM-CFD model, since the stresses are the same and the flow path are reduced N-fold from prototype to model, the pressure gradient should be scaled N-times from the prototype to model:

$$i_m = Ni_p \qquad\qquad\qquad\qquad\qquad\qquad\qquad\qquad\qquad \textbf{(7.6)}$$

Where i_m is the pressure gradient in the model and i_p is the pressure gradient in the prototype.

7.3.1.2 Equal pressure gradient scaling

In contrast to the traditional geotechnical centrifuge model, since the fluid flow in the soils are pressure driven, and the flow behavior is mainly determined by pressure (hydraulic) gradient instead of vertical stress within the soil, we can also assume equal hydraulic gradient between the model and the prototype, the model and the prototype are composed of the same porous media, then:

$$k_{pp} = k_{pm}, \nabla p_p = \nabla p_m \qquad\qquad\qquad\qquad\qquad\qquad \textbf{(7.7)}$$

Where ∇p_p is the pressure gradient in the prototype, and ∇p_m is the pressure gradient in the model. The gravity value is kept the same for both model and prototype.

7.3.2 Coupled DEM-CFD sheet pile model

The coupled DEM-CFD model is created as shown in Figure 7.2; the model shows the initial state of particles and fluid cells, and each fluid cell contains around 23 particles. The sheet pile wall is placed between fluid cell 35, 29, 23 and 54, 60, 66, by creating two no-flow boundaries at **be** and **eh**. The soil and the fluid are considered incompressible, and it is also assumed that the soil can be represented by an assembly of particles. It can be regarded as a 2D plane strain problem with the thickness of the model taken as the diameter of the particle. The simulation results will be calculated both using equal pressure gradient scaling. The particles that are slightly above the ground surface at points k and l are simply remnants of the initial hydrostatic packing process and could have been artificially restrained if desired.

7.3.3 Boundary condition for the sheet pile model

The boundary conditions for the flow under the sheet pile wall corresponding to Figure 7.2 are as listed in Table 7.2.

85
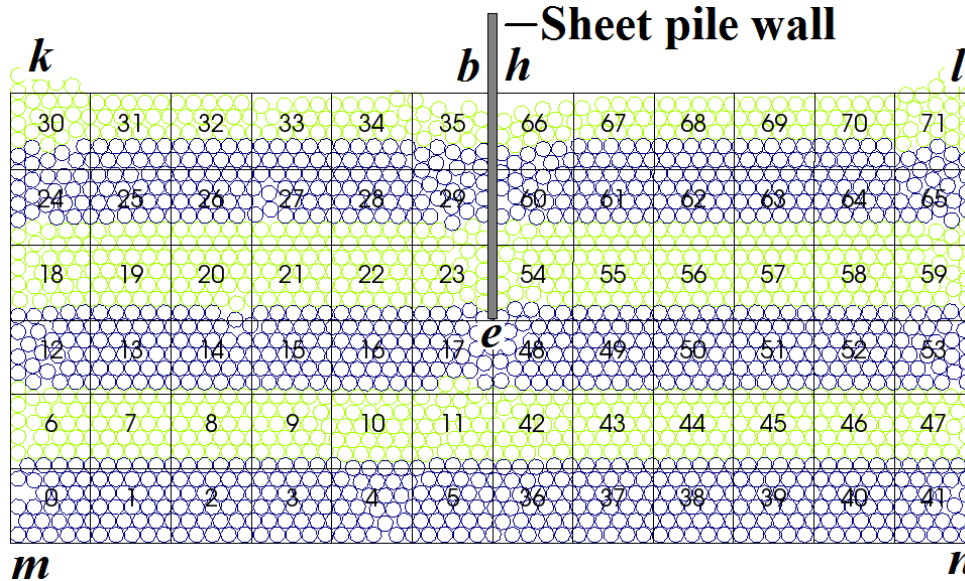
Figure 7.2 Fluid mesh and initial particle packing for the 2-D sheet pile wall problem

Table 7.2 Boundary conditions for the sheet pile model

Pressure boundary:		
Zero Gradient	*km, mn, ml*	
Fixed Value (Pa)	*kb*: $p=\rho_w g h$	*hl*: $p=0$
Velocity boundary:		
Zero Gradient	*kb, hl*	
Fixed Value (m/s)	*km, mn, ml*: U=(0, 0)	

Table 7.3 Physical and geometrical parameters for the 2D problem.

Parameter	Value	Unit
Solid (particle)		
Number, N_p	1800	
Radius, r	1.0×10^{-3}	m
Density, ρ_s	2650	kg/m^3
Contact stiffness, k_n	800	N/m
Friction angle	10, 20, 30	Degree
Fluid (Water at 20°C, 1atm)		
Density, ρ_w	1000	kg/m^3
Viscosity, μ	1.004×10^{-3}	Pa-s
Sheet pile configuration		
Width	0.22	m
Height	0.10	m
Thickness	1.0×10^{-3}	m
Fluid cell size $\Delta x \times \Delta y$	2.0×2.0	$(10^{-3}\text{m})^2$
Gravity constant	9.81	m/s^2

7.3.4 Determine material properties of the two dimensional model

The basic physical and geometric properties of the sheet pile model are as listed in Table 7.3, the permeability coefficient are then derived from these basic parameters.

The key parameter to estimate the flow under the sheet pile lies in the determination of the permeability coefficient. It can be roughly derived using Ergun's empirical equation (Ergun 1952) in a packed column of height H_{col}:

$$\frac{\Delta p}{H_{col}} = \frac{1-n}{dn^3}\left\{150\frac{1-n}{d}\mu u^* + 1.75\rho_w u^{*2}\right\} \tag{7.8}$$

where u^* is the superficial velocity and ρ_w is the density of water which now replaces the fluid density ρ_f in Eq. (3.2).

The hydraulic gradient is:

$$i = \frac{\Delta h}{H_{col}} = \frac{\Delta p}{\rho_w g H_{col}} = \frac{1-n}{\rho_w g dn^3}\left\{150\frac{1-n}{d}\mu u^* + 1.75\rho_w u^{*2}\right\} \tag{7.9}$$

The permeability k_p can be obtained as:

$$k_p = \frac{u^*}{i} = \frac{\rho_w g u^*}{\dfrac{1-n}{dn^3}\left\{150\dfrac{1-n}{d}\mu u^* + 1.75\rho_w u^{*2}\right\}} = \frac{d^2 n^3 \rho_w g}{150\mu\left(1-n\right)^2 + 1.75d\left(1-n\right)\rho_w u^*} \tag{7.10}$$

For the consolidation model, the final superficial velocity for the consolidation model is zero and Eq. (6.13) reduces to the Kozeny–Carman equation (Warren et al. 2005) Eq. (6.14):

$$k_p = \frac{d^2 n^3 \rho_w g}{150\mu\left(1-n\right)^2} \tag{7.11}$$

Using the particle and fluid parameters listed in Table 7.3, due to the slightly different porosity values in the two problems, the permeability coefficient k_p is found to be 0.0159m/s for the consolidation model.

7.4 Simulation procedure

7.4.1 Initial hydrostatic state

Before the boundary pressure conditions are applied, the particle assembly undergoes a settling procedure so that the hydrostatic state is approximately reached. The initial conditions are established in 2 steps:

(1) The 1800 equal diameter particles are packed sequentially with no space or overlap with the water level above the topmost particle.

(2) The particles then settle to the hydrostatic state under influence of gravity and buoyancy forces, i.e. the consolidation under gravity and buoyancy force is completed.

The simulation will take the state after step (2) as the initial condition for the simulation.

7.4.2 Applying the pressure gradient

Starting from the initial hydrostatic state above, a fluid pressure is then applied to the top left line *kb* of the sheet pile model while the top right line *hl* is fixed at *p=0* so a pressure gradient is

created within the saturated soil. The pressure gradient is increased up to that corresponding to a quick condition and the response of the model investigated over this range of pressure gradients.

7.5 Numerical solutions for the sheet pile problem

7.5.1 Equal pressure gradient scaling

Starting from the initial condition as shown in Figure 7.2, the coupled DEM-CFD solution will be discussed for a range of pressure gradients up to the critical value corresponding to a quick condition.

Transient and steady state pressure distribution for small pressure gradients

Figure 7.3 shows the computed contours of pore water pressure (which correspond to the equipotential lines in the flow net) at different solution times for an applied pressure in the model $\Delta p_m = 200 Pa$. This corresponds to an exit gradient i_e=0.48 which is well below the critical value of i_c=1.0. The computed pore water pressures are observed to change over the solutions until the system reaches a steady state after 4×10^{-3}s (Figure 3d). At this solution time the equal potential lines are found to be in close agreement with the classical flow net solution as shown in Figure 7.3(d).

7.5.2 Steady state quantity of flow under sheet pile wall

The classical solution of quantity of flow per unit width through the prototype is:

$$q = \frac{Q}{L} = kH \frac{n_f}{n_d} = 0.0159 \ 0.0204 \ \frac{4}{8} = 1.43 \times 10^{-4} (m^3/s)/m \tag{7.12}$$

The DEM-CFD solution for quantity of flow is the sum of flux from fluid cells number 66-71 across the surface on the right side of the flow domain and is shown in Table 7.4, which agree closely with the analytical solution, the details for the calculation is as shown in Table 7.4.

(a)

(b)

(c)

(d)
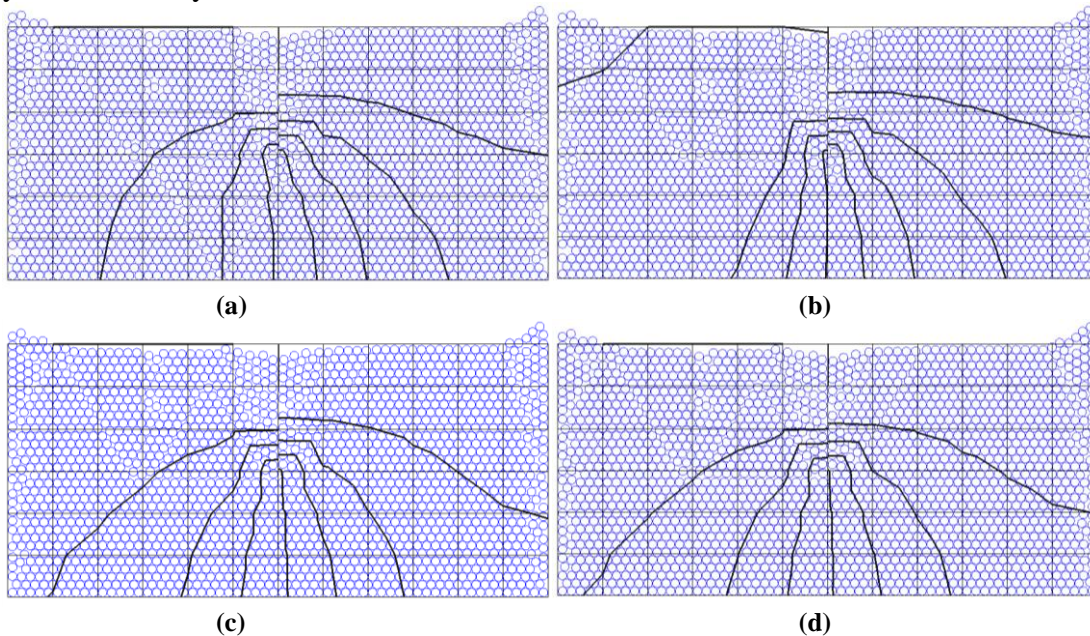
Figure 7.3 Pressure contour development for applied pressure 200Pa at different time (a) t=6×10⁻⁴s, (b) 8×10⁻⁴s, (c) t=1.8×10⁻³s, (d) 4×10⁻³s

Table 7.4 Quantity of flow under the model sheet pile wall using the DEM-CFD method.

Cell ID	Computed porosity	Pressure (Pa)	U_x (m/s)	U_y (m/s)	$U_y^*=U_y\times$ porosity (m/s)
66	0.5770	1.5435	0.0006	0.0171	0.009879327
67	0.4434	1.1400	0.0003	0.0073	0.003236165
68	0.4434	0.9636	-0.0001	0.0062	0.002747864
69	0.4657	0.8225	0.0001	0.0057	0.00267446
70	0.4657	0.7069	0.0001	0.0049	0.002271956
71	0.4657	0.7340	0.0000	0.0048	0.002256888
				Q/L =	1.15×10^{-4} (m³/s/m)

U_y^* is the superficial velocity in the *y* direction

7.5.3 Relationship between quantity of flow and pressure gradient

The pressure gradient applied to the model was increased, and the quantity of flow computed. The computed quantity of flow is shown as a function of the exit gradient in Figure 7.4. Also shown in Figure 7.4 is the quantity of flow calculated from Eqs. (7.1), where the permeability has been determined based on two different values of porosity from Eqs. (7.11). The upper curve corresponds to a mean porosity value n_{avg}=0.437 (corresponding permeability $k_{p,avg}$=0.0172m/s) obtained by averaging the porosity over the entire flow domain (fluid cells 0-71), while the lower bound analytical solution was obtained by using the minimum porosity n_{min} = 0.359 (permeability $k_{p,min}$=0.00738m/s) which corresponds to the minimum value of porosity determined from all fluid cells which occurs along the bottom of the flow domain. As expected, the computed DEM-CFD seepage obtained with spatially varying porosity is bounded by the two analytical solutions. While the flow as determined from Eqs. (7.1) is a linear function of the pressure and thus exit gradient according to Darcy's law, it is observed that the DEM-CFD solution is slightly nonlinear as the seepage forces changes the particle packing and porosity. At higher pressures as the exit gradient approaches 1.1, a sharp increase in the flow is observed corresponding to the disruption of the particle assembly as the exit gradient becomes critical and a quick condition is represented. While a quick condition is usually associated with exit gradients about 1.0, the exit gradient of which a quick condition occurs is actually a function of the porosity (Holtz and Kovacs 1981):

$$i_c = \left(\frac{\rho_s}{\rho_w}-1\right)\left(1-n\right) \tag{7.13}$$

where i_c is the critical gradient. The analytical solutions for seepage in Figure 7.4 have been marked to indicate the value of the exit gradient at which point a quick condition would be expected.

Figure 7.4 shows that the quantity of flow under the sheet pile approximately consists with Darcy's law when the exit gradient $i<1$(approximately linear), when the exit gradient $i>1$, the quantity of flow obtained from DEM-CFD starts to deviate from the trend predicted by Darcy's law.

Figure 7.4 Quantity of flow v.s. Pressure gradient

The chart shows Quantity of flow (m³/s)/m on the y-axis (0.00E+00 to 5.00E-04) versus Exit gradient on the x-axis (0 to 1.4). Legend: Quantity of flow, Darcy flow for mean porosity, Darcy flow for minimum porosity. Annotations: critical gradient-porosity line, n=0.473, n=0.360.
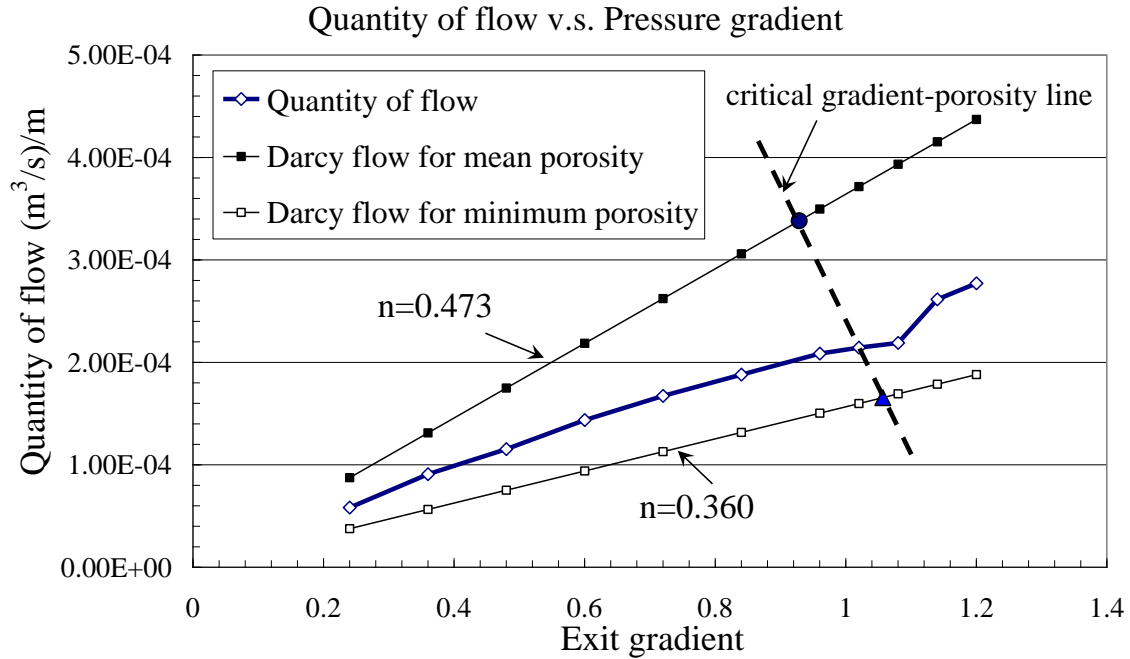
Figure 7.4 Quantity of flow with increasing pressure gradient

7.5.3.1 Pressure distribution for large pressure gradient close to quick

Figure 7.5 shows the pressure contours for conditions when exit gradient $i=1.2$. The particles close to the sheet pile where the gradient is the maximum start moving upwards and the pressure contour differs slightly from the classical flow net due to the porosity change within the model.

Figure 7.6 shows the contact plot comparison between exit gradient $i=0.48$ and $i=1.2$, where the width of the band increases with magnitude of the contact force, and the contact forces are scaled with reference to the maximum contact force over all the particle contacts. Figure 6(a) indicates that the contact forces on the downstream side of the sheet pile are only slightly less than those at the upstream side for low values of the exit gradient, while once a quick condition is reached (Figure 7.6(b)), the particle contact forces become very small in the exit region which indicates very low effective stresses and a possible quick condition.
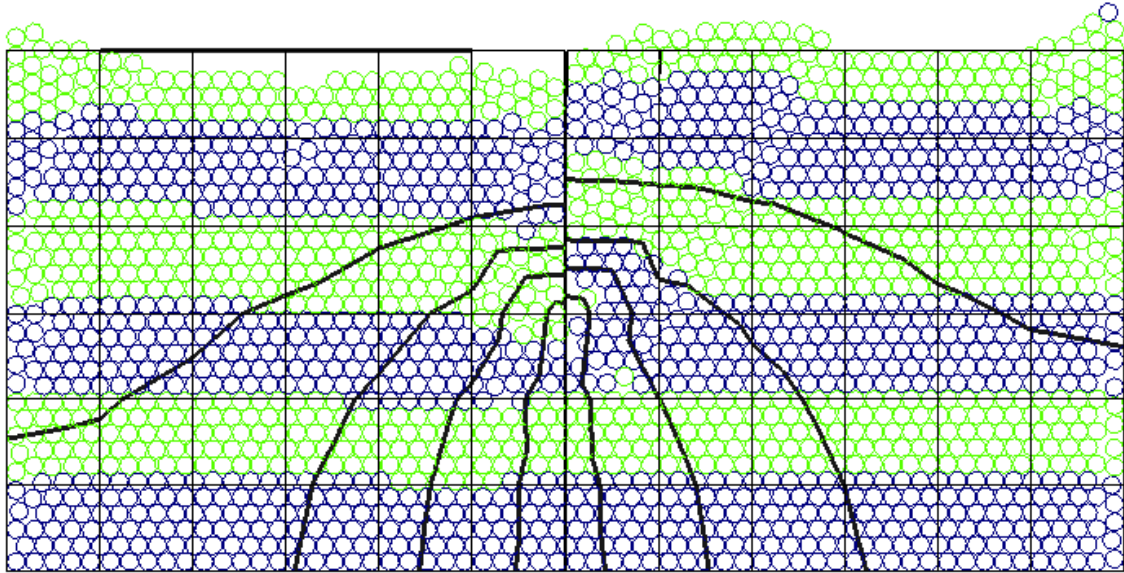
Figure 7.5. Pressure contour for exit gradient _i=1_.2. Note that the particles have moved above the ground surface in the area near the sheet pile. The particles above the ground surface near the edges of the flow domain remain from the initial packing.
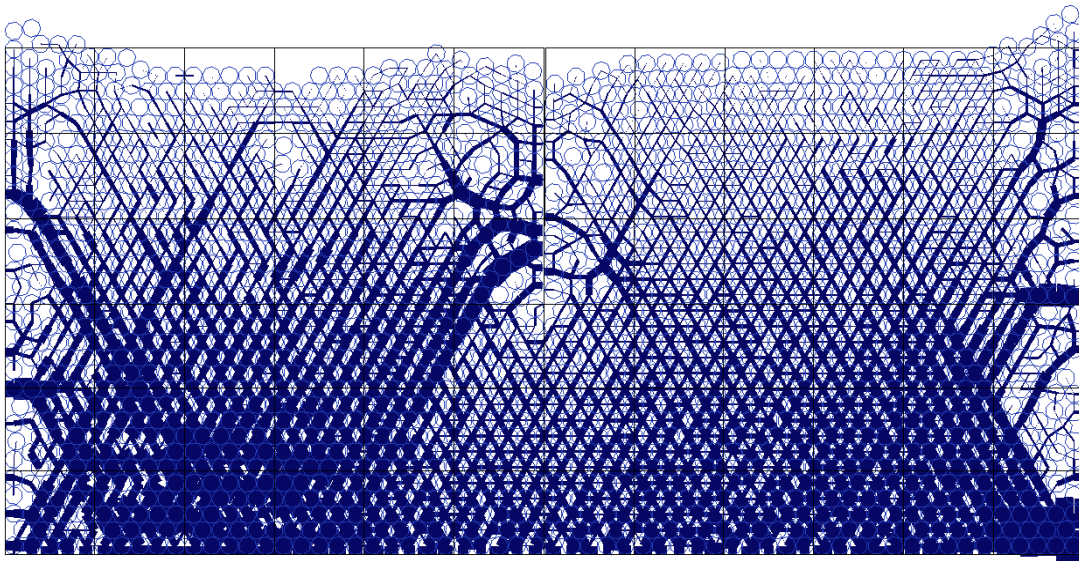
(a)
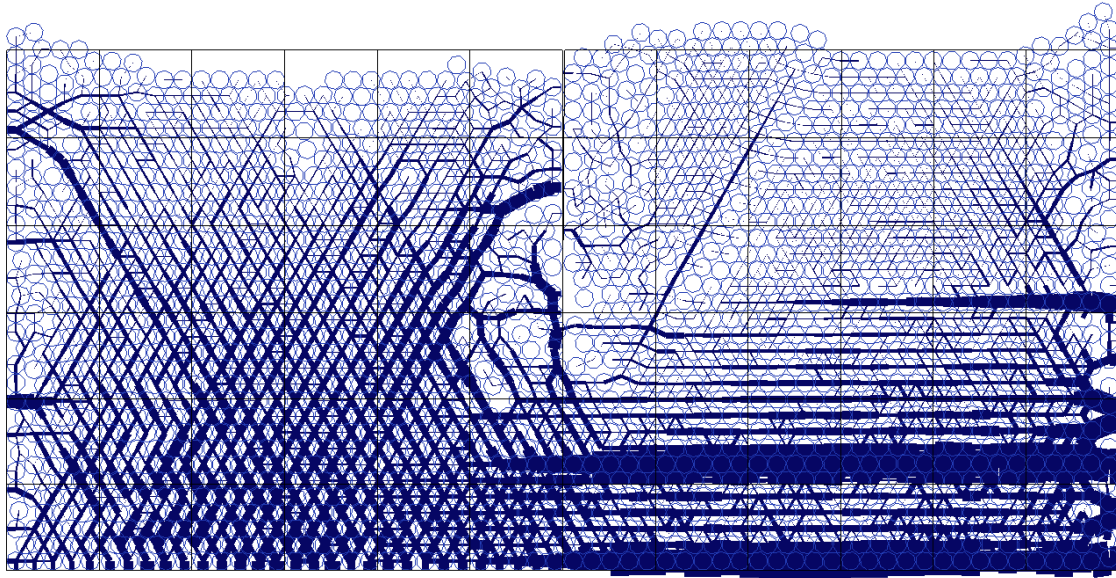
(b)

Figure 7.6 Comparison of contact force plot between particles with different exit gradient (the broader the band the higher the contact forces): (a) exit gradient *i*=0.48 and (b) *i*=1.2

7.5.4 Pressure contour and particle contact forces close to critical gradient

Figure 7.6 compares the contact forces between the steady state i=0.48 system and the exit gradient i=1.2 beyond critical, the particle contact forces in Figure 7.6(b) shows the particles are losing contact which indicates a possible quick condition.

7.6 Relationship between fluid mesh size and quantity of flow

The quantity of flow is calculated and compared using different fluid cell size with respect to the particle size, the calculated quantity of flow are summarized in Table 7.5, it is found that using the 12×6 mesh (Figure 7.7(b)) yields the closest quantity of flow value with the analytical solution, and 16×8 mesh (Figure 7.7(c)) also provide a relative close agreement with the analytical solution, the 24×12 mesh (Figure 7.7(d)) and the 8×4 mesh (Figure 7.7(a)) results tend to deviate from the analytical solution. This might suggest that the 2D sheet pile model will yield the best results when using the 12×6 mesh, which implies each fluid cell contains approximately 23 particles.

92
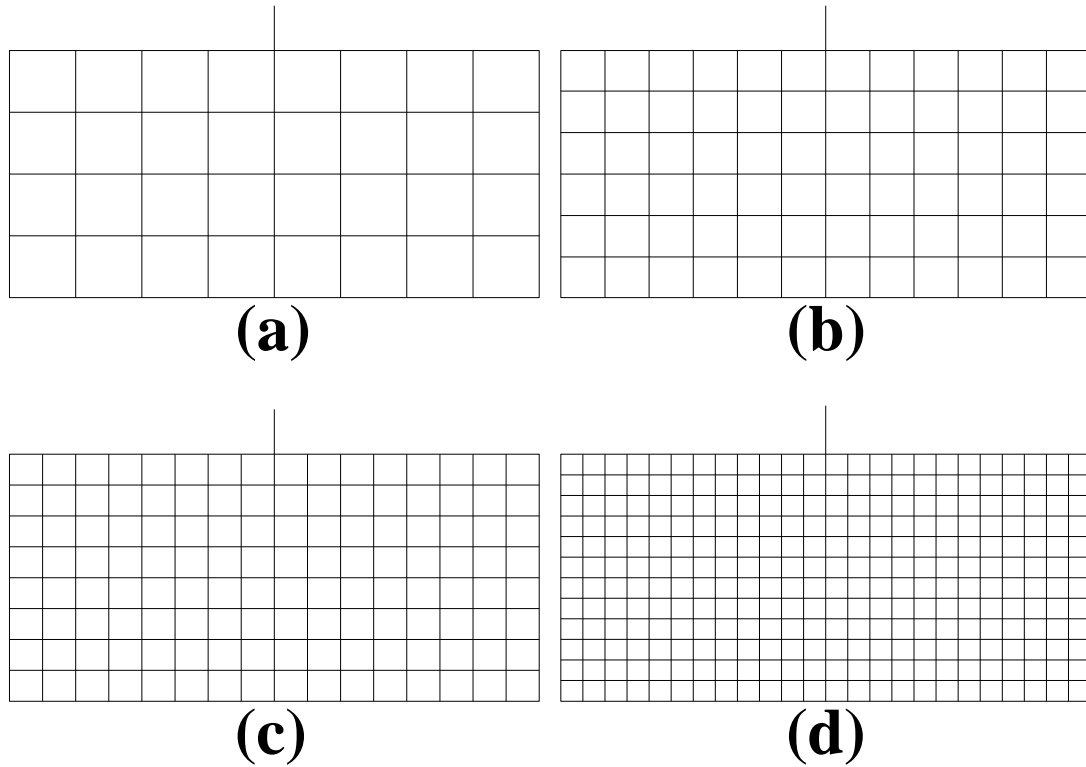
Figure 7.7 Different finite volume discretization of the fluid domain (a) 8×4 (b) 12×6(c) 16×8 (d) 24×12

Table 7.5 Quantity of flow using different finite volume mesh size

	FVM mesh size	Number of particles per cell	Quantity of flow 10^{-4} (m³/s/m)		% error compared to flow net solution
			DEM-CFD	Flow net	
(a)	8×4	53	0.81		43.4%
(b)	12×6	23	1.15	1.43	19.6%
(c)	16×8	13	1.04		27.3%
(d)	24×12	6	0.97		32.2%

7.7 Closure

A coupled DEM-CFD model was created for the classic fluid flow under sheet pile problem. In order to keep the number of particles relatively low to limit the computational demands, an equal pressure gradient scaling law is used to scale the problem domain of the model down while maintaining the permeability of the prototype. The calculated steady state pressure contours and quantity of flow from the model agree well with the classical solution from the flow net. The DEM/finite volume method is also able to present the transient pressure development during the early stages of the pressure application. The particle movement and contact forces within the particles as the exit gradient approaches the critical condition are also discussed. By taking advantage of the DEM, the model is also able to simulate the particle migration and the reduction of particle contact forces near the exit location as the pressure gradient is increased, which is not possible with the traditional continuum/porous media approach. The computed quantity of flow is shown to increase abruptly as the crucial gradient is approached, and the critical gradient is compared with that obtained from the continuum porous media approach for different uniform porosity values. The solution of this classic seepage problem suggests that the coupled DEM/finite volume method may have application in geotechnical engineering, particularly when the computer code can be cast into a parallel computing framework such that very large numbers of particles can be simulated. In the meantime, full scale problems can be approximated using the two methods of problem scaling discussed to limit the number particles to more reasonable values.

8 Coupled Discrete Element and Finite Volume Solution for Packing of a Chromatography Column

8.1 2D chromatography problem description

Band broadening makes the bands of packing material inside the chromatography column wider than the injection pulse, hence finally decreases the efficiency of the column (Guiochon et al. 1994). One of the major reasons for the band-broadening is the result of packing heterogeneity of the column. There has been experimental evidence by Knox and Parcher (1969), Knox et al. (1976) and Horne et al. (1966) which shows that the beds of the packed columns used in liquid chromatography are heterogeneous across the radius. These results have been explained by the assumption of a "wall effect" existence which would affect the packing material close to the column wall.

8.1.1 Experimental results

Experimental results by Yun and Guiochon (1997) to investigate the deformation pattern corresponding to axial compression in a packed bed due to the injection of the mobile phase (methanol) from the bottom of the column which provided a visualization of the packing process. The experiment shows a marked curve band toward the column wall and is similar to the deformation pattern observed earlier by Train (Train 1956, 1957). This is photographic evidence of the so called "wall effect" (Baur et al. 1988; Baur and R M Wightman 1989; Farkas et al. 1994, 1996). Due to this wall effect, the mobile phase velocity varies across the column accordingly, which reduces the efficiency of the column. It is further observed that the velocity is the maximum in the central region and lower close to the column wall, which suggests a nearly parabolic distribution (Farkas and Guiochon 1997).

8.2 Coupled DEM-CFD chromatography column model
8.2.1 Coupled DEM-CFD chromatography column model description

To investigate the conditions in a packed chromatography column and simulate the packing process and effects of wall friction, a 2 dimensional DEM analysis was performed. The slurry packing procedure of the chromatography column is investigated with the coupled DEM-CFD algorithm. The cylindrical column is simplified to a 2D plane model with the annular wall replaced by vertical plane wall as shown in Figure 8.2.
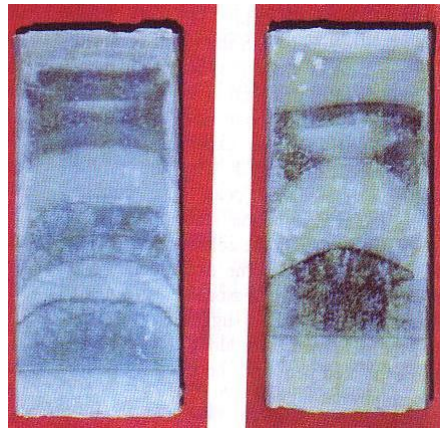
Figure 8.1 Axial cross-section of two column packed by slurry packing (Yun and Guiochon 1997)
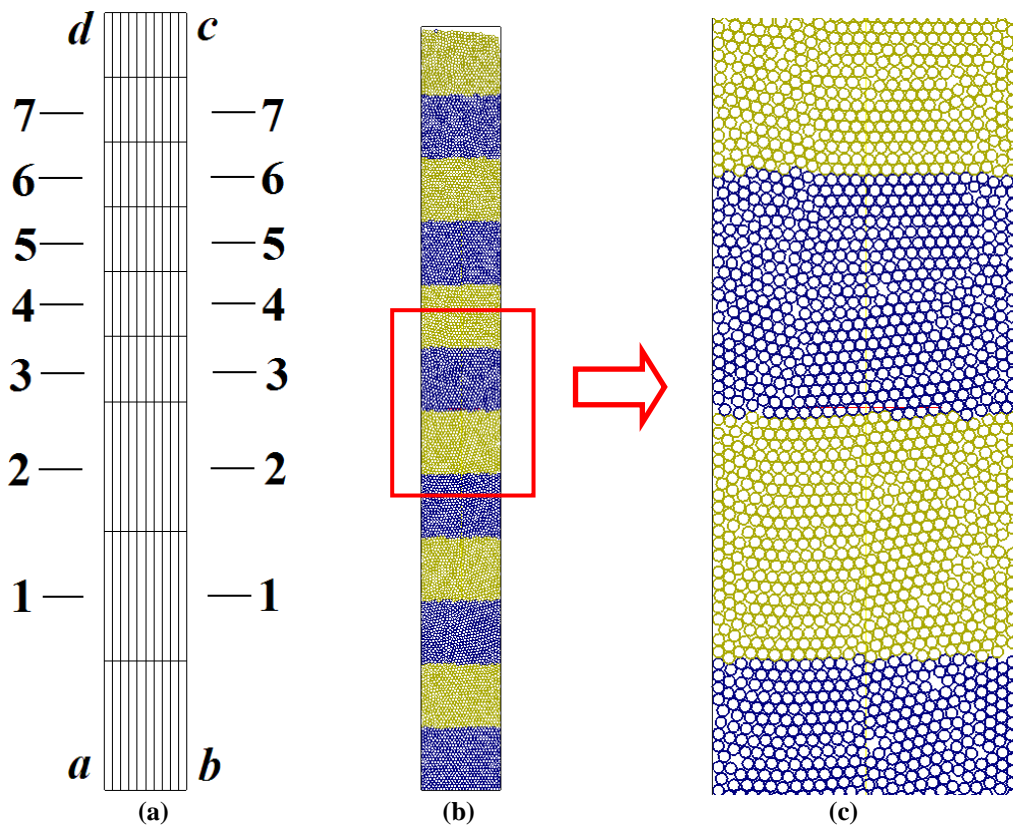
Figure 8.2 Fluid mesh and initial particle packing for the 2-D chromatography column (a) Fluid mesh (b) Colored initial particles (c) Magnified initial random packing

The packing material is divided into 12 color bands in order to reflect the initial particle positions and the final particle migration pattern, much like was done in the physical experiment of Figure 8.1 (Yun and Guiochon 1997). The initial particle packing process will be described in section 8.3.1.

8.2.2   Boundary conditions for the chromatography column model

The boundary conditions for the axial compression of the column corresponding to Figure 8.2 are as listed in Table 8.1. The mobile phase (methanol) is injected vertically from the bottom of the column with a large superficial velocity value of 2.0m/s. The velocity at the inlet is uniform across the width or diameter of the column, approximating the flow from the entrance frit in the chromatography column which is designed to achieve a near uniform entrance velocity. A zero fixed pressure boundary is specified at the top of the column, from which the methanol discharges.

8.2.3   Material properties of the chromatography column model

The basic physical and geometric properties of the 2D column model are as listed in Table 8.2. It is important to note that the internal particle friction is greater than the particle-wall friction, which is consistent with most laboratory investigations of particle solid contacts. The internal particle friction angle is assumed to be 30° as from Mihlbachler et al. (1998), while the particle-wall friction is 22° as from Yew (1999). These parameters are consistent with a silica packing material such as Zorbax (Yun and Guiochon 1997), and the contact stiffness is taken as a value typically used with sand particles.

Table 8.1. Boundary conditions for the chromatography column model

Pressure boundary:	(Figure 8.2a)	
Zero Gradient	*ab, bc, ad*	
Fixed Value (Pa)	*cd*: *p=0*	
Velocity boundary:		
Zero Gradient	*cd*	
Fixed Value (m/s)	*ad, bc*: U=(0, 0)	*ab*: U=(0, 2)

Table 8.2 Physical and geometrical parameters for the 2D problem.

Parameter		Value	Unit
Solid (silica particle)			
Number, N_p		6480	
Diameter, d		0.95~1.0	mm
Density, ρ_s		2650	kg/m^3
Contact stiffness, k_n		1.0×10^6	N/m
Friction angle	particle-wall	22	degree
	particle-particle	30	degree
Fluid (methanol at 20°C, 1 atm)			
Density, ρ_w		789.1	kg/m^3
Viscosity, μ		5.44×10^{-4}	Pa-s
Column configuration			
Width		0.025	m
Height		0.24	m
Thickness		1.0×10^{-3}	m
Wall-particle friction angle		22	degree
Fluid cell size $\Delta x\times\Delta y$		2.5×20	mm^2
Gravity constant		9.81	m/s^2

8.3 Simulation procedure
8.3.1 Initial hydrostatic state
Before the mobile phase methanol is injected, the particle assembly undergoes a settling procedure so that the hydrostatic state is approximately reached. The initial conditions are established in 2 steps:

(1) The 6480 particles are generated in rectangular space surrounded by the column walls with slight pseudo random variation of particle diameter from 0.95-1.0mm.

(2) The particles then settle to the hydrostatic state under the influence of gravity and buoyancy forces, i.e. the consolidation under gravity and buoyancy force is completed at the initial hydrostatic state. The simulation will take the state after step (2) as the initial condition for the simulation.

8.3.2 Applying the inlet velocity
Starting from the initial hydrostatic state above, the methanol is injected at the bottom of the column with a fixed superficial velocity U=2.0m/s. The value of U applied is greater than a value necessary to cause a quick condition. Because there is a wall (end frit) at the top of the column, the injection of flow will finally result in particles piled up at the column frit. The simulation is continued until the particles are close to equilibrium state and the pore pressure no longer changes with time, which indicates the flow field has reached the steady state.

8.3.3 Time step and simulation time
The DEM mechanical time step for the simulation is fixed at 5×10^{-7}s, while the fluid time step is fixed at 10 times the mechanical time step. The mechanical time step must be smaller than a critical step which is typically determined from translational motion and rotational motion of the smallest particle within the particle assembly:

$$t_{trans} < \sqrt{\frac{m}{k_{tran}}}, \; t_{rot} < \sqrt{\frac{I}{k_{rot}}} \qquad\qquad\qquad \textbf{(8.1)}$$

where t_{trans} and t_{rot} are the critical time step determined from translational motion and rotational motion, respectively; k_{tran} and k_{rot} are the translational and rotational stiffness, m is the particle mass and I is the particle moment of inertia. The actual mechanical time step must be smaller than both t_{trans} and t_{rot} calculated from Eqs. (8.1). It took the system around 60000 iterations to approximately reach a steady state at a real computation time of 0.03s. The simulation time on a Pentium Xeon Dual Core 2.8G Dell Precision workstation (2G memory) is about 25 hours. The currently coupled DEM-CFD code is just a serial code and therefore it is strongly expected that parallel algorithms will be used in the future to save simulation time.
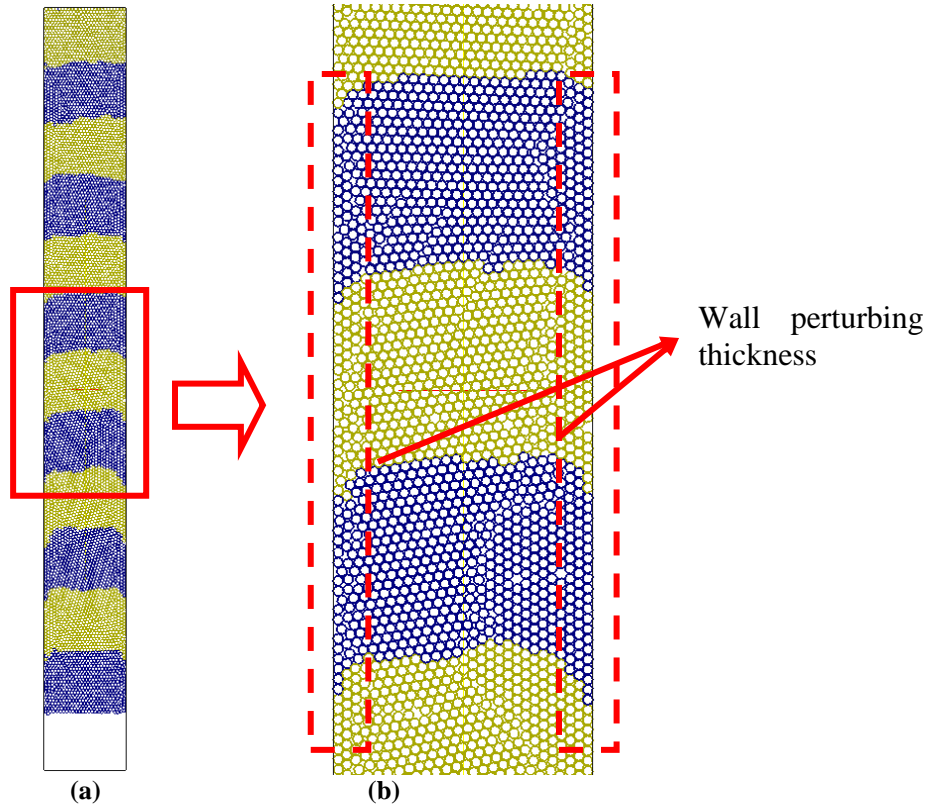
8.4 Simulated results for the column packing heterogeneity

8.4.1 Particle band profile for the packing heterogeneity

Figure 8.3 shows the band profile for the axial column compression. The particle materials are lifted and axially compressed by the upward velocity. The column lost approximately 1/12 of its original length (2cm) due to upward compression of the particles. It is evident that the final particle assembly shows a curved band toward the wall. In this simulation, the horizontal layer perturbed by the DEM wall seems to have a shear layer thickness of approximately 3 particle diameters as shown in Figure 8.3(b). In this simulation, the particle diameters (diameter 0.95-1mm) are about 100 times greater than those actually used in chromatography columns, which is typically around 10μm, therefore the wall perturbing thickness does not agree with (or cannot reflect) the experimental measurement (around 30 diameters for 10μm particles) by (Baur et al. 1988; 1989). However, the simulated results agree quite well with the results of limiting shear-layer thickness corresponding to 2.3-3.0 particle diameters by Johnson and Jackson (1987), which used 1.0mm polystyrene beads in friction-collision granular materials subject to plane shearing.

8.4.2 Pressure distribution for the final compressed column

Figure 8.4 shows the pore pressure distribution of the final steady state. The bottom pore pressure reaches a value of 5.46×10^6Pa (about 55atm). From the equal potential lines shown in Figure 8.4(b), the pressure drops within the particle-methanol porous media are equally spaced which indicates that the flow satisfies Darcy's law.

(a) **(b)**

Figure 8.3 Final particle band profile and magnified particle migration pattern

Wall perturbing thickness

p
5.460e+006
4.104e+006
2.747e+006
1.391e+006
3.435e+004

(a)   (b)   (c)
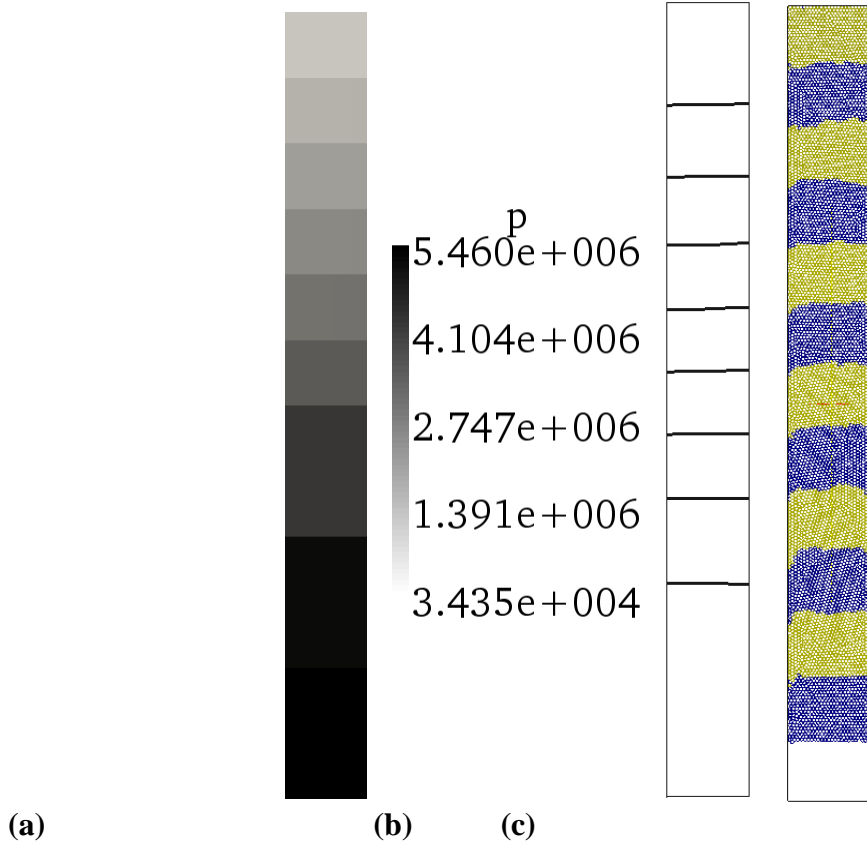
Figure 8.4 Pressure contour for final steady state

8.4.3 Porosity and velocity distribution for the final compressed column

In the Finite Volume method, the porosity and thus the flow velocity are taken as a constant within any fluid cell. Figure 8.5 depicts the velocity and porosity plot for the final compressed column, where a rectangular grid of 2.5mm by 20 mm fluid cells was used. As seen from the plots, the velocity and porosity values are not uniform, resulting from the heterogeneity introduced into the column during the packing process. A comparison of the computed porosity and velocity (Figure 8.6) across the column diameter are shown for various sections along the column as indicated in Figure 8.5. The results from Figure 8.6 suggest the relationship between the porosity and the mobile phase velocity value, and demonstrate that the porosity distribution is not uniform across the column. The areas with higher porosity tend to have higher velocities, since the mobile phase meets less resistance at high porosity cells.
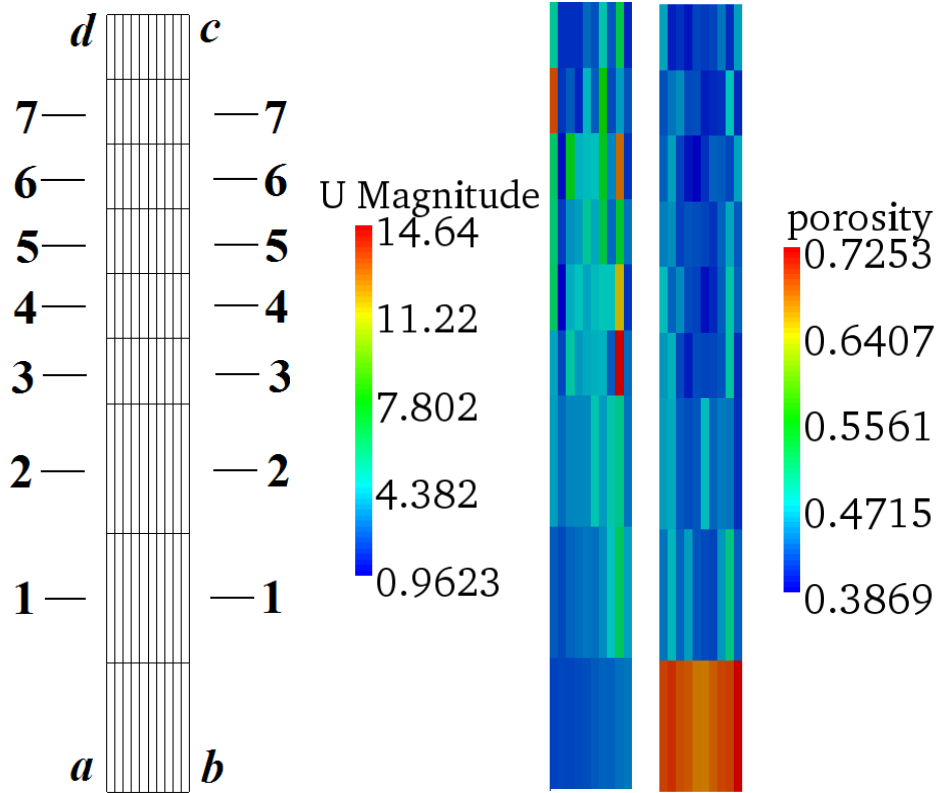

Figure 8.5 Velocity and porosity distribution. Cross sections 1-6 identify positions along which the computed porosity and velocity results are shown in Figure 6.

Experimental evidence from chromatography columns suggests that the mobile phase velocity is typically 2-3% higher in the column center than close to the wall (Yun and Guiochon 1997), and the variation of velocity across the column in roughly parabolic. This variation of mobile phase velocity is generally attributed to the heterogeneity of the column packing and leads to a significant reduction of column efficiency.

The DEM-CFD simulation in Figure 8.6 predicts a variation of velocity across the column of roughly more than 10 percent, which is much greater than that observed experimentally. This can be attributed to rather coarse nature of the model adopted to limit the number of particles in the simulation. In order to better reproduce the experimentally observed variation of flow velocity using the DEM-CFD coupled model, the porosity variation between adjacent fluid cells needs to be well below 2-3% level. For instance, in the current model, there are 10 fluid cells across the column in horizontal direction, which suggests that the porosity variation between adjacent cells should be around 2% divided by 10, which equals to 0.2%. This requires the fluid cell volume 2000 times larger than the particle volume, as opposed to the 100 times larger the particle volume in the current simulation. With the particle current model, DEM-CFD model cannot sufficiently model the actual porosity variation to simulate the experimental results.
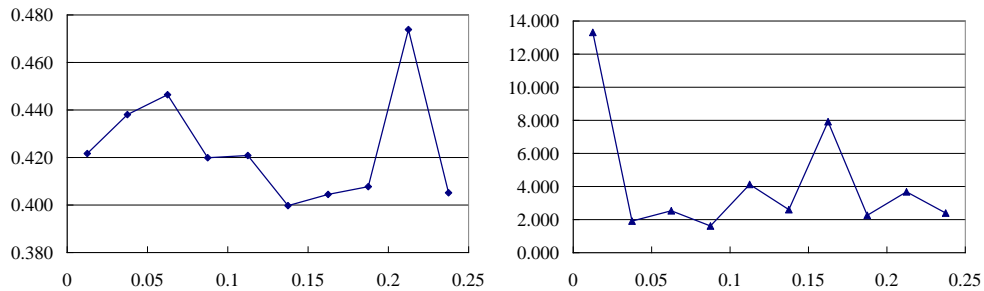
6-6
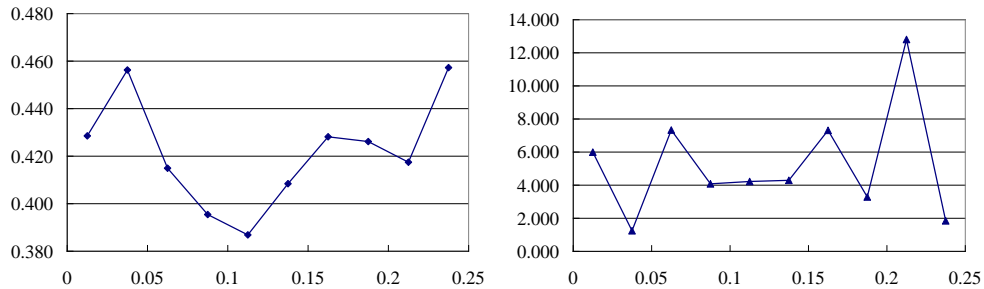
5-5
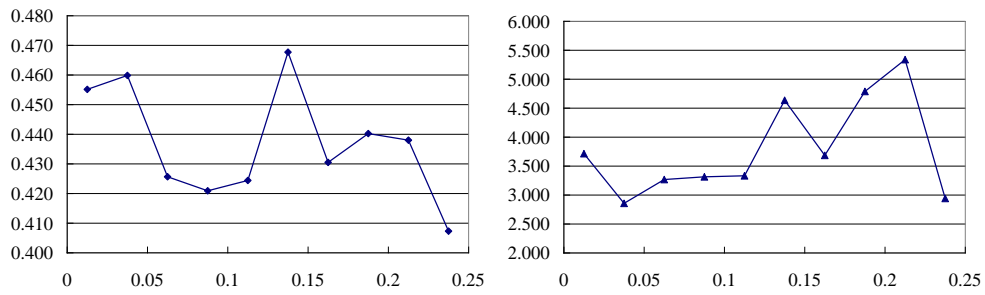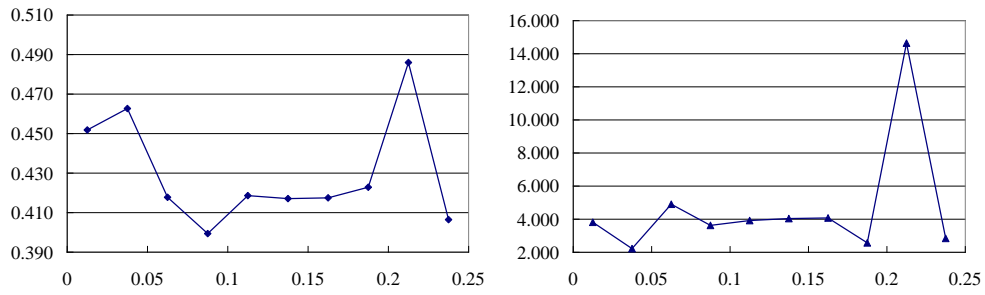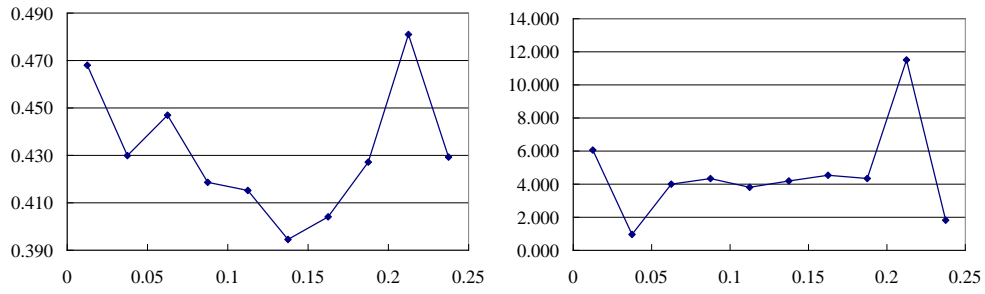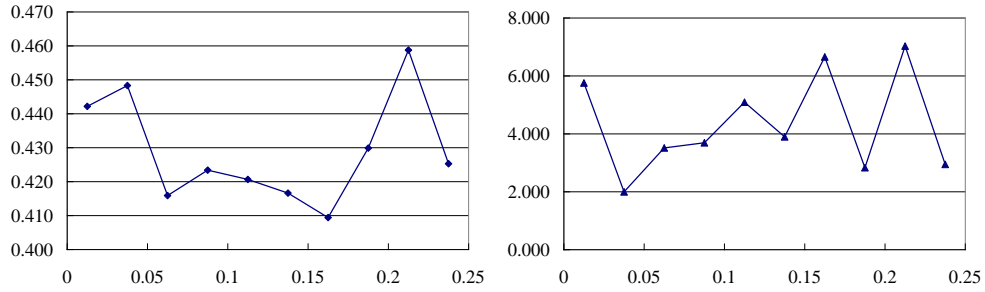
Figure 8.6 Variation of porosity and mobile phase velocity in the radial direction for cross section 1-6 in Figure 8.2. Left: porosity variation, vertical axis: porosity, horizontal axis: Distance from left wall (m);Right: velocity variation, vertical axis: methanol velocity (m/s), horizontal axis: Distance from left wall (m)

8.4.4 Effect of wall roughness on the band profile

(a)   **(b)**
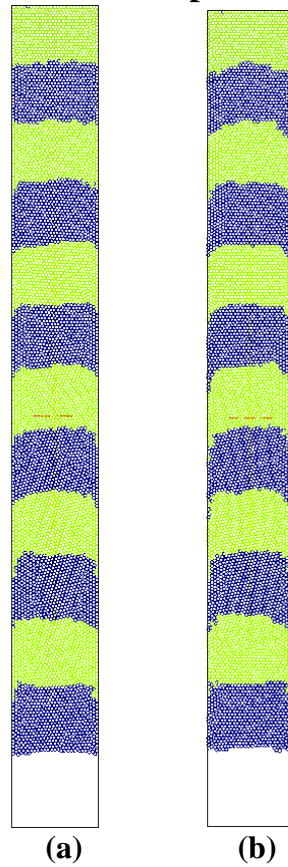
Figure 8.7 Effect of wall roughness of the band profile (a) left and right walls are regular DEM walls; (b) left and right walls are static particle walls

Figure 8.7(b) shows the same column but replacing the left and right regular DEM walls by static wall composed of particle diameters d_w=1mm in order to increase the wall roughness. In contrast to Figure 8.7(a), which uses the regular DEM wall, the band profile in Figure 8.7(b) showed larger curvature toward the column wall for the static particle wall model, which indicates that larger wall roughness will lead to more severe heterogeneity for the packing material inside the column.

8.5 Closure

The coupled DEM-CFD method is used to simulate the slurry packing of a chromatography column. The geometry was significantly simplified to conserve computational effort. The particle diameter was assumed to be approximately 100 times that typically used for silica packing material, and the cylindrical shape was approximated by planar flow. The coupled method is able to produce the shear effect on the packing material from wall during the axial upward compression procedure, providing a displacement filed similar to that observed in experiments.

Although the experimentally observed parabolic shaped velocity distribution was not repeated, the packing of a very heterogeneous column was simulated perhaps without reasonably considering the number of the particles in the column. This relationship is expected to be different if a larger number of particles within the fluid cell were used (at least 100 particles per fluid cell). The use of high performance parallel computational environment would make the solution of real problems possible, once the current DEM-CFD code can be written into a parallel framework.

9 Summary and Recommendations

The present study contributes to the field of discrete element method application in the following three ways:

9.1 Open source DEM code verification

The discrete element method is a highly computation intensive method, the results of which are sometimes very difficult to verify when a large number of particles are used. In order to verify the results, verification problems with well established analytical solutions must be identified and rely on assumptions consistent with the DEM. The verification problems used in this study: the 1D particle motion prediction with different damping coefficients, the 1D upward seepage/critical gradient problem, and the 1D consolidation problem, are all based on very idealistic assumptions. Although they might be of little engineering practice interest, such verification models enable the investigation of single parameter effects and the simple relationship between particles makes it easier to search and debug the DEM code. These problems also provide guidance for selecting the input parameters for larger scale problems, as with the discussion of the NDF value and the viscous damping effect in Chapter 6. It is recommended that simplified models, typically with a small number of particles be used and verified before carrying out large scale calculations.

9.2 The statistical approach in DEM method

In Chapter 4 and Chapter 5, a statistical approach using logistic regression is established with the 2D and 3D modeling of the sinkhole repair problem. While running different initial random particle positions and particle diameters, the transition in mean particle size from a stable to an unstable assembly of particles is described by a continuous smooth function rather than a step wise function. The use of this statistical method can be a useful tool in the future DEM application, since determining and changing an input random parameter is relatively easier than running different real experiments to collect data and then analyze them using statistical tools.

9.3 The coupled DEM-CFD model

The DEM-CFD method was originally proposed by Tsuji (1993) to investigate the fluidization of gas bed in powder technology. Chapter 6-8 discussed the application of the DEM-CFD method in a simplified 1D seepage/consolidation verification, 2D modeling of seepage flow under a sheet pile structure, and band broadening of the packing material inside a chromatography column. All of these models, by using the averaged Navier-Stokes equation, comply with Darcy's law when the particles within the fluid mesh are closely packed and the pressure gradient is below critical, although no Darcy's flow assumption is made throughout the calculation process. When the flow region is beyond critical, the method is still capable of predicting the behavior of fluid-particle assembly (as discussed in the 2D sheet pile analysis and slurry packing of chromatography column), where both analyses undergo a quick procedure during the simulation and Darcy's law is no longer capable of predicting the flow behavior. Based on these results, the coupled DEM-CFD method can be applied in most geotechnical engineering problems where Darcy's law dominates the fluid region and the discrete inter-particle behavior is important but difficult to obtain through the traditional continuum mechanics approach. It can also be used in cases when the fluid flow field cannot be calculated by Darcy's law, e.g. the behavior of a fluid particle system under large pressure gradient which is beyond quick, or the dilute flow when the fluid mesh domain is loosely packed by particles.

9.4 Future work

As seen from the previous chapters, the particle-fluid problem using DEM-CFD method is very computational intensive and has a serious limitation imposed by the computational power of the computer. Currently, research on the coupled model in this study is limited to relatively small scale and the particles are generally limited to several thousand level to adapt to the computation environment. For example, the number of particles used in real chromatography column problem or soil liquefaction under an earth dam might easily exceed 10^8, even for a simplified 2D model. As seen from the 2D sheet pile problem, although a scaling law provides a possible alternative, the large number of particles will still remain a serious issue for real engineering problems.

The most direct and apparent solution is the parallelization of the code. Based on the current YADE-OpenFOAM code coupling structure, it is therefore desirable to conduct research on the future framework of CFD-DEM parallelization, which includes:

(1)   Parallel framework between CFD fluid module and DEM solid particle module;
(2)   Parallel framework within the CFD fluid module;
(3)   Parallel framework within the DEM solid particle module;

There have been a number of previous investigating research studies on issue (2), the parallel CFD module. While there is little research on issue (1) and (3), especially (1), the parallel relationship between CFD and DEM are seldom discussed, but will have significant effect on the parallel model, and the communication of large quantity data between discrete element and the finite volume mesh also needs to be carefully optimized.

Another possible way of solving the computation limit is to change the mathematical nature of DEM mechanism for the solid particles, i.e. reducing the duty of the particle motion computation. The original DEM proposed by Cundall and Strack (1979) is in fact an explicit integration of velocity and hence displacement starting from the Newton's second law of motion under boundary constrains of contact. It is worthwhile to notice the Discontinuous Deformation Analysis (DDA) which is another type of discrete element method originally proposed by Shi (1993). Instead of traditional DEM which employs the explicit time marching scheme to solve the equations of motion directly (Cundall and Hart 1989), the system of equation in DDA is derived from minimizing the total potential energy of the particle assembly. This would be an implicit displacement method instead of a force method and guarantee that equilibrium is satisfied at all times, thus would be able to greatly reduce the computational needs required for explicit time integration. There has been previous research from Ke and Bray (1995) that used disk shape elements and therefore spherical element DDA analysis can also be extended.

References

Anderson, J., 1995. *Computational Fluid Dynamics. The Basic with Applications.*,

Anderson, T.B. & Jackson, R., 1967. A fluid mechanical description of fluidized beds. *Industrial & Engineering Chemistry Fundamentals*, 6(4), 527-539.

Bathurst, R.J. & Rothenburg, L., 1988. Micromechanical aspects of isotropic granular assemblies with linear contact interactions. *Journal of applied mechanics*, 55(1), 17-23.

Baur, J.E. et al., 1988. Fast-Scan Voltammetry of Biogenic Amines. *Analytical Chemistry*, 60, 1268-1272.

Baur, J.E. & Wightman, R.M., 1989. Microcylinder Electrodes as Sensitive Detectors for High-Efficiency, High-Speed Liquid Chromatography. *Journal of Chromatography*, 482, 65-73.

Bishop, R.E.D. & Johnson, D.C., 1960. *The mechanics of vibration*, Cambridge, U.K.: Cambridge University Press.

Brown, D.L., Henshaw, W.D. & Quinlan, D.J., 1999. Overture: An Object-Oriented Framework for Solving Partial Differential Equations on Overlapping Grids. In UCRL-JC-132017.

CD-adapco Group, 2001. STAR-CD Version 3.15 Methodology, Computational Dynamics. Ltd.

Chen, F., Ozgur, A. & Drumm, C.E., 2006. Simulation of Graded Rock Fill for Sinkhole Repair in Particle Flow Model. In Underground Construction and Ground Movement (GSP 155).

Cook, R., Malkus, D. & Plesha, M., 2001. *Concepts and applications of finite element analysis* 4th ed., New York: Wiley.

Courant, R. & Friedrichs, K.O., 1948. *Supersonic Flow and Shock Waves*, New York: Interscience Publishers, Inc.

Cundall, P.A., 1978. *Ball - a program to model granular media using the distinct element method.*, London: Dames and Moore, Advanced Technology Group.

Cundall, P.A., 1987. Distinct element models of rock and soil structure. In *Analytical and computational methods in engineering rock mechanics, E. T. Brown, ed.* London: George Allen and Unwin, pp. 129-163.

Cundall, P.A., 1998. Formation of a three dimensional Distinct Element Model-Part I. A Scheme to Detect and Report Contacts in a System Composed of Many Polyhedral Blocks. *International journal of rock mechanics and mining sciences*, 25(3), 107-116.

Cundall, P.A. & Hart, R.D., 1989. Numerical of discontinua. In Golden, Colo.

Cundall, P.A. & Strack, O.D.L., 1979. A discrete numerical model for granular assemblies. *Geotechnique*, 29, 47-65.

DEM Solutions, 2009. EDEM 2.1.2 User Guide. Available at: http://www.dem-solutions.com/downloads/manuals/edem212/EDEM2.1.2_user_guide.pdf [Accessed April 20, 2009].

Dobry, R. & Ng, T., 1992. Discrete Modeling of Stress-Strain Behavior of Media at Small and Large Strain. *Engineering Computations*, 9, 129-143.

Donzé, F.V. & Magnier, S.A., 1997. *Spherical Discrete Element Code*, Laboratory GEOTOP, Université du Québec à Montréal.

Drumm, E.C., Kane, W.F. & Yoon, C.J., 1990. Application of limit plasticity to the stability of sinkholes. *Engineering Geology*, 29, 213-225.

El Shamy, U. & Zeghal, M., 2005. Coupled Continuum-Discrete Model for Saturated Granular Soils. *Journal of Engineering Mechanics*, 131(4), 413-426.

Ergun, S., 1952. Fluid flow through packed columns. *Chemical Engineering Progress*, 48(2), 89-94.

Evgin, E., 2000. An experimental study and numerical simulation of liquefaction at a soil-structure interface. In Montreal: Canadian Geotechnical Society, pp. 1075–1082.

Farkas, T., Chambers, J.Q. & Guiochon, G., 1994. Column Efficiency and Radial Homogeneity in Liquid Chromatography. *Journal of Chromatography A*, 679, 231-245.

Farkas, T. & Guiochon, G., 1997. Contribution of the Radial Distribution of the Flow Velocity to Band Broadening in HPLC Columns. *Analytical Chemistry*, 69, 4592–4600.

Farkas, T., Sepaniak, M.J. & Guiochon, G., 1996. Column Radial Homogeneity in HPLC. *Journal of Chromatography A*, 740, 169-181.

Ferziger , J.H. & Peric , M., 2001. *Computational Methods for Fluid Dynamics* 3rd ed., Springer.

Fluent Inc., 2006. FLUENT 6.3 User's Guide. Available at: http://hpce.iitm.ac.in/Manuals/Fluent_6.3/Fluent.Inc/fluent6.3/help/pdf/ug/pdf.htm [Accessed May 1, 2007].

Galizzi, O. & Kozicki, J., 2005. YADE-Yet another dynamic engine. Available at: http://yade.berlios.de.

Ginsberg, J.H. & Genin, J., 1984. *Statics and dynamics*, Hoboken, NJ: Wiley.

Guiochon, G., Shirazi, G.S. & Katti , A., 1994. *Fundamentals of Preparative and Nonlinear Chromatography*, New York: Academic Press.

Hentz, S., Daudeville, L. & Donzé, F.V., 2004. Identification and validation of a discrete element model for concrete. *Journal of Engineering Mechanics*, 130(6), 709-719.

Hockney, R.W., 1970. The potential calculation and some applications. In *Alder, B., Fernbach, S., Rotenberg, M. (eds.): Methods in Computational Physics*. New York/London: Academic Press.

Holtz, R.D. & Kovacs, W.D., 1981. *An Introduction to Geotechnical Engineering*, Englewood Cliffs, NJ: Prentice-Hall, Inc.

Horne, D.S., Knox, J.H. & McLaren, L., 1966. A Comparison of Mobile Phase Peak Dispersion in Gas and Liquid Chromatography. *Sep. Sci. Technol.*, 1(531).

Hustrulid, A.I. & Mustoe, G.G.W., 1996. Engineering Analysis of Transfer Points Using Discrete Element Analysis. In Phoenix, AZ.

Issa, R.I., 1986. Solution of the implicitly discretized fluid flow equations by operator splitting. *Journal of Computational Physics*, 62(40-65).

Itasca Inc., 2004a. Fixed coarse-grid fluid scheme in PFC2D, The PFC2D user's manual. Available at: [Accessed November 13, 2007].

Itasca Inc., 2004b. The PFC2D user's manual. Available at: http://www.itascacg.com [Accessed September 16, 2005].

Jasak, H., 1996. *Error Analysis and Estimation for the Finite Volume Method with Applications to Fluid Flows*. PhD Thesis. Imperial College, University of London .

Jensen, R.P. et al., 2001. Effect of Particle Shape on Interface Behavior of DEM-Simulated Granular Materials. *The International Journal of Geomechanics*, 1(1), 1-19.

Johnson, P.C. & Jackson, R., 1987. Frictioinal-Collisioinal Constitutive Relations for Granular Materials with Application to Plane Shearing. *Journal of fluid Mechanics*, 176, 67-93.

Kawaguchi, T., Tanaka, T. & Tsuji, Y., 1998. Numerical simulation of two-dimensional fluidized beds using the discrete element method (comparison between the two- and three-dimensional models). *Powder Technology*, 96(2), 129-138 .

Ke, T. & Bray, J., 1995. Modeling of particulate media using discontinuous deformation analysis. *Journal of Engineering Mechanics*, 121(11), 1243-1234.

Kemmerly, P.R., 1984. Corrective Procedures for Sinkhole Collapse on the Western Highland Rim, Tennessee. *Transportation Research Record*, 978, 12-18.

Knox, J.H., Laird, G.R. & Raven, P.A., 1976. Interaction of Radial and Axial Dispersion in Liquid Chromatography in Relation to the 'Infinite Diameter Effect'. *Journal of Chromatography*, 122(7), 129-145.

Knox, J.H. & Parcher, J.F., 1969. Effect of the column to particle diameter ratio on the dispersion of unsorbed solutes in chromatography. *Analytical Chemistry*, 41(12), 1599-1606.

Knuth, D., 1997. *The Art of Computer Programming, Volume 3: Sorting and Searching* 3rd ed., Addison-Wesley.

Kozicki, J. & Donzé, F.V., 2008. A new open-source software developed for numerical simulations using discrete modeling methods. *Computer Methods in Applied Mechanics and Engineering*, 197, 4429-4443.

Kutner, M.H., Nachtsheim, C.J. & Neter, J., 2004. Chapter 14. Logistic regression, Poisson regression, and generalized linear models. In *Applied Linear Regression Models*. McGraw-Hill/Irwin, p. 701.

Lambe, T.W. & Whitman, R.V., 1969. *Soil mechanics*, New York: Wiley.

Lide, D.R., 1992. *Handbook of Chemistry and Physics (CRC)* 73rd ed., USA : Chemical Rubber Publishing Co.

Logg, A., 2009. FFC User Manual. Available at: http://www.fenics.org/pub/documents/ffc/ffc-user-manual/ffc-user-manual.pdf [Accessed March 24, 2009].

Maplesoft, 2005. Maple's help system. Available at: http://www.maplesoft.com [Accessed May 13, 2005].

Mihlbachler, K. et al., 1998. Measurement of the Degree of Cohesion of Two Native Silica Packing Materials. *Journal of Chromatography A*, 818(2), 155-168 .

Moore, H.L., 2006. A Proactive Approach to Planning and Designing Highways in East Tennessee Karst. *Environmental and Engineering Geoscience, Association of Engineering Geologists*, 12(2), 147-160.

Moore, H.L., 1981. Karst Problems Along Tennessee Highways: An Overview. In Austin, Texas.

von Neumann, J. & Richtmyer, R.D., 1950. A method for the numerical calculation of hydrodynamic shocks. *Journal of Applied Physics*, 21, 232-237.

Open Source Initiative, 2007. The Open Source Definition. Available at:
http://www.opensource.org/.

OpenCFD Ltd, 2008. The open source CFD toolbox, Programmer's Guide, Version 1.4.1.
Available at: http://foam.sourceforge.net/doc/Guides-a4/ProgrammersGuide.pdf
[Accessed May 13, 2008].

Patankar, S.V., 1980. *Numerical Heat Transfer and Fluid Flow*, Taylor & Francis.

Peron, H. et al., 2009. Discrete elementnext term modelling of drying shrinkage and cracking of
soils . *Computers and Geotechnics*, 36(2), 61-69.

Popp, K. & Schiehlen, W., 2008. *Ground Vehicle Dynamics*, Berlin: Springer.

Richard , S.W. & Rago , S.A., 2005. *Advanced Programming in the UNIX(R) Environment* 2nd
ed., Addison-Wesley Professional.

Richards, K. et al., 2004. Discrete-element modelling: methods and applications in the
environmental sciences. *Philosophical transactions - Royal Society. Mathematical,
physical and engineering sciences* , 362(1822), 1797-1816.

SAS Institute Inc., 2006. JMP Manual: Statistics and Graphics Guide. Available at:
http://www.jmp.com [Accessed July 5, 2008].

Shafipour, R. & Soroush, A., 2008. Fluid coupled-DEM modelling of undrained behavior of
granular media. *Computers and Geotechnics*, 35(5), 673-685.

Shi, G., 1993. *Block system modeling by discontinuous deformation analysis*, Computational
Mechanics Publications.

Sowers, G.F., 1996. *Building on Sinkholes: Design and Construction of Foundations in Karst
Terrain*, New York: ASCE.

Stone, J.M. & Norman, M.L., 1992. ZEUS-2D: A radiation magnetohydrodynamics code for
astrophysical flows in two space dimensions. I-The hydrodynamic algorithms and tests.
Astrophysical Journal Supplement Series, 80(2), 753-790.

Succi, S., 2001. *The Lattice Boltzmann Equation for Fluid Dynamics and Beyond*, Oxford
University Press.

Suzuki, K. et al., 2007. Simulation of Upward Seepage Flow in a Single Column of Spheres
Using Discrete-Element Method with Fluid-Particle Interaction. *Journal of Geotechnical
and Geoenvironmental Engineering*, 133(1), 104-110.

Tanaka, T., Kawaguchi, T. & Tsuji, Y., 1993. Discrete particle simulation of flow patterns in two-dimensional gas fluidized beds. *International Journal of Modern Physics B*, 7(9/10), 1889 - 1898.

Taylor, D., 1948. *Fundamentals of soil mechanics*, New York: John Wiley & Sons.

Terzaghi, K., 1943. *Theoretical soil mechanics*, New York: Wiley.

Thomson, W.T., 1993. *Theory of Vibration with Applications*, Prentice Hall.

Thornton, C. & Liu, L., 2000. DEM simulations of uniaxial compression and decompression. In *Compaction of Soils, Granulates and Powders By D. Kolymbas, W. Fellin*. Taylor & Francis.

Train, D., 1956. An Investigation into the Compaction of Powders. *Journal of Pharmacy and Pharmacology*, 8, 745.

Train, D., 1957. Transmission of Forces through a Powder Mass during the Process of Pelleting. *Transactions of the American Institute of Chemical Engineers*, 35(4), 258-266.

Tsuji, Y., Kawaguchi, T. & Tanaka, T., 1993. Discrete particle simulation of two-dimensional fluidized bed. *Powder technology*, 77(11), 79-87.

Warren, L.M., Julian, C.S. & Peter, H., 2005. *Unit Operations of Chemical Engineering* 7th ed., New York: McGraw-Hill.

Wikipedia, 2007. Porous medium. Available at: http://en.wikipedia.org/wiki/Porous_medium [Accessed May 15, 2007].

Williams, J.R., Hocking, G. & Mustoe, G.G.W., 1985. The theoretical basis of the discrete element method. In Balkema, Rotterdam, The Netherlands, pp. 897-906.

Yao, M. & Anandarajah, M., 2003. Three-Dimensional Discrete Element Method of Analysis of Clays. *Journal of Engineering Mechanics*, 129(6), 585-596.

Yew, B.G., 1999. *Application of Soil Mechanics and the Finite Element Method to High Performance Liquid Chromatography Columns*. Master's Degree Dissertation. The University of Tennessee, Knoxville, TN.

Yun, T. & Guiochon, G., 1997. Visualization of the Heterogeneity of Column Beds. *Journal of Chromatography A*, 760(1), 17-24.

Yuu, S., Umekage, T. & Johno, Y., 2000. Numerical simulation of air and particle motions in bubbling fluidized bed of small particles . *Powder Technology*, 110(1-2), 158-168.

Zureick, A., Bennett, R.M. & Ellingwood, B.R., 2006. Statistical Characterization of Fiber-Reinforced Polymer Composite Material Properties for Structural Design. *Journal of Structural Engineering*, 132(8).

Vita

Feng Chen was born in Liuhe, Jiangsu China P.R. He attended elementary schools in Jiading District Shanghai, China and graduated from Shanghai Jiading No.1 Senior School in July 1997. In September 1997 he entered Tongji University in Shanghai China and in July 2001 received the Bachelor' Degree in Building Engineering. He received Master' Degree in Structural Engineering in March 2004. He entered the University of Tennessee, Knoxville in August 2004 and is a candidate for the Doctor of Philosophy Degree in Civil Engineering.